

# Mass transfer in gas fluidized beds : scaling, modeling and particle size influence

**Citation for published version (APA):**

Lare, van, C. E. J. (1991). *Mass transfer in gas fluidized beds : scaling, modeling and particle size influence*. [Phd Thesis 1 (Research TU/e / Graduation TU/e), Chemical Engineering and Chemistry]. Technische Universiteit Eindhoven. <https://doi.org/10.6100/IR348157>

**DOI:**

[10.6100/IR348157](https://doi.org/10.6100/IR348157)

**Document status and date:**

Published: 01/01/1991

**Document Version:**

Publisher's PDF, also known as Version of Record (includes final page, issue and volume numbers)

**Please check the document version of this publication:**

- A submitted manuscript is the version of the article upon submission and before peer-review. There can be important differences between the submitted version and the official published version of record. People interested in the research are advised to contact the author for the final version of the publication, or visit the DOI to the publisher's website.
- The final author version and the galley proof are versions of the publication after peer review.
- The final published version features the final layout of the paper including the volume, issue and page numbers.

[Link to publication](#)

**General rights**

Copyright and moral rights for the publications made accessible in the public portal are retained by the authors and/or other copyright owners and it is a condition of accessing publications that users recognise and abide by the legal requirements associated with these rights.

- Users may download and print one copy of any publication from the public portal for the purpose of private study or research.
- You may not further distribute the material or use it for any profit-making activity or commercial gain
- You may freely distribute the URL identifying the publication in the public portal.

If the publication is distributed under the terms of Article 25fa of the Dutch Copyright Act, indicated by the "Taverne" license above, please follow below link for the End User Agreement:

[www.tue.nl/taverne](http://www.tue.nl/taverne)

**Take down policy**

If you believe that this document breaches copyright please contact us at:

[openaccess@tue.nl](mailto:openaccess@tue.nl)

providing details and we will investigate your claim.

# Mass transfer in gas fluidized beds: scaling, modeling and particle size influence

Proefschrift

ter verkrijging van de graad van doctor aan de  
Technische Universiteit Eindhoven, op gezag van  
de Rector Magnificus, prof. dr. J.H. van Lint, voor  
een commissie aangewezen door het College  
van Dekanen in het openbaar te verdedigen op  
vrijdag 5 april 1991 om 16.00 uur

door

Cornelis Elisabeth Johannes van Lare

Geboren te Horn

Dit proefschrift is goedgekeurd door de promotor:

Prof. dr. ir. D. Thoenes

Omslagontwerp:

Robert Engelke

*Men moet iets leren door het te doen; want alhoewel je denkt dat je iets kunt,  
je weet het pas zeker als je het geprobeerd hebt.*

*Sophocles.*

Voor mijn ouders.

Voor Yvonne.

## SUMMARY

---

In a gas fluidized bed a gas is led through a reactor filled with particles supported by a distributor plate. If sufficient gas is led through, bubbles will form. These bubbles maintain the particle circulation which results in the excellent heat transfer properties of a fluid bed reactor. But they also may contain most of the gas, leading to a short circuit of the gas. To maximize the conversion of a heterogeneously catalyzed gas phase reaction, the mass transfer from the bubble phase to the so called dense phase (which contains the solid particles) has to be as high as possible.

Consider a mass transfer controlled fluid bed system, where the reaction is such that it is best to have a relatively low conversion, because then a maximum selectivity and/or yield is obtained. To maximize the production quantity, but also minimize the reactor dimensions and prevent the blowing out of powders, it would be best to use large particle powders in these situations. The question is whether the mass transfer from bubble phase to dense phase is sufficiently large for these powders.

A parameter that describes the resistance to mass transfer from the bubble phase to the dense phase is the height of a mass transfer unit  $H_k$ . Based on theoretical considerations it was calculated that the height of a mass transfer unit increases with increasing particle size for A and small B type powders and that it decreases with increasing particle size for large B and D type powders. This is however no more than an expected trend, which was confirmed by experiments (reported in literature) on one injected bubble. However hydrodynamics and mass transfer are completely different for a bubbling bed. Therefore experiments had to be performed to check this theory.

The model that was used to analyze the experimental data was a two phase model: bubble phase and dense phase in plug flow (with or without axial dispersion) and mass transfer between these two phases (the Van Deemter model).

First of all a sensitivity analysis was performed to investigate the influence of the Peclet numbers and mass transfer coefficient on a non steady state system. This was done with a new numerical technique: the decoupling method. Combined with data from literature it was concluded that the Peclet numbers had little influence. In general the superficial velocity in the

bubble phase is that high that a diffusional influence on this phase can be neglected. Furthermore the relative gas flow through the dense phase is that small that the influence of a diffusional component in this phase is of little influence on the total behavior of a fluidized bed.

The dispersion coefficients were neglected in analyzing the experimental data obtained from a chemically reacting system in steady state: the ozone decomposition on a ferric oxide/sand catalyst of  $67 \mu\text{m}$  in a fluid bed reactor with a diameter of 10 cm. It was found that for this catalyst the height of a mass transfer unit was about 18 cm.

Particle size influences many parameters. Therefore a parameter that describes all fluid bed systems is necessary to compare different reactor types, reactions and particle types and sizes. A "scaling parameter"  $S$  was proposed to this end. Our data and a lot of literature data were analyzed statistically to estimate this parameter. This scaling parameter can also be used for scaling up fluid bed reactors, since it contains the bed height, the bed diameter and the superficial velocity. It was shown that for A type powders the height of a mass transfer unit indeed increases with increasing particle size with a constant scaling parameter as reference. This result confirmed the theoretically predicted trend for A type powders. For coarse powders more experimental data were needed.

Residence time distribution measurements were performed in a fluid bed with a diameter of 25 cm with quartz sand powders of 106, 165, 230, 316 and 398  $\mu\text{m}$ . The experimental curves were fitted using the decoupling method and the results for the various powders were compared with the scaling parameter as reference. The height of a mass transfer unit indeed showed the expected trend: with constant scaling parameter,  $H_k$  increased with increasing particle size, up to about 230  $\mu\text{m}$ . After the maximum it decreased with increasing particle size.

Hydrodynamic measurements were also performed. The signals obtained from a capacitive probe were analyzed with a new statistical method. The results from these experiments and computational technique were in agreement with theories known from the literature. Furthermore it was possible to gain information on the stable bubble height  $h^*$ . This is the height at which an equilibrium between coalescence and splitting is reached. It appeared that  $h^*$  was linearly dependent on particle size only.

All experimental results were combined to give a mass transfer model that

was composed of theoretical models found in literature. We were able to get a simple model entirely based on physical and theoretical grounds. With this model it was possible to predict all our own and literature data reasonably well. The model was then used to perform some simple design computations. This showed that there can be situations where large B type powders can be more efficient than small particle powders.

## SAMENVATTING

---

In een gas gefluïdiseerd bed wordt een gas geleid door een reaktor gevuld met deeltjes, die liggen op een verdeelplaat. Als er voldoende gas wordt doorgeleid ontstaan bellen. Deze bellen zorgen voor een deeltjescirculatie, hetgeen resulteert in de goede warmte-overdrachtseigenschappen van een fluidbed. Voor een zo hoog mogelijke conversie van een gas-vast gekatalyseerde reactie moet de stofoverdracht van de bellen naar de, deeltjes bevattende, dichte fase zo groot mogelijk zijn.

Stel je hebt een stofoverdracht bepaald fluidbed-systeem, waarbij de reactie zodanig is dat een bepaalde (relatief lage) conversie het meest gunstig is in verband met een gewenste produkt-opbrengst. Wanneer men zoveel mogelijk wenst te produceren, maar tegelijkertijd het overmatig uitblazen van poeders vermeden moet worden (zonder te veel cyclonen te gebruiken) en de reaktordimensies geminimaliseerd moeten worden, dan is het het beste om grove poeders te gebruiken. Immers, bij grove poeders kan en moet een grote superficiële gassnelheid gebruikt worden. De vraag is echter of de stofoverdracht van de bellenfase naar de dichte fase voldoende groot is, wanneer grote deeltjes gebruikt worden.

Een parameter die de weerstand tegen stofoverdracht van de bellenfase naar de dichte fase beschrijft is de hoogte van een stofoverdrachtstrap  $H_k$ . Uit een theorie werd berekend dat  $H_k$  stijgt bij toenemende deeltjesgrootte voor A en kleine B poeders en dat  $H_k$  enigszins daalt bij toenemende deeltjesgrootte voor grote B en D poeders. Dit is slechts een verwachte trend, die bevestigd werd uit experimenten, vermeld in de literatuur, voor één (geïnjecteerde) bel. Hydrodynamica en stofoverdracht zijn volledig verschillend voor een heterogeen gefluïdiseerd bed. Experimenten moesten derhalve uitwijzen of deze theorie juist is voor dergelijke (in de praktijk meest voorkomende) bedden.

Het model dat werd gebruikt om de experimentele data te analyseren was een twee-fasen model: bellenfase en dichte fase in propstroom (met of zonder axiale dispersie) en stofoverdracht tussen deze twee fasen (het van Deemter model).

Allereerst werd een gevoeligheidsanalyse uitgevoerd, om de invloed van de Peclet-getallen en de stofoverdrachtscoëfficiënt te onderzoeken voor een niet-stationair systeem. Dit werd gedaan met een nieuwe numerieke methode: de



"decoupling"-methode. Gecombineerd met data uit de literatuur werd er geconcludeerd dat de Peclet-getallen weinig invloed hadden. In het algemeen is de superficiële gassnelheid in de bellenfase zo groot dat een invloed van de diffusie verwaarloosd kan worden voor deze fase. De relatieve gasdoorstroming van de dichte fase is zodanig klein dat de invloed van de diffusie in deze fase een kleine invloed heeft op het overall gedrag van een gefluïdiseerd bed.

De dispersie werd verwaarloosd voor beide fasen en dit werd gebruikt om de data te analyseren die werden verkregen uit een chemisch reactiesysteem in stationaire toestand: de decompositie van ozon op een ijzeroxide katalysator van 67  $\mu\text{m}$  in een fluidbed-reactor met een diameter van 10 cm. Voor deze katalysator werd een hoogte van een stofoverdrachtstrap van ongeveer 18 cm gevonden.

De deeltjesgrootte beïnvloedt zeer veel parameters. Om verschillende reaktortypes, reacties en deeltjestypen en -grootten te kunnen vergelijken is één parameter nodig die alle fluidbed-systemen beschrijft. Daarom werd een schalingsparameter gedefinieerd, die verkregen werd door onze data en vele data uit de literatuur statistisch te analyseren. Deze schalingsparameter kan ook gebruikt worden in het opschalen van fluid bed reactoren, aangezien het de bedhoogte, beddiameter en superficiële gassnelheid bevat. Met de schalingsparameter als referentie werd voor A poeders aangetoond dat de hoogte van een stofoverdrachtstrap inderdaad stijgt bij toenemende deeltjesgrootte. Voor grovere poeders waren meer experimentele data nodig.

Verblijftijdspreidingsmetingen werden uitgevoerd in een fluidbed met een diameter van 25 cm met kwarts-zand poeders met deeltjesgrootten van 106, 165, 230, 316 en 398  $\mu\text{m}$ . De experimenteel gemeten curven werden numeriek gefit, waarbij de "decoupling"-methode werd gebruikt. De resultaten voor de verschillende poeders werden vergeleken met de schalingsparameter als referentie. De hoogte van een stofoverdrachtstrap  $H_k$  vertoonde inderdaad de verwachte trend: bij een constante schalingsparameter steeg  $H_k$  bij toenemende deeltjesgrootte tot ongeveer 230  $\mu\text{m}$ . Na het maximum daalde  $H_k$  weer bij toenemende deeltjesgrootte.

Hydrodynamische experimenten werden ook uitgevoerd. De signalen die verkregen werden met een capacitieve probe werden geanalyseerd met een nieuw ontwikkelde statistische methode. De resultaten van de experimenten en rekentechniek waren in overeenstemming met theorieën uit de literatuur. Het bleek verder ook mogelijk om informatie te verkrijgen over de stabiele

belhoogte  $h^*$ . Dit is de hoogte waar een evenwicht tussen coalescentie en splitsing van de bellen is bereikt. Het leek er op dat  $h^*$  lineair afhankelijk is van alleen de deeltjesgrootte.

Alle experimentele resultaten werden gecombineerd tot een model, gebaseerd op theorieën uit de literatuur. Het was mogelijk een eenvoudig model te definieëren geheel gebaseerd op theoretische en fysische overwegingen. Met dit model konden al onze data en alle literatuurdata bevredigend beschreven worden. Daarna werd het model gebruikt om eenvoudige ontwerpberekeningen uit te voeren. Deze lieten zien dat er situaties zijn waar het gunstiger is grote B poeders te gebruiken in plaats van de meer gangbare kleine A poeders.

# TABLE OF CONTENTS

## List of symbols

<b>Introduction</b>	1
<b>Chapter 1. Theory</b>	3
1.1 Basic principles	3
1.2 Hydrodynamics	5
1.3 Mass transfer	9
1.4 Model description	11
1.5 Mass transfer as a function of particle size	16
1.6 Scope of this thesis	18
<b>Chapter 2. Numerical solution of differential equations, derived from a two phase model.</b>	19
2.1 Introduction	19
2.2 The decoupling method	20
2.3 Algorithm	26
2.3.1 Definition of feed- and end conditions	28
2.4 Results and Discussion	29
2.5 Concluding remarks	35
Appendix 2.A	37
<b>Chapter 3. Chemical model reaction: ozone decomposition.</b>	41
3.1 Introduction	41
3.2 Experimental	43
3.2.1 The equipment	43
3.2.2 Experiments	46
3.3 Results and Discussion	50
3.4 Concluding remarks	51
Appendix 3.A	52
Appendix 3.B	52

<b>Chapter 4.</b>	<b>Scaling of mass transfer</b>	<b>58</b>
4.1	Introduction	58
4.2	Data analysis	58
4.3	Results and Discussion	61
4.4	Conclusions	71
<b>Chapter 5.</b>	<b>Mass transfer from RTD measurements</b>	<b>72</b>
5.1	Introduction	72
5.2	Experimental	72
5.2.1	The fluid bed reactor	72
5.2.2	Measuring equipment	75
5.2.3	The measurements	77
5.2.4	Data processing	79
5.3	Results and Discussion	81
5.4	Concluding remarks	88
	Appendix 5.A	90
<b>Chapter 6.</b>	<b>Investigation on bubble characteristics and stable bubble height.</b>	<b>91</b>
6.1	Introduction	91
6.2	Experimental method	92
6.3	Statistical signal analysis	97
6.4	Determination of local fluidizing state	107
6.5	Results and Discussion	108
6.6	Concluding remarks	124
<b>Chapter 7.</b>	<b>Mass transfer modeling and reactor design.</b>	<b>125</b>
7.1	Introduction	125
7.2	Modeling	126
7.3	Model computations	133
7.4	An example of a reactor design	137
7.4.1	Heat transfer	142
7.4.2	Design calculations	144
7.5	Concluding remarks	150
	Appendix 7.A	151

<b>References</b>	154
<b>Curriculum Vitae</b>	159
<b>Nawoord</b>	160

## List of Symbols

a	specific bubble surface.	[m <sup>2</sup> /m <sup>3</sup> ]
a <sub>d</sub>	coefficient in Dirac pulse.	[-]
A	cross sectional area of reactor.	[m <sup>2</sup> ]
A <sub>0</sub>	total free surface of distributor.	[m <sup>2</sup> ]
Ar	Archimedes number.	[-]
B	constant in eq. (7.22), from Bock (1983).	[-]
C <sub>b</sub>	gas concentration in bubble phase.	[mol/m <sup>3</sup> ]
C <sub>d</sub>	gas concentration in dense phase.	[mol/m <sup>3</sup> ]
C <sub>e</sub>	exit concentration.	[mol/m <sup>3</sup> ]
C <sub>g</sub>	gas concentration.	[mol/m <sup>3</sup> ]
C <sub>0</sub>	total amount of gas injected.	[mol/m <sup>3</sup> ]
C <sub>f</sub>	feed concentration.	[mol/m <sup>3</sup> ]
C <sub>1</sub>	entrance concentration.	[mol/m <sup>3</sup> ]
C <sub>out</sub>	average concentration of gas, leaving the reactor.	[mol/m <sup>3</sup> ]
C <sub>03,max</sub>	maximum obtainable ozone concentration.	[mol/m <sup>3</sup> ]
c	constant.	[-]
c <sub>g</sub>	heat capacity of gas.	[J/kg·K]
c <sub>p</sub>	heat capacity of particles.	[J/kg·K]
c <sub>1</sub>	constant in equation (4.3).	[-]
c <sub>2</sub>	constant in equation (4.3).	[-]
D	bed diameter.	[m]
D <sub>e</sub>	effective bed diameter.	[m]
D <sub>g</sub>	diffusion coefficient of gas.	[m <sup>2</sup> /s]
D <sub>T</sub>	heat exchange pipe diameter.	[m]
d <sub>b</sub>	average equivalent bubble diameter.	[cm]
d <sub>j</sub>	eigenvalues of matrix A.	[-]
d <sub>p</sub>	average particle size.	[μm]
d <sub>p,opt</sub>	optimal particle size.	[μm]
E	enhancement factor for mass transfer.	[-]
E[1]	mean pierced length.	[cm]
$\overline{E[1]}$	radial averaged mean pierced length.	[cm]
E <sub>b</sub>	Eddy dispersion coefficient for bubble phase.	[m <sup>2</sup> /s]
E <sub>d</sub>	Eddy dispersion coefficient for dense phase.	[m <sup>2</sup> /s]
E(θ)	dimensionless response (= C <sub>out</sub> (θ)/C <sub>0</sub> ).	[-]

$E(t)$	dimensionless response ( $= C_{out}(t)/C_0$ ).	[-]
$f(x)$	probability distribution of value $x$ .	[-]
$F(t)$	cumulative probability distribution for $t$ .	[-]
$F$	molar air flow rate (in chapter 3).	[mol/s]
	factor introduced by Werther (1977) (eq. 7.8).	[-]
$f_b$	fraction of gas in the bubble phase.	[-]
$f_{cat}$	fraction of catalyst in fluid bed.	[-]
$\tilde{f}_j$	elements of $\tilde{F}^{-1}$ vector.	[-]
$g$	acceleration constant due to gravity.	[m/s <sup>2</sup> ]
$h^*$	stable bubble height.	[m, cm]
$h$	differential bed height.	[m, cm]
$h_0$	initial bubble height ( $= 4 \cdot \sqrt{A_0}$ ).	[m, cm]
$h_w$	overall heat transfer coefficient.	[W/(m <sup>2</sup> ·K)]
$h_g$	heat transfer coefficient due to gas convection.	[W/(m <sup>2</sup> ·K)]
$h_p$	heat transfer coefficient due to particle convection.	[W/(m <sup>2</sup> ·K)]
$h_r$	heat transfer coefficient due to radiation.	[W/(m <sup>2</sup> ·K)]
$H$	total bed height.	[m, cm]
$\Delta H$	heat of reaction.	[kJ/mol]
$H_{hw}$	height necessary to remove all heat.	[m]
$H_{xa}$	height necessary to obtain a given conversion.	[m]
$Ha$	Hatta number.	[-]
$H_b$	bubbling bed height.	[m]
$H_d$	bed height with dense phase expansion.	[m]
$H_0$	initial bed height.	[m]
$H_{mf}$	bed height at minimum fluidization.	[m, cm]
$H_k$	height of a mass transfer unit.	[m, cm]
$i$	subscript.	[-]
$j$	subscript.	[-]
$k$	bubble frequency.	[s <sup>-1</sup> ]
$k_1$	reaction rate constant.	[s <sup>-1</sup> ]
$k_2$	reaction rate constant.	[s <sup>-1</sup> ]
$K_e$	mass transfer coefficient based on total gas volume.	[s <sup>-1</sup> ]
$k_m$	reaction constant based on catalyst mass.	[kg/(m <sup>3</sup> ·s)]
$k_d$	reaction rate constant, based on dense phase volume.	[s <sup>-1</sup> ]
$k_r$	reaction rate constant, based on fluid bed volume.	[s <sup>-1</sup> ]

$k_g$	mass transfer coefficient.	[m/s]
$k_{g,eff}$	effective mass transfer coefficient.	[m/s]
$l_i$	local pierced length.	[cm]
$M$	real average (in Chapter 6).	[ms]
	molecular weight (in Chapter 7).	[g/mol]
$M_i$	measured value in RTD experiments.	[V]
$n$	total number of bubbles counted.	[-]
	factor in n-type theory (eq. (1.6)).	[-]
$N_p$	number of heat exchange pipes.	[-]
$N_k$	number mass transfer units.	[-]
$N_r$	number of reaction units.	[-]
$N_t$	total number of transfer units.	[-]
$\Delta P$	bed pressure drop.	[N/m <sup>2</sup> ]
$P$	absolute pressure.	[N/m <sup>2</sup> ]
$Pr$	Prandtl number.	[-]
$P_D$	amount produced of component D.	[ton/year]
$Pe_b$	Peclet number for bubble phase.	[-]
$Pe_d$	Peclet number for dense phase.	[-]
$p_j$	elements of particulate vector $P^i(\sigma)$ .	[-]
$p_a$	partial pressure of component a.	[N/m <sup>2</sup> ]
$Q$	volumetric air flow rate.	[m <sup>3</sup> /s]
$Q_b$	volumetric gas flow through bubble phase.	[m <sup>3</sup> /s]
$Q_d$	volumetric gas flow through dense phase.	[m <sup>3</sup> /s]
$Q_w$	amount of heat.	[kJ/s]
$r$	radial position.	[cm]
$r_a$	reaction rate velocity.	[mol/(m <sup>3</sup> ·s)]
$r_{03}$	reaction rate velocity in ozone generator.	[mol/(m <sup>3</sup> ·s)]
$R$	radius of fluid bed reactor.	[cm]
	gas constant (= 8.31) (in chapter 3).	[J/(mol·K)]
$R_b$	radius of cloud.	[cm]
$R_c$	radius of bubble.	[cm]
$S$	Scaling parameter.	[m, cm]
$S_a$	real deviation (in chapter 6).	[ms]
$S_D$	selectivity with respect to component D.	[-]
$s$	distance between two probe points (= 10 mm).	[mm]
$t$	real time.	[s]
$\Delta t$	time step.	[s]



T	total measuring time.	[s]
	absolute temperature.	[K]
$\Delta T$	temperature difference.	[K]
$t_c$	contact time in eq. (7.22).	[s]
$t_j$	transformation elements for $p_j$ -elements.	[-]
$t_a$	bubble rising time.	[s]
$t_b$	bubble contact time.	[s]
$t_{trig}$	trigger time.	[s]
$t_0$	time at which bubble hits lower probe.	[s]
$t_m$	time at which maximum capacity change is reached.	[s]
$t_3$	time at which probe hits "bottom" of bubble.	[s]
$t_4$	time at which bubble has passed probe completely.	[s]
U	superficial gas velocity.	[m/s]
$U_{mf}$	minimum fluidization velocity.	[m/s]
$U_{max}$	superficial velocity at which $h_g$ reaches maximum.	[m/s]
$u_{b,i}$	local bubble velocity.	[cm/s]
U	superficial velocity.	[m/s]
$u_b$	bubble velocity	[m/s] or [cm/s]
$u_{b,\infty}$	rise velocity of a single bubble.	[m/s]
$u_d$	dense phase gas velocity.	[m/s]
$U_{mf}$	minimum fluidization velocity.	[m/s] or [cm/s]
$\dot{V}_b$	local visible bubble gas flow	[cm <sup>3</sup> /cm <sup>2</sup> ·s] or [m <sup>3</sup> /m <sup>2</sup> ·s]
$V_b$	radial averaged visible bubble gas flow.	[cm <sup>3</sup> /cm <sup>2</sup> ·s] or [m <sup>3</sup> /m <sup>2</sup> ·s]
W	catalyst mass.	[kg]
x	value of probe signal.	[V]
$X_a$	conversion.	[-]
$X_{a,hw}$	conversion obtained when a bed height of $H_{hw}$ is used.	[-]
$Y_D$	yield of product D.	[-]
y	value of probe signal.	[V]
	mole fraction of ozone (in chapter 3).	[-]
$y_{max}$	maximum value of probe signal.	[V]
z	height above distributor in eq. (7.22).	[m]
z'	bed height at which hydrodynamic factors become constant in eq. (7.22), from Bock (1983).	[m]

## Greek

$\alpha$	slope of trapezium.	[-]
$\beta$	gas parameter for bubble phase.	[-]
$\gamma$	gas parameter for dense phase.	[-]
	accomodation coefficient, from Bock (1983).	[-]
$\delta$	bubble hold up.	[-]
$\delta_f$	film thickness.	[m]
$\epsilon$	fixed bed porosity.	[-]
$\epsilon_b$	bubble hold up from Bock (1983) (chapter 7).	[-]
$\epsilon_d$	dense phase porosity.	[-]
$\epsilon_{mf}$	dense phase porosity at minimum fluidization velocity.	[-]
$\epsilon_{rel}$	relative error.	[-]
$\zeta$	parameter for boundary conditions.	[-]
	ratio of ozone concentration and maximum obtainable ozone concentration.	[-]
$\kappa$	constant in eq. (7.8), from Werther (1977).	[-]
$\lambda_H$	heat conductivity coefficient.	[W/m·K]
$\lambda_m$	free path length of gas molecules.	[m]
$\vartheta$	dimensionless time ( = $t/\tau$ ).	[-]
$\vartheta_{step}$	dimensionless time step for Dirac pulse.	[-]
$\vartheta_{stop}$	dimensionless time at which computations are stopped.	[-]
$\Delta\vartheta$	stepsize for dimensionless time.	[-]
$\theta$	starting value in probability distribution $f(x)$ .	[-]
$\mu$	average value of log-normal distribution (chapter 6).	[-]
	average residence time calculated by program simulation (in chapter 2).	[s]
$\varphi$	dense phase through flow factor.	[-]
$\varphi_{xy}$	cross correlation of signals x and y.	[-]
$\phi$	factor in relation for bubble velocity (Werther (1977)).	[-]
$\phi_H$	ratio of film volume and dense phase volume.	[-]
$\phi_{mA}$	mass flow rate of A.	[kg/s]
$\phi_{mol,A}$	molar flow rate of A.	[mol/s]
$\psi$	shape factor for bubbles.	[-]
$\rho_p$	particle density.	[kg/m <sup>3</sup> ]
$\rho_f$	fluidum density.	[kg/m <sup>3</sup> ]

$\sigma$	dimensionless height (= $h/H$ ).	[-]
	deviation of log-normal distribution (in chapter 6 only)	[-]
$\sigma_a$	deviation of bubble rising time $t_a$ .	[ms]
$\Delta\sigma$	step size for dimensionless height.	[-]
$\tau$	time difference between two probe signals. (in Chapter 6 only).	[s]
	average residence time, based on total amount of gas in reactor.	[s]
$\tau_b$	average residence time, based on gas in bubble phase.	[s]
$\tau_d$	average residence time, based on gas in dense phase.	[s]
$\xi$	total gas fraction in reactor ( $= \delta + (1-\delta) \cdot \epsilon_d$ ).	[-]

### Matrices/Vectors (in Chapter 2)

<b>A</b>	matrix containing original parameters.
<b>c</b>	constant vector for homogeneous solution.
<b>D</b>	diagonal matrix containing the eigenvalues of <b>A</b> .
<b>E</b>	matrix obtained by evaluating the boundary conditions.
<b>F</b>	vector containing concentrations from time step $i-1$ .
$\tilde{F}$	"decoupled" <b>F</b> -vector ( $= Q^{-1} \cdot F$ ).
<b>g</b>	vector obtained evaluating the feed and boundary conditions.
<b>P</b>	matrix for particulate solution.
$\tilde{P}$	<b>P</b> -matrix with extracted $\Delta\theta$ -value.
<b>Q</b>	matrix containing the eigenvectors of <b>A</b> .
$\tilde{R}$	<b>F</b> -vector with extracted $\Delta\theta$ -values.
<b>X</b>	original vector containing bubble and dense phase concentrations.
<b>Y</b>	"decoupled" <b>X</b> -vector ( $= Q^{-1} \cdot X$ ).
$Y_h$	homogeneous part of solution differential equation.

## INTRODUCTION

A fluidized bed is formed by passing a fluid, usually a gas, upwards through a bed of particles, supported by a porous plate or a perforated distributor. When the gas velocity becomes high enough, the gravitational force acting on the particles is counterbalanced by the force exerted by the flowing gas and the particles start to "float". A fluidlike system is obtained. At a certain superficial gas velocity bubbles will form.

The earliest commercial use of the fluidization process started around the 1930's and was for the purpose of carrying out a chemical reaction. Since that time there have been many successful applications of fluid bed reactors. Although there has been extensive research in this area since the late 1950's, scale up and design are still difficult and tedious. Nevertheless, the process is still widely used, because of its advantages over other systems. Due to the vigorous particle motions the reactor can operate under virtual isothermal conditions. Process heat control is relatively simple, due to the high heat transfer from the bed to the walls of the vessel and/or heat exchange pipes. Furthermore solids handling is easy, because of the fluidlike behavior of the bed.

At the same time this vigorous motion of particles, caused by the rising bubbles, can be the source of problems. Entrainment of solids may lead to loss of expensive materials or product. Attrition, erosion and agglomeration may cause serious experimental problems. Bypassing of gas via bubbles will always reduce the conversion of a gas/solid catalyzed reaction. This effect will be counteracted by an effective mass transfer between the bubble and the dense phase.

The mass transfer from the bubble phase to the dense phase depends on many factors. A very important but still not sufficiently investigated parameter is the particle size of the powder. The main idea was the following: consider a reaction where it is best to have a relatively low conversion, because then a maximum yield of the wanted product is obtained. To produce a fair amount of the wanted product a large throughput has to be used. With fine powders an excessive large reactor diameter and/or many cyclones are necessary to prevent the blowing out of the particles. For a better process control and reasonable reactor dimensions it might be more favorable to use coarse particles in these situations. The question is whether the mass transfer from

the bubble phase to the dense phase is sufficiently large for the coarse particle systems. For this reason this thesis is concerned with the influence of the particle size on the mass transfer from the bubble phase to the dense phase and consequently derive rules to simplify scale up.

**1.1 Basic principles**

The fluidizing gas is fed into the reactor through a distributor on which the particles are lying. At low gas flow rates the systems behaves like a fixed bed and the bed pressure drop increases with increasing superficial gas velocity, according to the relation given by Ergun (1952). At the minimum fluidization velocity  $U_{mf}$  the particles start more or less to float and the bed pressure drop about equals the weight of the bed per unit area (fig. 1.1). For superficial gas velocities significantly larger than  $U_{mf}$  the pressure drop remains constant. The superficial velocity at which bubbles start to form is called the (minimum) bubbling velocity  $U_{mb}$ . Depending on the powder properties, expansion of the bed between  $U_{mf}$  and  $U_{mb}$  can set in. This is called homogeneous fluidization.

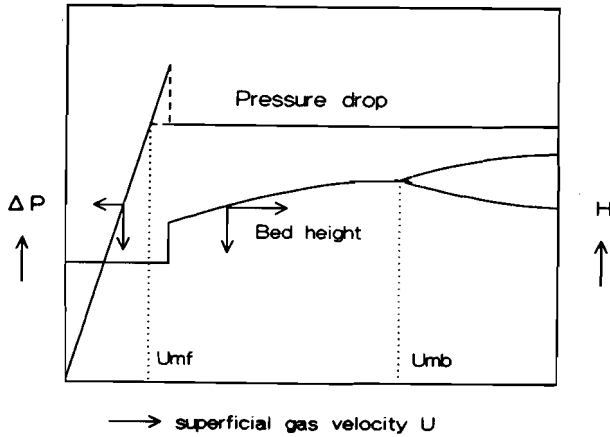


**Figure 1.1** *Bed pressure drop and bed height as a function of superficial gas velocity (schematical).*

The fluidization behavior of a powder depends upon its particle size  $d_p$ , particle density  $\rho_p$ , the fluidum density  $\rho_f$  and the fluid viscosity  $\mu$ . According to their behavior Geldart (1973) proposed the following classification for fluidization at ambient conditions (fig. 1.2):

- *C powders* cohesive; small particles ( $d_p < 30 \mu\text{m}$ ); difficult to fluidize. Channeling occurs readily.
- *A powders* aeratable; relatively small particles ( $30 < d_p < 150 \mu\text{m}$ ); easy to fluidize.  $U_{mf} < U_{mb}$ . Homogeneous expansion may occur.
- *B powders* bubbling from the onset of fluidization; larger particles.  $150 < d_p < \text{about } 500 - 600 \mu\text{m}$ . Easy to fluidize.  $U_{mf} = U_{mb}$ .
- *D powders* dense particles. Large particles.  $d_p > \text{about } 500 - 600 \mu\text{m}$ .  $U_{mf} = U_{mb}$ .

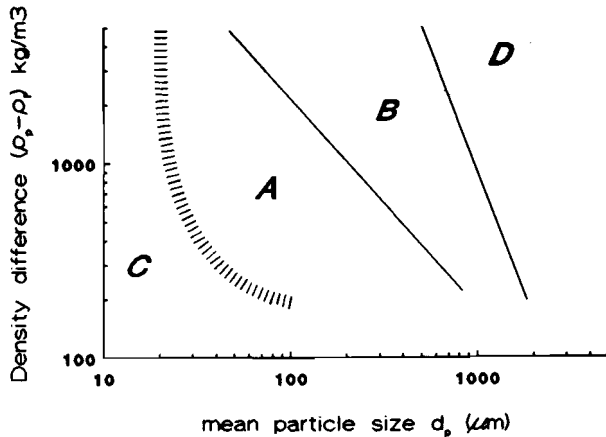


Figure 1.2 Powder classification according to Geldart (1973).

Several empirical relations can be found for calculating  $U_{mf}$ . A well known one is the relation given by Wen and Yu (1966):

$$U_{mf} = \mu \cdot ( [(33.7)^2 + 0.0408 \cdot Ar]^{1/2} - 33.7 ) / (d_p \cdot \rho_f) \quad (1.1)$$

$$\text{with } Ar = \frac{d_p^3 \cdot \rho_f \cdot (\rho_p - \rho_f) \cdot g}{\mu^2}$$

## 1.2 Hydrodynamics

If gas is fed at a sufficient rate into the bed bubbles will form. These bubbles are the essence of the typical behavior of a fluid bed and therefore they have been the subject of many studies. They maintain the particle movement, which gives the very good heat transfer properties. But they also contain most of the gas fed into the reactor, which gives a short circuiting of the gas.

A single bubble rises similar to a bubble in a liquid: the bubble velocity is proportional to  $d_b^{1/2}$  ( $d_b$  = bubble diameter). Bubbles rise faster in a swarm of bubbles, which was expressed by a relation proposed by Davidson and Harrison (1963):

$$u_{b,\infty} = 0.711 \cdot \sqrt{g \cdot d_b} \quad (1.2a)$$

$$\text{and } u_b = u_{b,\infty} + (U - U_{mf}) \quad (1.2b)$$

Here  $u_{b,\infty}$  is the bubble rise velocity of a single bubble,  $u_b$  the bubble rise velocity in a swarm of bubbles and  $U$  is the superficial gas velocity. Werther (1978) developed another relation in which the bubble velocity was also assumed to be dependent of bed diameter. This is an effect that is probably due to an overall particle circulation. This relation will be discussed in chapters 6 and 7.

Relations for bubble diameters are very often given with constraints. Experiments are always performed under unique circumstances: given bed diameter, distributor type, reactor dimensions, bed height, gas velocities, etc. A problem in obtaining data on hydrodynamics, conversion and heat



transfer, is the more or less stochastic nature of a fluid bed. Most relations concerning fluidized beds are considered to be deterministic. Some stochastic descriptions have been tried based on population balances and Monte Carlo simulations (Argyriou et al. (1971), Shah et al (1977a, 1977b.) and Sweet et al. (1987)) They appear to be promising but rather complex and still use deterministic equations. Due to this stochastic behavior there seems to be a great variance in the data. For this reason there are numerous relations known for  $d_b$ . A listing of several relations can be found in a paper of Darton et al. (1977) and several textbooks, e.g. Darton et al. (1977), Werther (1976), Rowe (1976), Mori and Wen (1975) and Kato and Wen (1969).

As bubbles rise in the bed, they grow larger due to three main effects:

- 1) *Expansion* due to decrease of hydrostatic pressure.
- 2) *Extraction* of gas from the dense phase.
- 3) *Coalescence* of bubbles.

Darton et al. (1977) developed a theory based on the coalescence principle. Their model led to the following equation:

$$d_b = 0.54 \cdot (U - U_{mf})^{2/5} \cdot (h + 4 \cdot \sqrt{A_0})^{4/5} \cdot g^{-1/5} \quad (1.3)$$

with  $A_0$  being the total free surface of the distributor and  $h$  the height in the bed. The constant 0.54 was determined by analyzing many literature data.

Another important feature of the bubbles is the formation of clouds around the bubble boundary, under certain conditions. Davidson and Harrison (1963) predicted the occurrence of these clouds, based on calculations of gas and particle streamlines. Experimental evidence had already been found by Rowe (1962) with tracer experiments. For fine powders the bubbles rise faster through the dense phase than the interstitial dense phase gas (so called "fast" bubbles). Gas escaping from the top of the bubble is transported via the cloud to the bottom where it re-enters the bubble. This way gas can get even "trapped" inside the bubble. The size of the cloud depends upon the  $u_b/u_d$ -ratio as given in equation 1.4. (Davidson and Harrison, 1963) (fig. 1.3).

$$\frac{R_c}{R_b} = \left[ \frac{u_b + 2 \cdot u_d}{u_b - u_d} \right]^{1/3} \quad (1.4)$$

where  $R_c$  and  $R_b$  are the cloud and bubble radius respectively and  $u_d$  is the interstitial gas velocity through the dense phase.

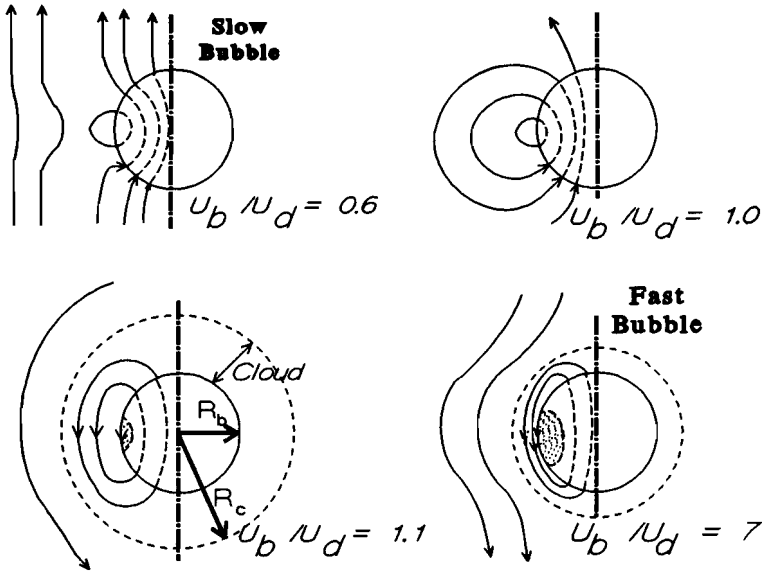


**Figure 1.3** Gas streamlines and cloud sizes as a function of  $u_b/u_d$ . From Kunii and Levenspiel (1969).

Figure 1.3 shows that "slow" bubbles have no cloud at all. "Slow" means here slow compared to the dense phase gas velocity: for coarse particles  $U_{mf}$  (and therefore  $u_d$ ) can become very large and the dense phase gas flows through the bubbles in the same axial direction as the bubbles move. Although the bubbles

formed in the coarse powders are called "slow", they can rise faster than bubbles formed in the fine particle powders, depending on the excess gas velocity  $(U - U_{mf})$  used.

Toomey and Johnstone (1952) postulated the two phase theory which states that all excess gas, above minimum fluidization, rises in the form of bubbles. Other workers, however, have found some indications that more gas can flow through the dense phase than given by the two phase theory (e.g. Clift and Grace (1985)). We define an extra through flow factor  $\varphi$ , by which the volumetric gas flow through the dense phase  $Q_d$  is given by:

$$Q_d = \varphi \cdot U_{mf} \cdot A = u_d \cdot (1-\delta) \cdot \varepsilon_d \cdot A \quad (1.5a)$$

and the volumetric flow through the bubble phase  $Q_b$  by:

$$Q_b = (U - \varphi \cdot U_{mf}) \cdot A = u_b \cdot \delta \cdot A \quad (1.5b)$$

Here  $u_d$  is the interstitial gas velocity through the dense phase,  $\delta$  is the bubble hold up,  $\varepsilon_d$  is the dense phase porosity and  $A$  is the cross sectional area of the bed.

Instead of using this factor  $\varphi$  a modified two phase (n-type) theory is also used in the literature (Clift and Grace, 1985):

$$Q_b/A = U - U_{mf} \cdot (1 + n \cdot \delta) \quad (1.6)$$

The parameter  $n$  was found to vary much for different systems. For simplicity we chose to use the factor  $\varphi$ . If necessary  $n$  can be calculated from equations (1.5b) and (1.6).

Collapse experiments can be used to determine bubble hold up and dense phase porosity (Rietema (1967)). In these experiments the gas supply is suddenly shut off. When the bubbles have left the bed, the fluid bed surface will sink with a velocity equal to the superficial dense phase gas velocity (fig. 1.4).

Bubble hold up and dense phase porosity can be determined with the following equations:

$$\delta = \frac{H_b - H_d}{H_b} \quad \text{and} \quad \epsilon_d = \frac{H_d - H_o}{H_d} \quad (1.7)$$

This method is of course only applicable with powders that have a homogeneous expansion.

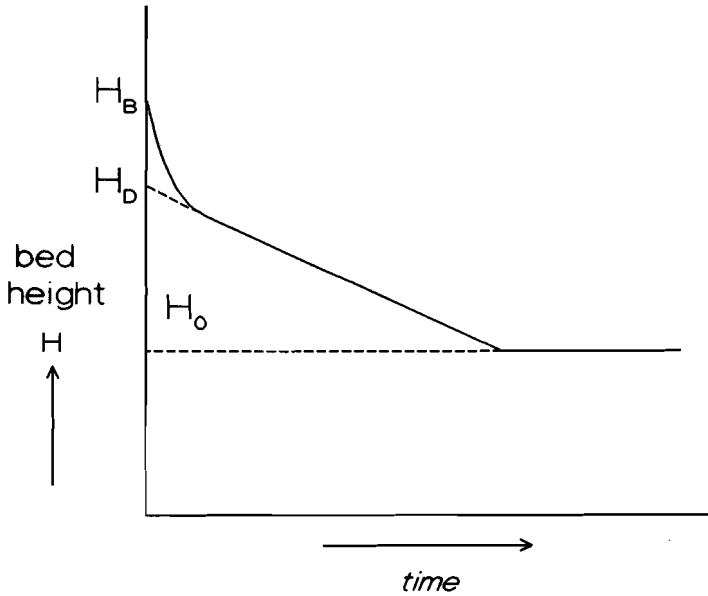


**Figure 1.4** *Bed height as a function of time in a collapse experiment.*

### 1.3 Mass transfer

At commonly used gas flow rates, most gas fed into a fluid bed reactor is transported upwards in the form of bubbles. The reactive component has to be transferred to the dense phase. To describe this mass transfer mechanism several models have been proposed. Reviews of these models can be found in several text books (for instance Yates, 1983).

Basically the mass transfer mechanism can be described with a convection term and a diffusion term (fig. 1.5). The convection term consists of the circulation of gas inside the bubble and cloud and of the direct through flow through the bubble. The molecular diffusion from the bubble phase to the dense phase also influences the mass transfer process.

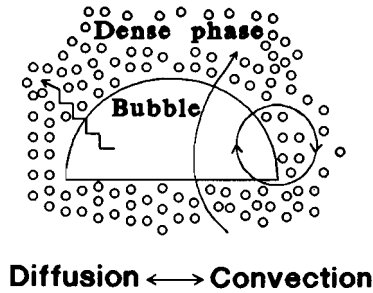


**Figure 1.5** *Schematic presentation of mass transfer from bubble phase to dense phase.*

Kunii and Levenspiel (1968) developed a theory with all these terms and taking transfer from bubble to cloud and from cloud to dense phase. Two partial transfer coefficients and one overall transfer coefficient were defined. Sit and Grace (1978, 1981), used a more simple description. They defined one mass transfer coefficient  $k_g$  with a convection and a diffusion term.

$$k_g = \frac{U_{mf}}{3} + \left[ \frac{4 \cdot D_g \cdot \epsilon_{mf} \cdot u_b}{\pi \cdot d_b} \right]^{1/2} \quad D_g = \text{gas diffusion coefficient.} \quad (1.8a)$$

The diffusion term is obtained from the Higbie penetration model and is defined in analogy with the Kunii and Levenspiel model (1969). In this model the contact time for the two phases is essential. A package of the dense phase gas can interchange during that contact time. In most situations  $u_b \gg u_d$  and therefore the contact time will be roughly proportional to  $d_b/u_b$ . Kunii and Levenspiel (1968) and Sit and Grace (1978) used this definition. For large particles the assumption that  $u_b \gg u_d$ , does not have to be correct. Therefore the velocity *difference* has to be used and we define a contact time proportional to  $d_b/(u_b - u_d)$ . This leads to:

$$k_g = \frac{U_{mf}}{3} + \left[ \frac{4 \cdot D_g \cdot \epsilon_{mf} \cdot (u_b - u_d)}{\pi \cdot d_b} \right]^{1/2} \quad (1.8b)$$

Some well known examples of other models for  $k_g$  are those of Davidson and Harrison (1963), Kunii and Levenspiel (1968) and Chiba and Kobayashi (1970).

A distinction may be made on the basis of the complexity of mass transfer models, as discussed by van Swaaij (1985). The Level I models regard a fluid bed as a black box. When applying such a black box Level I model, information, obtained from small beds, can only be extrapolated to large beds if sufficient data are available. Usually this means a long way in scale up. The Level II models (computation of  $k_g$ ) use the effective average bubble size as a fitting parameter (e.g. Kunii and Levenspiel (1990)). With Level III models bubble growth is taken into consideration. Especially these last type of models appear to be promising for scale up, but they all are based on data obtained from A or fine B type powders.

If the physical behavior is known a priori for all scales, scale up becomes much more easier, because the Level III models can then be used. However, there are still risks involved in scale-up. We chose to start with a Level I model for our data analysis and to use Level III models for the modeling of a fluid bed aimed at scale-up.

#### 1.4 Model description

Several models have been proposed for describing gas fluidized beds. The Van Deemter model (1961) and Bubble Dispersion Model (BDM) (see e.g. Dry and Judd (1985)) are simple physical descriptions of a gas fluidized bed with just a few (unknown) fitting parameters. Experiments could be explained well with these models (see e.g. Van Swaaij and Zuiderweg (1972), Werther (1978), Bauer (1980), Dry and Judd (1985) and Van Lare et al. (1990)). They are mostly used for describing the behavior of A or B type powders, according to the Geldart classification (Geldart, 1973).

In the present investigation first a similar model will be used. The bubble and the dense phase are described as plug flow zones with axial dispersion and mass transfer between both phases is allowed for (fig. 1.6).

The superficial velocity is  $U$  and the gas flows through the dense phase with a volumetric flow rate of  $\varphi U_{mf} A$ . The factor  $\varphi$  accounts for the fact that more gas can flow through the dense phase than corresponds with the two phase theory of Toomey and Johnstone (1952) (where  $\varphi = 1$ ). For A-type powders several values of  $\varphi$  are reported (Grace and Clift, 1974). However, these deviations are not very important for A type powders, because of the large  $U/(\varphi U_{mf})$ -values commonly used.

A volumetric mass transfer coefficient  $K_e$  (that is equal to  $k_g \cdot a$ ) and Eddy dispersion coefficients for the bubble phase ( $E_b$ ) and for the dense phase ( $E_d$ ) are defined. The bubble holdup  $\delta$ , the dense phase porosity  $\epsilon_d$  and the parameters  $\varphi$ ,  $K_e$ ,  $E_b$  and  $E_d$  are taken to be independent of the height  $h$ , implying that height averaged values are used. By definition reaction can only take place in the dense phase, because there are no (catalyst-)particles in the bubble phase. A reaction rate constant  $k_m$  is defined, based on catalyst mass and a first order reaction is assumed.

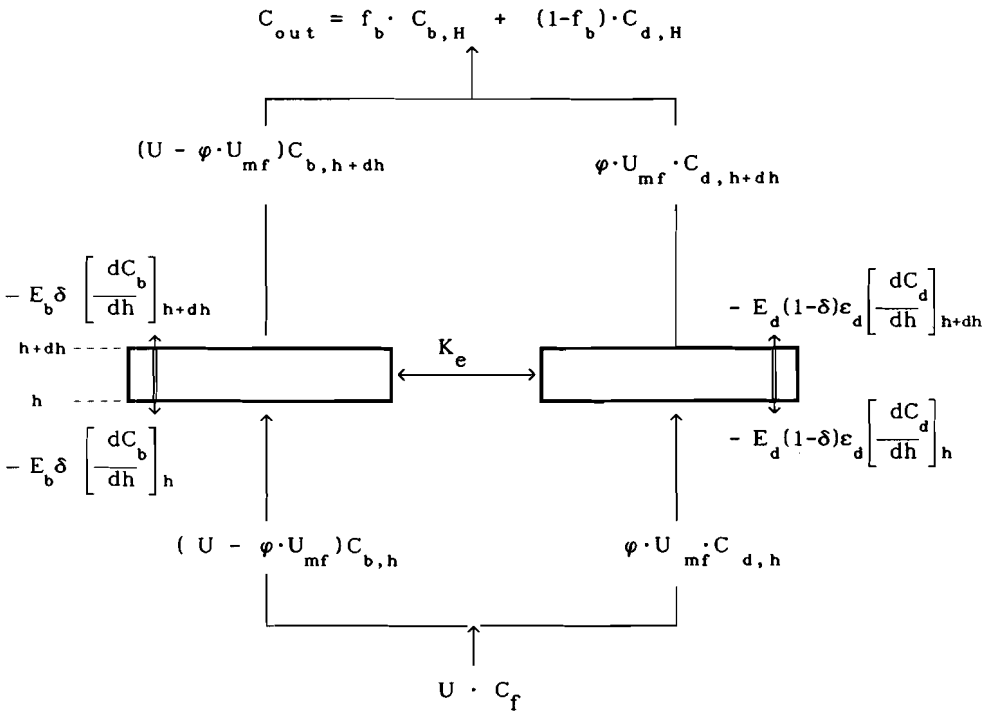


Figure 1.6 Schematic presentation of the two phase model: bubble phase and dense phase in plug flow with axial dispersion.

Taking a mass balance over a slice dh for a non-steady state leads to:

$$\delta \cdot \frac{\partial C_b}{\partial t} = -(U - \varphi U_{mf}) \cdot \frac{\partial C_b}{\partial h} - K_e \cdot (C_b - C_d) + E_b \cdot \delta \cdot \frac{\partial^2 C}{\partial h^2} \quad (1.9a)$$

$$(1-\delta) \cdot \varepsilon_d \cdot \frac{\partial C_d}{\partial t} = -\varphi U_{mf} \cdot \frac{\partial C_d}{\partial h} - K_e \cdot (C_d - C_b) + E_d \cdot (1-\delta) \cdot \varepsilon_d \cdot \frac{\partial^2 C_d}{\partial h^2} - k_m \cdot (1-\delta) \cdot (1-\varepsilon_d) \cdot \rho_p \cdot C_d \quad (1.9b)$$

These equations can be used to evaluate experiments with chemically reacting systems and residence time distribution measurements and the following boundary conditions hold:

For  $t \leq 0$  there is no (tracer)gas in the reactor:

$$C_b(0, h) = 0 \quad (1.10a)$$

$$C_d(0, h) = 0 \quad (1.10b)$$

Gas is fed at the distributor ( $h = 0$ ) and there is axial mixing in the column:

$$C_b(t, 0) = C_f(t) + \frac{1}{f_b \cdot Pe_b} \cdot \frac{\partial C_b}{\partial h} \Bigg|_{h=0} \quad (t > 0) \quad (1.10c)$$

$$C_d(t, 0) = C_f(t) + \frac{1}{(1-f_b) \cdot Pe_d} \cdot \frac{\partial C_d}{\partial h} \Bigg|_{h=0} \quad (t > 0) \quad (1.10d)$$

$$\text{with } f_b = (U - \varphi U_{mf})/U = \text{fraction of gas in the bubble phase} \quad (1.10e)$$

No concentration gradients are assumed at the fluid bed surface:



$$\left. \frac{\partial C_b}{\partial h} \right]_{h=H} = 0 \quad (1.10e)$$

$$\left. \frac{\partial C_d}{\partial h} \right]_{h=H} = 0 \quad (1.10f)$$

We define an average residence time  $\tau$  based on the total gas volume in the fluid bed and on the total gas throughflow in the reactor and not only on the fraction of gas passing through the bubble phase. For A/B type powders the difference is very small. However for D type powders, it is essential to take the fraction of gas in the dense phase into account. Furthermore we define an average residence time for the gas in the bubble phase ( $\tau_b$ ) and for the gas in the dense phase ( $\tau_d$ ):

$$\tau_b = \frac{H}{u_b} = \frac{H \cdot \delta}{U - \varphi U_{mf}} \quad (1.11a)$$

$$\tau_d = \frac{H}{u_d} = \frac{H \cdot (1-\delta) \cdot \varepsilon_d}{\varphi U_{mf}} \quad (1.11b)$$

$$\tau = f_b \cdot \tau_b + (1-f_b) \cdot \tau_d = \frac{H \cdot \xi}{U}, \quad \text{with } \xi = \delta + (1-\delta) \cdot \varepsilon_d \quad (1.11c)$$

Making equations (1.9) and (1.10) dimensionless leads to:

$$\frac{\partial C_b}{\partial \vartheta} + \beta \cdot \frac{\partial C_b}{\partial \sigma} + N_k \cdot \frac{\xi}{\delta} \cdot (C_b - C_d) - \frac{1}{Pe_b} \cdot \frac{\xi}{\delta} \cdot \frac{\partial^2 C_b}{\partial \sigma^2} = 0 \quad (1.12)$$

$$\frac{\partial C_d}{\partial \vartheta} + \gamma \cdot \frac{\partial C_d}{\partial \sigma} + \frac{N_k \cdot \xi}{(1-\delta) \cdot \varepsilon_d} \cdot (C_d - C_b) - \dots \dots \dots$$

$$\dots \dots \dots - \frac{1}{Pe_d} \cdot \frac{\xi}{(1-\delta) \cdot \varepsilon_d} \cdot \frac{\partial^2 C_d}{\partial \sigma^2} + N_r \cdot \frac{\xi}{(1-\delta) \cdot \varepsilon_d} \cdot C_d = 0 \quad (1.13)$$

With boundary conditions:

$$C_b(0, \sigma) = 0 \quad (1.14)$$

$$C_d(0, \sigma) = 0 \quad (1.15)$$

$$C_b(\vartheta, 0) = C_f(\vartheta) + \left. \frac{1}{f_b \cdot Pe_b} \cdot \frac{\partial C_b}{\partial \sigma} \right]_{\sigma=0} \quad (\vartheta > 0) \quad (1.16)$$

$$C_d(\vartheta, 0) = C_f(\vartheta) + \left. \frac{1}{(1-f_b) \cdot Pe_d} \cdot \frac{\partial C_d}{\partial \sigma} \right]_{\sigma=0} \quad (\vartheta > 0) \quad (1.17)$$

$$\left. \frac{\partial C_b}{\partial \sigma} \right]_{\sigma=1} = 0 \quad (1.18)$$

$$\left. \frac{\partial C_d}{\partial \sigma} \right]_{\sigma=1} = 0 \quad (1.19)$$

The dimensionless variables and coefficients are defined as follows:

$$\beta = f_b \cdot \xi / \delta$$

$$\vartheta = \frac{t}{\tau}$$

$$\sigma = \frac{h}{H}$$

$$\gamma = \frac{(1-f_b) \cdot \xi}{(1-\delta) \cdot \varepsilon_d}$$

$$N_k = \frac{K_e \cdot H}{U}$$

$$N_r = \frac{k_m \cdot (1-\delta) \cdot (1-\varepsilon_d) \cdot \rho_p \cdot H}{U}$$

$$Pe_b = \frac{H \cdot U}{\delta \cdot E_b}$$

$$Pe_d = \frac{H \cdot U}{E_d \cdot (1-\delta) \cdot \varepsilon_d}$$

(1.20)

If we assume that the bubble-phase is in ideal plug flow ( $E_b = 0$ ), we get the van Deemter model (1961). If we neglect the dense phase flow we get the well known simplifications:

$$f_b = 1 \quad \text{and} \quad \xi = \delta, \quad \text{so} \quad \beta = 1 \quad \text{and} \quad \gamma = 0 \quad (1.21)$$

In the steady state ( $\partial C / \partial \vartheta = 0$ ), this leads to the modified Van Deemter model (Van Swaaij and Zuiderweg, 1972).

### 1.5 Mass transfer as a function of particle size

The height of a mass transfer unit  $H_k$  gives qualitative and quantitative information about the mass transfer and is defined as follows:

$$H_k = \frac{H}{N_k} = \frac{U}{K_e} = \frac{U}{k_g \cdot a} \quad (1.22)$$

in which  $a$  is the specific (volumetric) bubble surface area, obtained from:

$$a = \frac{6 \cdot \delta}{d_b} \quad (1.23)$$

The bubble holdup  $\delta$  was estimated from:

$$\delta = \frac{U - U_{mf}}{u_b} \quad (\Leftrightarrow \varphi = 1) \quad (1.24)$$

The average bubble diameter was estimated from the integrated relation given by Darton et al. (1977) (equation 1.3):

$$\bar{d}_b = \frac{0.19}{H} \cdot (U - U_{mf})^{2/5} \left[ (H + 4\sqrt{A_0})^{9/5} - (4\sqrt{A_0})^{9/5} \right] \quad (1.25)$$

The average bubble velocity has been calculated with equations 1.2a and 1.2b and the minimum fluidization velocity with the equation given by Wen and Yu (1966) (eq. 1.1). In order to estimate a relation between  $H_k$  and  $d_p$ , the two phase theory of Toomey and Johnstone (1952) ( $\phi = 1$ ) was used. Calculations were performed with  $H = 1.0$  m,  $\epsilon_d = 0.4$ ,  $A_0 = 0$  (since for porous plates  $A_0$  is very small) and  $U/U_{mf} = 2$ . A constant  $U/U_{mf}$  value was used, because this determines the fraction of gas that enters the reactor in the bubble phase. Substitution of equations 1.8a, 1.23, 1.24 and 1.25 in equation 1.22 gave results as shown in fig. 1.7.

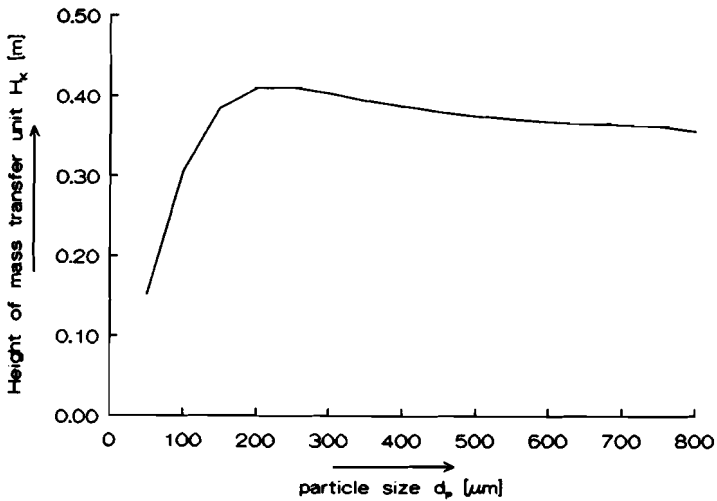


**Figure 1.7** Predicted value of  $H_k$  versus  $d_p$ , with  $H = 1$  m,  $\epsilon_d = 0.4$  and  $U/U_{mf} = 2$ . See text.

Figure 1.7 shows that  $H_k$  is expected to increase with increasing  $d_p$  for A and small B powders and decrease gradually for large B and D powders. It has

to be emphasized that the relation given by Sit and Grace (1978, 1981) is still no more than a theory, with only qualitative and no quantitative experimental confirmation. Furthermore the assumption that  $\varphi = 1$  is doubtful. Therefore fig. 1.7 only shows an expected trend that has to be verified experimentally. For a single bubble bed, where one bubble is injected into a fluidized bed held at incipient fluidization, this trend was also found by Borodulya et al. (1981). However, hydrodynamics and therefore mass transfer are quite different in a freely bubbling bed.

## 1.6 Scope of this thesis

In this thesis experimental and theoretical work on the mass transfer from the bubble phase to the dense phase in a freely bubbling bed will be discussed. Two experimental methods will be described. First of all a chemical reacting system (CRS), for which the ozone decomposition was chosen as a model reaction. Secondly residence time distribution measurements (RTD) were performed. For solving the equations describing the non steady state a new numerical method was used.

The height of a mass transfer unit  $H_k$  can be determined as a function of  $d_p$  and  $U$ , but these parameters cannot be varied completely independently of each other, because larger particles require a larger flow rate. Furthermore a lot of other parameters such as maximum bubble diameter,  $U_{mf}$ , bubbling point and hydrodynamic behavior are also dependent on these and other variables. Therefore a parameter has to be found that is descriptive for all fluid bed systems with equal particle properties. This parameter can then also be used as a tool in scale up.

In chapter 2 the numerical method for solving the basic model equations (steady state and non steady state) will be presented. Chapter 3 describes the investigation concerning the model reaction. In chapter 4 results from chapter 3 will be used, together with many literature data, to obtain a parameter that is descriptive for all fluid bed systems. In chapter 5 results are presented of the RTD measurements. In chapter 6 the hydrodynamic measurements will be discussed. The final conclusions and some model computations will be presented in chapter 7.

## CHAPTER 2

### NUMERICAL SOLUTION OF DIFFERENTIAL EQUATIONS, DERIVED FROM A TWO PHASE MODEL

---

#### 2.1 Introduction

Residence Time Distribution measurement (RTD) is a strong and (experimentally) relatively simple method in determining physical parameters, such as mass transfer or mixing coefficients. Therefore the RTD curve has to be measured experimentally and fitted numerically. In principle this method can also be applied to Chemically Reacting Systems (CRS). In both cases the system under consideration must be described mathematically. It is not unlikely one obtains a system of equations that is not solvable analytically and sometimes even not numerically.

The numerical methods, that are most frequently used for non steady state problems, are the Crank-Nicholson-technique (for instance Eigenberger and Butt, 1976) and orthogonal collocation (Villadsen and Stewart, 1967). Both methods can lead to erroneous answers and/or excessive calculation-time for stiff problems (Hlavacek and Van Rompay, 1981).

Van Loon (1987) obtained good results for steady state stiff boundary value problems, using the decoupling method. It was tried whether this approach could be employed for non steady state equations. It then could be used for a sensitivity analysis.

A numerical method will be described for solving a set of (stiff) parabolic differential equations, describing the non steady state behavior of gas fluidized beds. This method decouples the equations into a "decoupled space". There the solution is calculated and by back transformation the final solution is obtained (analogous to Laplace-transformation). The model description has been given in chapter 1.4.

**2.2 The decoupling method**

The Crank Nicholson technique uses a finite difference in the space variable  $\sigma$ . We, however, use an Euler approximation for the time variable  $\vartheta$ :

$$\frac{\partial C_x}{\partial \vartheta} \approx \frac{C_{x,i} - C_{x,i-1}}{\vartheta_i - \vartheta_{i-1}} = \frac{C_{x,i} - C_{x,i-1}}{\Delta\vartheta}, \text{ with } x = b,d. \tag{2.1}$$

Substitution in equations 1.12 and 1.13 leads to:

$$\frac{\partial^2 C_{b,1}}{\partial \sigma^2} = f_b \cdot Pe_b \cdot \frac{\partial C_{b,1}}{\partial \sigma} + N_k \cdot Pe_b \cdot (C_{b,1} - C_{d,1}) + \frac{C_{b,1} - C_{b,1-1}}{\Delta\vartheta} \cdot \frac{Pe_b \cdot \delta}{\xi} \tag{2.2}$$

$$\begin{aligned} \frac{\partial^2 C_{d,1}}{\partial \sigma^2} &= (1-f_b) \cdot Pe_d \cdot \frac{\partial C_{d,1}}{\partial \sigma} + N_k \cdot Pe_d \cdot (C_{d,1} - C_{b,1}) + N_r \cdot Pe_d \cdot C_{d,1} + \dots \\ &\dots + \frac{C_{d,1} - C_{d,1-1}}{\Delta\vartheta} \cdot \frac{Pe_d \cdot (1-\delta) \cdot \epsilon_d}{\xi} \end{aligned} \tag{2.3}$$

Writing equations 2.2 and 2.3 in matrix-form gives:

$$\begin{aligned}
\frac{d}{d\sigma} \begin{bmatrix} C_{b,1} \\ C_{d,1} \\ \partial C_{b,1} / \partial \sigma \\ \partial C_{d,1} / \partial \sigma \end{bmatrix} &= \begin{bmatrix} 0 & 0 & 1 & 0 \\ 0 & 0 & 0 & 1 \\ Pe_b (N_k + \delta / (\xi \cdot \Delta \theta)) & -N_k \cdot Pe_b & f_b \cdot Pe_b & 0 \\ -N_k \cdot Pe_d & Pe_d (N_k + N_r + (1-\delta) \varepsilon_d / (\xi \cdot \Delta \theta)) & 0 & (1-f_b) Pe_d \end{bmatrix} \begin{bmatrix} C_{b,1} \\ C_{d,1} \\ \partial C_{b,1} / \partial \sigma \\ \partial C_{d,1} / \partial \sigma \end{bmatrix} \\
&\dots + \begin{bmatrix} 0 \\ 0 \\ -(Pe_b \cdot \delta / (\xi \cdot \Delta \theta)) \cdot C_{b,1-1} \\ - \frac{Pe_d \cdot (1-\delta) \varepsilon_d}{\xi \cdot \Delta \theta} \cdot C_{d,1-1} \end{bmatrix} \quad (2.4)
\end{aligned}$$

In short:

$$\frac{d}{d\sigma} X^i(\sigma) = A \cdot X^i(\sigma) + F^{i-1}(\sigma) \quad (2.5)$$

This equation is similar to equations describing dynamic systems (Palm, 1983).

Due to the  $A$  matrix the  $x_j^i$ -terms are coupled. A small computational error will accumulate and be amplified, because of the iteration process, that is necessary for calculating the solution at every time step. This is the well known problem of stiffness. If a diagonal matrix  $D$  can be found instead of the matrix  $A$ , a set of ordinary differential equations will be obtained. Therefore the matrix  $Q$  and the vector  $Y$  are defined such that the following holds:

$$A \cdot Q = Q \cdot D \text{ and } X = Q \cdot Y \Leftrightarrow Y = Q^{-1} \cdot X \quad (2.6)$$

The matrix  $D$  contains the eigenvalues of the matrix  $A$ . The matrix  $Q$  contains the eigenvectors of  $A$ .



$$\mathbf{D} = \begin{bmatrix} d_1 & 0 & 0 & 0 \\ 0 & d_2 & 0 & 0 \\ 0 & 0 & d_3 & 0 \\ 0 & 0 & 0 & d_4 \end{bmatrix} \quad \text{and} \quad \mathbf{Q} = \begin{bmatrix} q_{11} & q_{12} & q_{13} & q_{14} \\ q_{21} & q_{22} & q_{23} & q_{24} \\ q_{31} & q_{32} & q_{33} & q_{34} \\ q_{41} & q_{42} & q_{43} & q_{44} \end{bmatrix} \quad (2.7)$$

Two negative and two positive eigenvalues were always found, due to the definition of the  $\mathbf{A}$  matrix. We chose to take  $d_1, d_2 < 0$  and  $d_3, d_4 > 0$ . This is however not important, as long as the boundary conditions are correctly evaluated. The eigenvector  $\mathbf{q}(i,j)$  belongs to the eigenvalue  $d_j$  ( $i,j = 1,2,3,4$ ).

Substitution of equation 2.6 in equation 2.5 yields:

$$\mathbf{Q} \cdot \frac{d}{d\sigma} \mathbf{Y}^i(\sigma) = \mathbf{A} \cdot \mathbf{Q} \cdot \mathbf{Y}^i(\sigma) + \mathbf{F}^{i-1} \quad (2.8)$$

$$\Rightarrow \mathbf{Q} \cdot \frac{d}{d\sigma} \mathbf{Y}^i(\sigma) = \mathbf{Q} \cdot \mathbf{D} \cdot \mathbf{Y}^i(\sigma) + \mathbf{F}^{i-1}(\sigma) \quad (2.9)$$

$$\Rightarrow \frac{d}{d\sigma} \mathbf{Y}^i(\sigma) = \mathbf{D} \cdot \mathbf{Y}^i(\sigma) + \tilde{\mathbf{F}}^{i-1}(\sigma), \quad (2.10)$$

$$\text{with } \tilde{\mathbf{F}}^{i-1}(\sigma) = \mathbf{Q}^{-1} \cdot \mathbf{F}^{i-1}(\sigma)$$

Due to the  $\mathbf{D}$ -matrix the  $y_j^i$ -terms are now decoupled. Equation 2.10 can be solved by standard procedures for the solution of inhomogeneous differential equations. First a homogeneous solution  $\mathbf{Y}_h^i(\sigma)$  is defined:

$$\mathbf{Y}_h^i(\sigma) = \begin{bmatrix} e^{d_1 \sigma} & 0 & 0 & 0 \\ 0 & e^{d_2 \sigma} & 0 & 0 \\ 0 & 0 & e^{d_3 (\sigma-1)} & 0 \\ 0 & 0 & 0 & e^{d_4 (\sigma-1)} \end{bmatrix} \quad (2.11)$$

The  $(\sigma-1)$ -term has been chosen to make sure that the solution can easily be calculated at  $\sigma = 1$ , as will be shown later.

The particular solution can be determined using the following equations:

$$\frac{d}{d\sigma} p_j(\sigma) = d_j \cdot p_j(\sigma) + \tilde{f}_j^{i-1}(\sigma) \quad (j = 1,2,3,4)$$

$$\text{with } p_1(0) = 0, p_2(0) = 0, p_3(1) = 0, p_4(1) = 0. \quad (2.12)$$

This gives for the complete solution:

$$Y^i(\sigma) = c^i \cdot Y_h^i(\sigma) + P^i(\sigma) \quad (2.13)$$

Here the  $P^i(\sigma)$ -vector contains the  $p_j^i(\sigma)$ -terms, obtained from equation 2.12. The constant-vector  $c^i$  can be found by evaluating the boundary conditions. Writing equations (1.16) to (1.17) in  $x_j^i$ -terms yields:

$$x_1^i(0) = c_f + \zeta_1 \cdot x_3^i(0) \quad \text{with } \zeta_1 = 1/(f_b \cdot Pe_b) \quad (2.14)$$

$$x_2^i(0) = c_f + \zeta_2 \cdot x_4^i(0) \quad \text{with } \zeta_2 = 1/((1-f_b) \cdot Pe_d) \quad (2.15)$$

$$x_3^i(1) = 0 \quad (2.16)$$

$$x_4^i(1) = 0 \quad (2.17)$$

This leads to:

$$[1 \ 0 \ -\zeta_1 \ 0] \cdot X^1(0) = c_f \quad (2.18)$$

$$[0 \ 1 \ 0 \ -\zeta_2] \cdot X^1(0) = c_f \quad (2.19)$$

$$[0 \ 0 \ 1 \ 0 \ 1] \cdot X^1(1) = 0 \quad (2.20)$$

$$[0 \ 0 \ 0 \ 1 \ 1] \cdot X^1(1) = 0 \quad (2.21)$$

Substitution of  $X = Q \cdot Y$  gives:

$[1 \ 0 \ -\zeta_1 \ 0] \cdot Q \cdot Y^1(0) = c_f$ , etc. Evaluating these equations with equation 2.13 leads to:

$$E \cdot c^i = g^i \quad (2.22)$$

with:

$$E = \begin{bmatrix} q_{11} - \zeta_1 \cdot q_{31} & q_{12} - \zeta_1 \cdot q_{32} & (q_{13} - \zeta_1 \cdot q_{33})e^{-d_3} & (q_{14} - \zeta_1 \cdot q_{34})e^{-d_4} \\ q_{21} - \zeta_2 \cdot q_{41} & q_{22} - \zeta_2 \cdot q_{42} & (q_{23} - \zeta_2 \cdot q_{43})e^{-d_3} & (q_{24} - \zeta_2 \cdot q_{44})e^{-d_4} \\ q_{31}e^{d_1} & q_{32}e^{d_2} & q_{33} & q_{34} \\ q_{41}e^{d_1} & q_{42}e^{d_2} & q_{43} & q_{44} \end{bmatrix}$$

$$\text{and } \mathbf{g}^i = \begin{bmatrix} c_f - p_3^1(0) \cdot (q_{13} - \zeta_1 \cdot q_{33}) - p_4^1(0) \cdot (q_{14} - \zeta_1 \cdot q_{34}) \\ c_f - p_3^1(0) \cdot (q_{23} - \zeta_2 \cdot q_{43}) - p_4^1(0) \cdot (q_{24} - \zeta_2 \cdot q_{44}) \\ - p_1^1(1) \cdot q_{31} - p_2^1(1) \cdot q_{32} \\ - p_1^1(1) \cdot q_{41} - p_2^1(1) \cdot q_{42} \end{bmatrix} \quad (2.23)$$

$$\text{The following holds :} \quad \mathbf{c}^i = \mathbf{E}^{-1} \cdot \mathbf{g}^i \quad (2.24)$$

Because the inverse matrix  $\mathbf{E}^{-1}$  can introduce some computational inaccuracies (NAG, 1980), it was always checked whether the constant vector  $\mathbf{c}^i$  calculated by equation 2.24 fulfilled equation 2.22. This was always the case.

For  $p_j^1(\sigma)$  equation 2.12 holds. In finding  $p_3^1(\sigma)$  and  $p_4^1(\sigma)$  the end conditions for these variables have to be transformed into initial conditions. We have:

$$dp_j^1(\sigma)/d\sigma = d_j^1 \cdot p_j^1(\sigma) + \tilde{f}_j^{1-1}(\sigma) \quad \text{with} \quad p_j^1(1) = 0 \quad (j = 3, 4) \quad (2.25)$$

We now define

$$t_j^1(\sigma) = p_j^1(1-\sigma). \quad (j = 3, 4) \quad (2.26)$$

This leads to:

$$dt_j^1(\sigma)/d\sigma = - dp_j^1(1-\sigma)/d\sigma = - d_j \cdot p_j^1(1-\sigma) - \tilde{f}_j^{1-1}(1-\sigma). \quad (j = 3, 4) \quad (2.27)$$

Therefore

$$dt_j^1(\sigma)/d\sigma = - d_j \cdot t_j^1(\sigma) - \tilde{f}_j^{1-1}(1-\sigma) \quad \text{with} \quad t_j^1(0) = 0 \quad (j = 3, 4) \quad (2.28)$$

The end condition is now transformed into an initial condition and computation is possible. When  $t_j^1(\sigma)$  has been calculated,  $p_j^1(\sigma)$  can be found by interchanging the values according to equation 2.26.

In calculating  $p_j^1(\sigma)$ ,  $\tilde{f}_j^{i-1}(\sigma)$  has to be known. This means that an  $\tilde{f}_j^{i-1}$ -value has to be known at every possible  $\sigma$ . This is done by curve-fitting the concentration-profile of the preceding time-step (i-1) with a cubic-spline fit (Hayes, 1974). The integration-routine can calculate every  $\tilde{f}_j^{i-1}$ -value at every desired  $\sigma$ -value, and not only at the points specified by the user.

A semi analytical solution of equation 2.12 is also possible. Then a polynomial curve fit of the concentration profiles has to be substituted in the analytical solution. Of course this is only possible if the curve fit can describe the actual curve with high enough accuracy. To start with and for simplicity, a numerical solution using the Gear method was used.

For calculational purposes (stability) the equations for  $P^1(\sigma)$  have been changed somewhat by eliminating  $\Delta\theta$ . By means of the  $F^{i-1}$ -vector  $\Delta\theta$  is introduced (eq. 2.8). Multiplying by  $\Delta\theta$  leads to:

$$d\tilde{P}^i(\sigma)/d\sigma = D \cdot \tilde{P}^i(\sigma) + \tilde{R}^{i-1}(\sigma) \quad (2.29)$$

$$\text{with} \quad \tilde{P}^i(\sigma) = \Delta\theta \cdot P^i(\sigma) \quad \text{and} \quad \tilde{R}^{i-1}(\sigma) = \Delta\theta \cdot \tilde{F}^{i-1}(\sigma) \quad (2.30)$$

With the  $\tilde{R}^{i-1}$ - vector  $\Delta\theta$  is now eliminated. This doesn't change anything about the preceding.

The same derivations can of course be used when neglecting one or two of the axial dispersion coefficients  $E_b$  and/or  $E_d$ . The resulting matrices for ( $E_b = 0, E_d \neq 0$ ) and ( $E_b = 0, E_d = 0$ ) are given in Appendix 2.A. It is furthermore stressed that with this method it is necessary for the parameters to be independent of height (except for the concentrations of course). Otherwise the decoupling with the matrices can not be performed.

### 2.3 Algorithm

Calculations were done with the NAG-library (1980 - 1989). Computation can of course also be done with other libraries and if necessary routines can be written by the user himself.

All used routines will be given at every step. A summary of all the major steps is:

- 1) Find  $Q$  and  $D$ , such that  $AQ = QD$ . (eigenvalues and eigenvectors).
- 2) Define  $Y^i(\sigma) = Q^{-1} \cdot X^i(\sigma)$ , leading to  $dY^i(\sigma)/d\sigma = D \cdot Y^i(\sigma) + \tilde{F}^{i-1}(\sigma)$ ,  
with  $\tilde{F}^{i-1}(\sigma) = Q^{-1} \cdot F^{i-1}(\sigma)$ .
- 3) Compute  $Y^i(\sigma)$  from the homogeneous and particulate solution:  
 $Y^i(\sigma) = c^i \cdot Y_h^i(\sigma) + P^i(\sigma)$ , with  $c^i = E^{-1} \cdot g^i$ .
- 4) The final solution is found by back-transformation:  $X^i(\sigma) = Q \cdot Y^i(\sigma)$ .

The accuracy of the calculation can be controlled in three ways. First of all the integration routine (for  $\tilde{P}^i(\sigma)$ ) requires a tolerance. Secondly the user can specify many or few  $\sigma$ -points at which a solution is desired. Thirdly the  $\Delta\theta$ -value has a direct control over the  $A$ -matrix and therefore also over the  $Q$  and  $D$  matrices.

A flow sheet is given in fig. 2.1. Eigenvalues and eigenvectors were calculated with the NAG routine F02AGF. The inverse matrix with the routine F01AAF. A cubic spline fit was done with E02BAF and an evaluation of the fit was done with E02BBF. Furthermore the integration routine D02EBF (Gear method routine) was used.

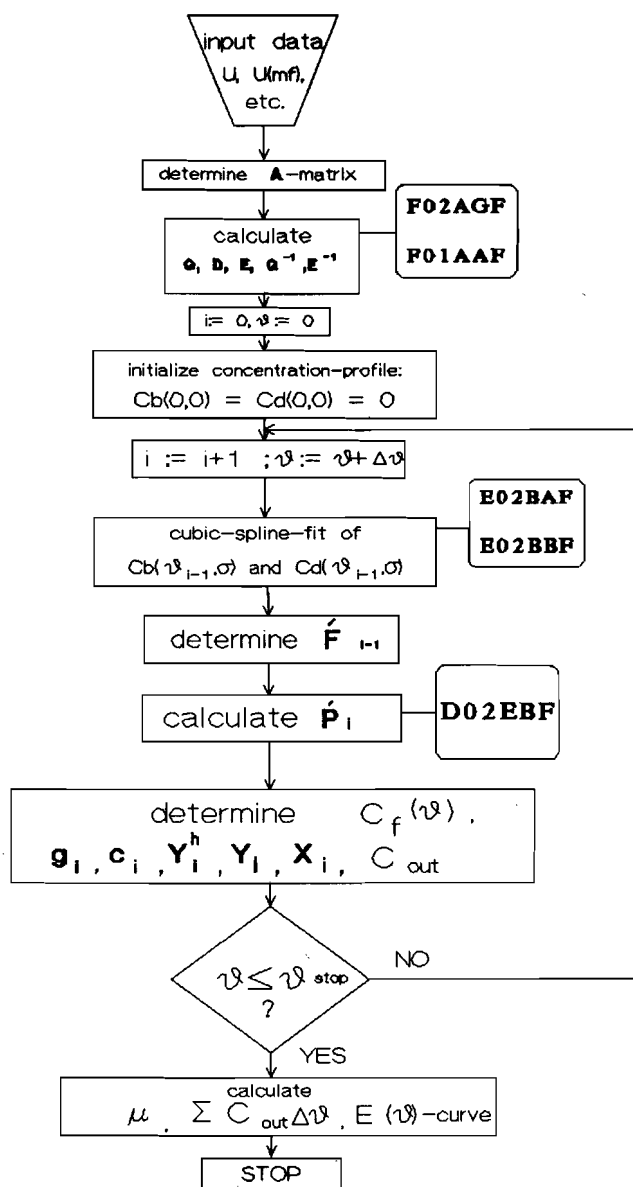


Figure 2.1 Flowsheet of program, using the decoupling method.

### 2.3.1 Definition of feed- and end conditions

For the RTD the injection-pulse has been defined as a Dirac-pulse :

$$C_f(t) = a_d \cdot \exp(-\pi^2 \cdot a_d^2 \cdot (t - t_{\text{step}})^2) \quad (2.31)$$

The  $t_{\text{step}}$ -value has been introduced to make sure that the pulse is injected completely and gradually (numerically speaking). For the final RTD-curve this  $t_{\text{step}}$ -value has to be subtracted from the  $t$ -values. The response on a Dirac-pulse with  $t_{\text{step}}$  equal to zero will be known.

Making equation 2.31 dimensionless yields:

$$C_f(\theta) = a_d \cdot \exp(-\pi^2 \cdot a_d^2 \cdot (H \cdot \xi / U)^2 \cdot (\theta - \theta_{\text{step}})^2) \quad (2.32)$$

Because the surface under a Dirac-pulse equals unity this leads to:

$$\int_0^{\infty} C_f(\theta) d\theta = 1/\tau = I \quad (2.33)$$

with  $\tau$  being the average residence-time and  $I$  the integral amount of tracer gas injected.

The total amount of tracer gas entering the reactor has to leave the reactor (no reaction) and therefore:

$$\int_0^{\infty} C_f(\theta) d\theta = \int_0^{\infty} C_{\text{out}}(\theta) d\theta = 1/\tau \quad (2.34)$$

Because  $I$  equals  $1/\tau$ , this also leads to the condition that the surface under the  $E(\theta)$ -curve (which is the dimensionless response), equals unity:

$$\int_0^{\infty} C_{\text{out}}(\theta) d\theta = 1/\tau = I \quad \Rightarrow \quad \int_0^{\infty} \frac{C_{\text{out}}(\theta)}{I} d\theta = \int_0^{\infty} E(\theta) d\theta = 1 \quad (2.35)$$

It was checked whether the calculations fulfilled these conditions, by taking a summation-value according to:

$$\sum_0^{\vartheta_{\text{stop}}} C_{\text{out}}(\vartheta) \cdot \Delta\vartheta = 1/\tau = \frac{U}{H \cdot \xi} \quad (2.36)$$

The  $\vartheta_{\text{stop}}$ -value has always been taken large enough to acquire a constant summation value, implying that  $\vartheta_{\text{stop}} \rightarrow \infty$ .

Another check was performed by calculating the average residence time from the simulated curves. This value has to be equal to  $\vartheta = 1$ .

To fulfill equation 2.32 numerically, we computed an  $a_d$  value according to

$$\text{minimize } \left\{ \left( \sum_0^{\vartheta_{\text{stop}}} C_f(\vartheta) \cdot \Delta\vartheta \right) - (1/\tau) \right\} \quad (2.37)$$

## 2.4 Results and discussion

The program was written in FORTRAN and run on VAX/VMS. The CPU-time was in the order of 1-5 minutes, depending upon matrix type, step sizes and tolerance used with the calculations. For all calculations the input parameters listed in table 2.1 were used. As an example these values were used, because they are usually encountered in reactors on laboratory scale. For instance Fan and Fan (1979, 1980) used values of the same order of magnitude. They also showed that Pe could be taken independent of height and therefore an average Pe value was used. Computation is of course also possible with values that refer to commercial units.

We defined a relative error in the following way:

$$\epsilon_{\text{rel}} = \frac{|\text{value calculated} - \text{value wanted}|}{|\text{value wanted}|} \cdot 100 \% \quad (2.38)$$

Relative errors were calculated, based on the theoretically expected (value wanted) and on the actually calculated residence time and surface beneath the curve. The best  $\Delta\vartheta$  and  $\Delta\sigma$  values, as well as knots for the cubic spline fit,



were determined by taking those values that gave stable solutions with a small relative error. The boundaries for the integration routine were taken to be  $\sigma = 0$  and  $\sigma = 1$ . All solutions were calculated with  $\Delta\sigma = 0.01$  and  $\Delta\phi = 0.01$ . The step size in placing the knots was taken to be 0.02.

U	=	0.1	m/s
U <sub>mf</sub>	=	0.01	m/s
$\delta$	=	0.05	
$\epsilon_d$	=	0.40	
H	=	1.0	m
$\phi$	=	1.0	

**Table 2.1** List of parameter values used in computation.

The tolerance in calculating  $\tilde{p}_1(\sigma)$  was  $10^{-5}$ . If necessary  $10^{-7}$  was taken. This way a maximum relative error of  $\approx 5\%$  was always found. Most calculations returned a relative error of 1 - 3% .

First of all a comparison was made between the finite difference method (NAG-routine D03PGF) and the decoupling method. Results for  $Pe_b = 20$ ,  $Pe_d = 20$  and  $N_k = 2$  are shown in fig. 2.2. This shows that both methods lead to the same result. The difference only occurs in the height of the top. Place and shape of the first peak, caused by the bubbles, are equal. Dense phase gas leaves the reactor more slowly and gradually, giving the tail. Shape and place of the tail are again the same for both methods.

Due to the stiffness the finite difference method often returned erroneous answers, particularly at somewhat "low" Pe-numbers ( $Pe \leq 10$ ) and "high"  $N_k$  numbers ( $N_k \geq 5 - 10$ ). The decoupling method always returned a stable solution with a relative error of less than 5%.

Computations were also made with the steady state reaction system, for which the governing mass balance equations were solved analytically. Concentration profile in height and resulting conversion were the same as for the steady state reaction system, using the decoupling method and the analytical solutions.

Various computations were made with different parameter values.

Neglecting one or two  $Pe$ -terms leads, in principle, to different systems. This is because the resulting matrices are completely different. Yet comparable solutions were obtained, as is shown in figures 2.3 to 2.9. This indicates the stability of the decoupling method.

All this shows that the decoupling method is a stable method leading to good results.

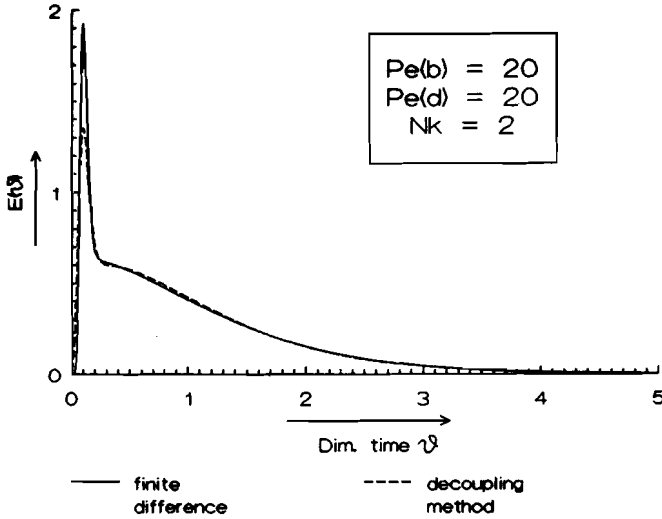


**Figure 2.2** Comparison of residence time distribution of finite difference and decoupling method.

Figure 2.3 shows results for the  $(2 \times 2)$ -matrix, with  $Pe_b \rightarrow \infty$ ,  $Pe_d \rightarrow \infty$  and  $N_k$  as the parameter (Appendix 2.A). At  $N_k = 2$  gas exchange is relatively small and, because bubbles rise much faster than the dense phase gas, a peak occurs. When the gas exchange increases the curve maximum shifts more towards  $\vartheta = 1$ , because more gas is transported upwards in the relatively slow dense phase. If the exchange would get infinitely great, equilibrium would be reached and the gas would rise in plug flow. Therefore there will be a gaussian peak at  $\vartheta = 1$  for large  $N_k$  numbers. The average residence time of the total gas is described with equation 1.11a and of the bubble phase with equation 1.11b. This shows that  $\tau_b/\tau \approx \delta/\xi \approx 0.12$  (with  $\delta = 0.05$  and  $\epsilon_d = 0.4$ ). This value is indeed found from fig. 2.3.

Comparable results were obtained with the  $(3 \times 3)$ -matrix, with  $Pe_b \rightarrow \infty$ ,

$Pe_d = 10$  and  $N_k$  as the parameter (fig. 2.4). As can be seen from figures 2.3 and 2.4, the influence of  $N_k$  is sufficient to obtain a reliable  $N_k$  value from RTD measurements. For a two phase model with one stagnant phase, similar results were presented by Westerterp, Van Swaij and Beenackers (1984).

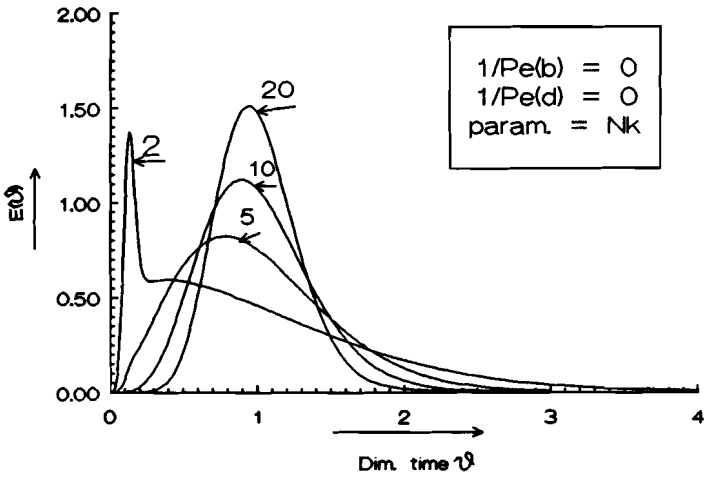


Figure 2.3 Residence time distribution with fixed  $Pe_d$  and  $Pe_b$  and variable  $N_k$  ( $2 \times 2$  matrix).

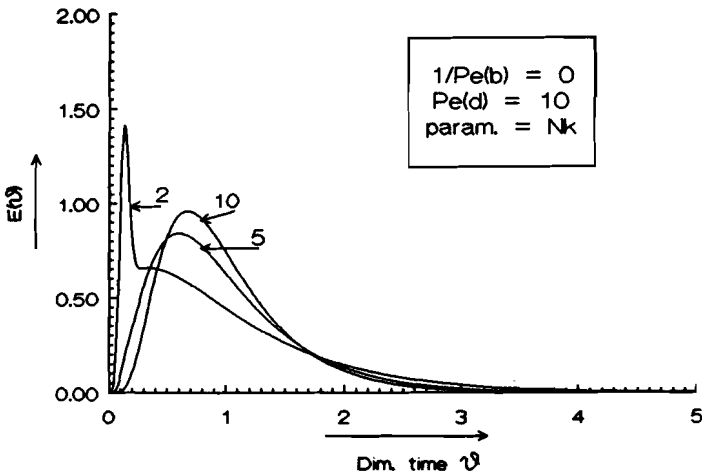


Figure 2.4 Residence time distribution with fixed  $Pe_d$  and  $Pe_b$  and variable  $N_k$  ( $3 \times 3$  matrix).

The influence of the  $Pe_d$  number is shown in fig. 2.5. At  $N_k = 2$  the influence is not obvious because most gas flows through the reactor in the bubble phase and the gas exchange to the dense phase is relatively small. With  $N_k = 10$  (fig. 2.6), the influence is much more obvious, due to the higher exchange to the dense phase. At low  $Pe_d$  numbers the dense phase approaches an ideal mixed system. Therefore the top of the curve will shift towards  $\theta = 0$ . Similar results for the  $(4 \times 4)$ -matrix are shown in the figures 2.7 to 2.9.

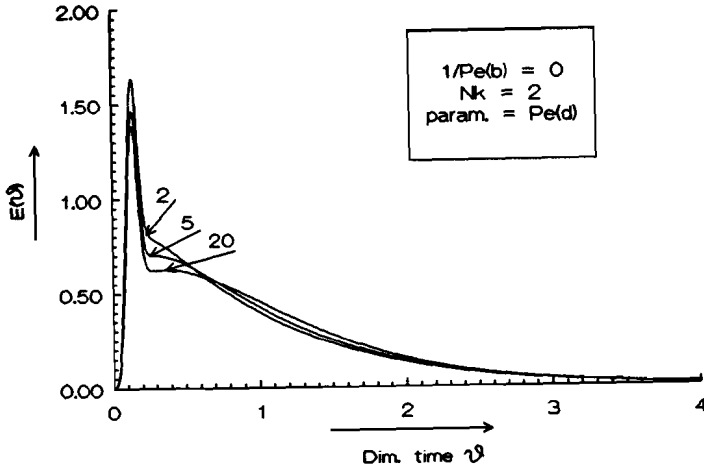


Figure 2.5 RTD with fixed  $Pe_b$  and  $N_k$  and variable  $Pe_d$  ((3 x 3) matrix).

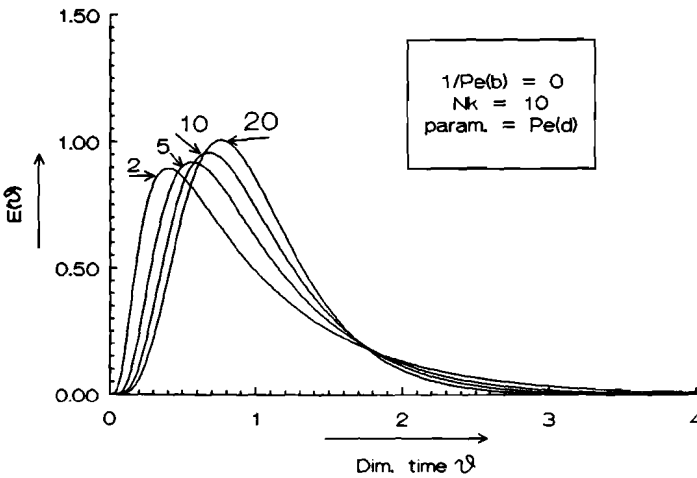


Figure 2.6 RTD with fixed  $Pe_b$  and  $N_k$  and variable  $Pe_d$  ((3 x 3) matrix).

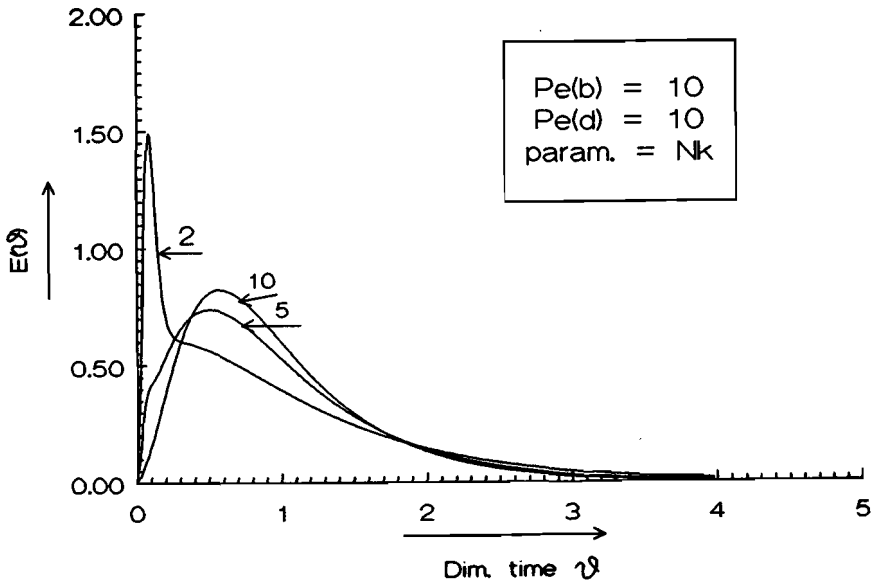


Figure 2.7 RTD with fixed  $Pe_b$  and  $Pe_d$  and variable  $N_k$  ((4 x 4) matrix).

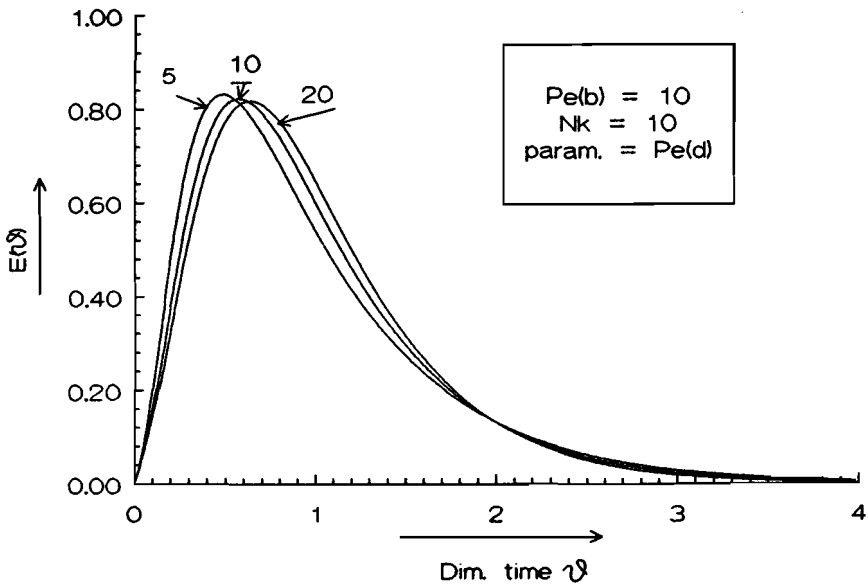


Figure 2.8 RTD with fixed  $Pe_b$  and  $N_k$  and variable  $Pe_d$  ((4 x 4) matrix).

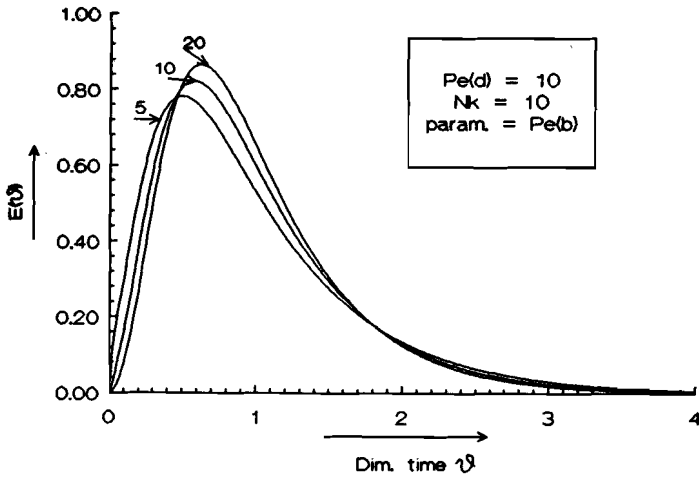


Figure 2.9 RTD with fixed  $N_k$  and  $Pe_d$  and variable  $Pe_b$  ( $(4 \times 4)$  matrix).

### 2.5 Concluding remarks

A finite difference was taken in the time variable in stead of in the space variable. After rewriting these equations, using rather elementary mathematics, the equations were decoupled. Comparable computations were performed with the standard Crank-Nicholson technique and the decoupling method. This showed that both methods gave the same results, if calculation was possible with the Crank-Nicholson technique.

The advantages of the decoupling method are that it is straightforward, mathematically not very complex and that it leads to good and stable solutions. Of course it should be possible to use the decoupling method for other non steady state and steady state systems. In principle it can be used for a system of many equations, as long as it is possible to calculate the eigenvectors, eigenvalues and inverse matrices with high enough accuracy. An

example of another system than we used, was given by Tuin (1989).

To start with a grid with uniform spacing was taken. It will of course be more efficient economically if a non uniform spacing is used. For simplicity this was not done, but a non uniform spacing would not affect the decoupling method itself. A semi analytical solution for equation 2.12, describing the particular part, might give also some improvement. This, however, is only the case if an accurate polynomial curve fit is possible. More research is needed in these areas.

**Appendix 2.A**

1) Matrix definition when neglecting  $Pe_b$ - term.

Original equations :

$$\frac{\partial C_b}{\partial \vartheta} + \beta \cdot \frac{\partial C_b}{\partial \sigma} + N_k \cdot \frac{\xi}{\delta} \cdot (C_b - C_d) = 0 \quad (A.2.1)$$

$$\frac{\partial C_d}{\partial \vartheta} + \gamma \cdot \frac{\partial C_d}{\partial \sigma} + \frac{N_k \cdot \xi}{(1-\delta) \cdot \epsilon_d} \cdot (C_d - C_b) - \dots$$

$$\dots - \frac{1}{Pe_d} \cdot \frac{\xi}{(1-\delta) \cdot \epsilon_d} \cdot \frac{\partial^2 C_d}{\partial \sigma^2} + N_r \cdot \frac{\xi}{(1-\delta) \cdot \epsilon_d} \cdot C_d = 0 \quad (A.2.2)$$

With boundary conditions:

$$C_b(0, \sigma) = 0 \quad (A.2.3)$$

$$C_d(0, \sigma) = 0 \quad (A.2.4)$$

$$C_b(\vartheta, 0) = C_f(\vartheta) \quad (\vartheta > 0) \quad (A.2.5)$$

$$C_d(\vartheta, 0) = C_f(\vartheta) + \frac{1}{(1-f_b) \cdot Pe_d} \cdot \frac{\partial C_d}{\partial \sigma} \Bigg|_{\sigma=0} \quad (\vartheta > 0) \quad (A.2.6)$$

$$\frac{\partial C_d}{\partial \sigma} \Bigg|_{\sigma=1} = 0 \quad (A.2.7)$$

Euler approximation of time variable:



$$\frac{\partial C_{b,i}}{\partial \sigma} = -\frac{N_k}{f_b} (C_{b,i} - C_{d,i}) - \frac{C_{b,i} - C_{b,i-1}}{\Delta \theta} \cdot \frac{1}{\beta} \quad (\text{A.2.8})$$

$$\begin{aligned} \frac{\partial^2 C_{d,i}}{\partial \sigma^2} &= (1-f_b) \cdot Pe_d \cdot \frac{\partial C_{d,i}}{\partial \sigma} + N_k \cdot Pe_d \cdot (C_{d,i} - C_{b,i}) + N_r \cdot Pe_d \cdot C_{d,i} + \dots \\ &\dots + \frac{C_{d,i} - C_{d,i-1}}{\Delta \theta} \cdot \frac{Pe_d \cdot (1-\delta) \cdot \epsilon_d}{\xi} \end{aligned} \quad (\text{A.2.9})$$

Taking  $N_r = 0$  (no reaction) leads to:

$$\begin{aligned} \frac{d}{d\sigma} \begin{bmatrix} C_{b,i} \\ C_{d,i} \\ \partial C_{d,i} / \partial \sigma \end{bmatrix} &= \begin{bmatrix} -(N_k/f_b + 1/(\beta \cdot \Delta \theta)) & N_k/f_b & 0 \\ 0 & 0 & 1 \\ -N_k \cdot Pe_d & Pe_d (N_k + (1-\delta) \epsilon_d / (\xi \cdot \Delta \theta)) & (1-f_b) Pe_d \end{bmatrix} \begin{bmatrix} C_{b,i} \\ C_{d,i} \\ \partial C_{d,i} / \partial \sigma \end{bmatrix} + \\ &\dots + \begin{bmatrix} \frac{1}{\beta \cdot \Delta \theta} C_{b,i-1} \\ 0 \\ -\frac{Pe_d \cdot (1-\delta) \epsilon_d}{\xi \cdot \Delta \theta} C_{d,i-1} \end{bmatrix} \end{aligned} \quad (\text{A.2.10})$$

2) Matrix definition when neglecting  $Pe_b$  and  $Pe_d$  terms.

Original equations:

$$\frac{\partial C_b}{\partial \vartheta} + \beta \cdot \frac{\partial C_b}{\partial \sigma} + N_k \cdot \frac{\xi}{\delta} \cdot (C_b - C_d) = 0 \quad (\text{A.2.11})$$

$$\frac{\partial C_d}{\partial \vartheta} + \gamma \cdot \frac{\partial C_d}{\partial \sigma} + \frac{N_k \cdot \xi}{(1-\delta) \cdot \varepsilon_d} \cdot (C_d - C_b) + N_r \cdot \frac{\xi}{(1-\delta) \cdot \varepsilon_d} \cdot C_d = 0 \quad (\text{A.2.12})$$

With boundary conditions

$$C_b(0, \sigma) = 0 \quad (\text{A.2.13})$$

$$C_d(0, \sigma) = 0 \quad (\text{A.2.14})$$

$$C_b(\vartheta, 0) = C_f(\vartheta) \quad (\vartheta > 0) \quad (\text{A.2.15})$$

$$C_d(\vartheta, 0) = C_f(\vartheta) \quad (\vartheta > 0) \quad (\text{A.2.16})$$

Taking an Euler approximation in the time variable and  $N_r = 0$ :

$$\frac{\partial C_{b,1}}{\partial \sigma} = - \frac{N_k}{f_b} (C_{b,1} - C_{d,1}) - \frac{C_{b,1} - C_{b,1-1}}{\Delta \vartheta} \cdot \frac{1}{\beta} \quad (\text{A.2.17})$$

$$\frac{\partial C_{d,1}}{\partial \sigma} = - \frac{N_k}{(1-f_b)} (C_{d,1} - C_{b,1}) - \frac{C_{d,1} - C_{d,1-1}}{\Delta \vartheta} \cdot \frac{1}{\gamma} \quad (\text{A.2.18})$$

Writing in matrix form yields:

$$\begin{aligned}
 \frac{d}{d\sigma} \begin{bmatrix} C_{b,1} \\ C_{d,1} \end{bmatrix} &= \begin{bmatrix} -(N_k/f_b + 1/(\beta \cdot \Delta\theta)) & N_k/f_b \\ N_k/(1-f_b) & -(N_k/(1-f_b) + 1/(\gamma \cdot \Delta\theta)) \end{bmatrix} \begin{bmatrix} C_{b,1} \\ C_{d,1} \end{bmatrix} + \\
 &\dots + \begin{bmatrix} \frac{1}{\beta \cdot \Delta\theta} C_{b,1-1} \\ \frac{1}{\gamma \cdot \Delta\theta} C_{d,1-1} \end{bmatrix} \quad (\text{A.2.19})
 \end{aligned}$$

### 3.1 Introduction

In this chapter a steady state system with chemical reaction will be described. To determine the mass transfer from the bubble phase to the dense phase the decomposition of ozone on a ferric oxide catalyst was used as a model reaction and the Van Deemter model (1961) was used for the data analysis.

#### Fixed bed

The reaction rate constant  $k_m$  ( $m^3/kg \cdot s$ ) is based on catalyst mass and is determined in a fixed bed reactor. Taking a mass balance over a slice  $dh$ , assuming steady state, isothermal conditions, a first order reaction and neglecting axial dispersion leads to:

$$\frac{F}{A} \cdot \frac{dy}{dh} = - k_m \cdot \rho_p \cdot (1-\varepsilon) \cdot C_g \quad (3.1)$$

Here  $F$  equals molar air flow rate (mol/s),  $y$  the mole fraction (ozone),  $A$  the cross sectional area of the fixed bed,  $C_g$  the (ozone) gas concentration and  $\varepsilon$  the bed porosity. Because a relatively small amount of ozone was mixed with the air stream, the gas volume change due to reaction was neglected. The ozone concentration  $C_g$  can be expressed as a function of pressure and mole fraction  $y$  using the ideal gas law ( $PV = nRT$ ). Therefore the following holds:

$$\frac{dy}{dh} = - \frac{k_m \cdot A \cdot \rho_p \cdot P \cdot (1-\varepsilon)}{F \cdot R \cdot T} \cdot y \quad (3.2)$$

The pressure  $P$  changes linearly with fixed bed height if the superficial gas velocity is taken to be constant with the height (Ergun (1952)). Because the pressure difference between the top and the bottom of the bed will be small, due to the small superficial velocity, the average pressure was substituted in equation 3.2. Integrating leads to:

$$\ln \left[ \frac{y_H}{y_0} \right] = - \frac{k_m \cdot A \cdot \rho_p \cdot H \cdot (1-\epsilon)}{2 \cdot F \cdot R \cdot T} (P_H + P_0) \quad (3.3)$$

Here the subscripts H and 0 denote fixed bed end and beginning respectively. Catalyst mass W equals:

$$W = A \cdot H \cdot \rho_p \cdot (1-\epsilon) \quad (3.4)$$

Substituting eq. 3.4 in eq. 3.3 and rewriting gives:

$$k_m = - \frac{2 \cdot F \cdot R \cdot T}{W \cdot [P_H + P_0]} \cdot \ln \left[ \frac{y_H}{y_0} \right] \quad (3.5)$$

This equation was used to determine  $k_m$ .

### Fluid bed

If a steady state for the fluid bed is assumed, the time derivatives in equations 1.9 and 1.10 are equal to zero. Based on the calculations discussed in chapter 2 the mixing term for the bubble phase was neglected. Therefore the following holds for the (ozone) concentration:

$$f_b \cdot \frac{dC_b}{d\sigma} + N_k \cdot (C_b - C_d) = 0 \quad (3.6)$$

$$(1-f_b) \cdot \frac{dC_d}{d\sigma} - \frac{1}{Pe_d} \cdot \frac{d^2 C_d}{d\sigma^2} + N_k \cdot (C_d - C_b) + N_r \cdot C_d = 0 \quad (3.7)$$

Van Swaaij and Zuiderweg (1972) showed that axial dispersion could be neglected (i.e.  $Pe_d \rightarrow \infty$ ) for the reaction with the catalyst they used (quartz sand (147  $\mu\text{m}$ ) coated with ferric oxide). Furthermore we did calculations with  $Pe_d = 0$  (ideally mixed dense phase) and  $Pe_d \rightarrow \infty$  (ideal plug flow) and virtually the same results were obtained concerning  $H_k$  for A/B powders. This is caused by the relative small amount of gas in the dense phase. The same small influence was found by calculations of residence time

distributions, as was shown in Chapter 2. The axial dispersion for the dense phase was therefore neglected.

For the calculation of the number of reaction units  $N_r$  the reaction rate constant  $k_m$  is used. Definitions based on dense phase volume (giving  $k_d$  [1/s]) or fluid bed volume (giving  $k_r$  [1/s]) can also be used. Assuming that  $\delta \approx 1 - H_{mf}/H$  leads to:

$$N_r = \frac{k_m \cdot (1-\delta) \cdot (1-\epsilon_d) \cdot \rho_p \cdot H}{U} = \frac{k_m \cdot W}{Q} = \frac{k_d \cdot (1-\delta) \cdot H}{U} \approx \frac{k_d \cdot H_{mf}}{U} = \frac{k_r \cdot H}{U} \quad (3.8)$$

Here  $Q$  is the volumetric air flow rate. Equation (3.8) shows that  $k_d$  can easily be calculated from  $k_m$  and vice versa.

For A powders most of the gas enters the bed in the bubble phase, which means that  $f_b$  equals 1 ( $U \gg \varphi \cdot U_{mf}$ ). Solving equations 3.6 and 3.7 for  $Pe_d = \infty$  and  $f_b = 1$  gives:

$$\frac{C_e}{C_1} = \exp(-N_t) \quad \text{with} \quad \frac{1}{N_t} = \frac{1}{N_k} + \frac{1}{N_r} \quad (3.9)$$

With  $N_r$  known and conversion measured,  $N_k$  (and therefore  $H_k$ ) can be calculated from equation 3.9. This equation was therefore used to determine  $H_k$ .

## 3.2 Experimental

The decomposition of ozone was chosen as a model reaction, because it is reported to be a first order reaction and process control is relatively simple, due to low temperatures and atmospheric pressure that can be used. Furthermore the reaction has been used by various other investigators and proven to give good results (Frye et al. (1958), Orcutt et al. (1962), Kobayashi and Arai (1965), Van Swaaij and Zuiderweg (1972), Fryer and Potter (1976), Calderbank et al. (1976) and Bauer (1980)).

### 3.2.1 The equipment

A schematic drawing of the equipment is given in fig. 3.1.

The fluid bed and the fixed bed were both made of stainless steel. The fluid bed had an internal diameter of 100 mm and a length of 1 m. The fixed bed had an internal diameter of 10 mm and a length of 243 mm. Both reactors contained a porous plate distributor and could be heated. Bed temperatures were measured by thermocouples. The fluid bed was thermally isolated and divided into seven single heating sections. The wall temperature of each section could be measured. Pressures up to 14 bar could be used. To determine the bed height, pressure differences were measured at three points. The ozone that had not been converted was destroyed by leading the air through an ozone destructor, which was a fixed bed of magnetite particles (operated at about 300 - 350 °C).

Inlet and outlet concentrations were measured with a U.V. spectrophotometer, which was constructed in such a way that it could be used for high pressure experiments: a stainless steel through flow cuvet was used. The U.V. lamp section and the detection section (using a Hamamatsu R 1384 solar blind foto tube) were separated from the cuvet by quartz glass. A filter for 254 nm was placed between detector and lamp, because ozone has a maximum absorbance at that wave length. Slides could be placed in front of the detector to control the amount of light passed through. The U.V. spectrophotometer was calibrated by a iodometric method (see Appendix 3.A), using a normal procedure and the Low Absorbance Method (LAM) (Skoog and West (1982)) (see Appendix 3.B for calibration results). With measured transmission it was now possible to determine the ozone *concentration* and with known pressure and temperature in the U.V. spectrophotometer, the ozone *mole fraction* could be calculated.

The ozone was produced by means of corona discharges in an ozone generator (fig. 3.2). The voltage between the electrodes could be regulated up to 25,000 V by means of the transformer. Because of these high voltages extensive safety devices were built in. The air flowed between the two electrodes: the outer electrode was a stainless steel tube with a length of 546 mm (i.d.: 25 mm, o.d.: 40 mm) and the inner electrode was made of glass (borium-silicium) with a thin gold layer in it (i.d.: 22 mm, o.d.: 24 mm). These dimensions were the results of experiments with several glass tubes, varying the inner and outer diameters and air flow rate through the generator. Experiments were performed to determine the ozone outlet concentration of the generator as a function of the superficial velocity and the pressure. It was

found that small variations in these two process conditions could have a large influence on the amount of ozone produced (see Appendix 3.B). It was therefore necessary to measure inlet concentration in every fluid and fixed bed experiment.

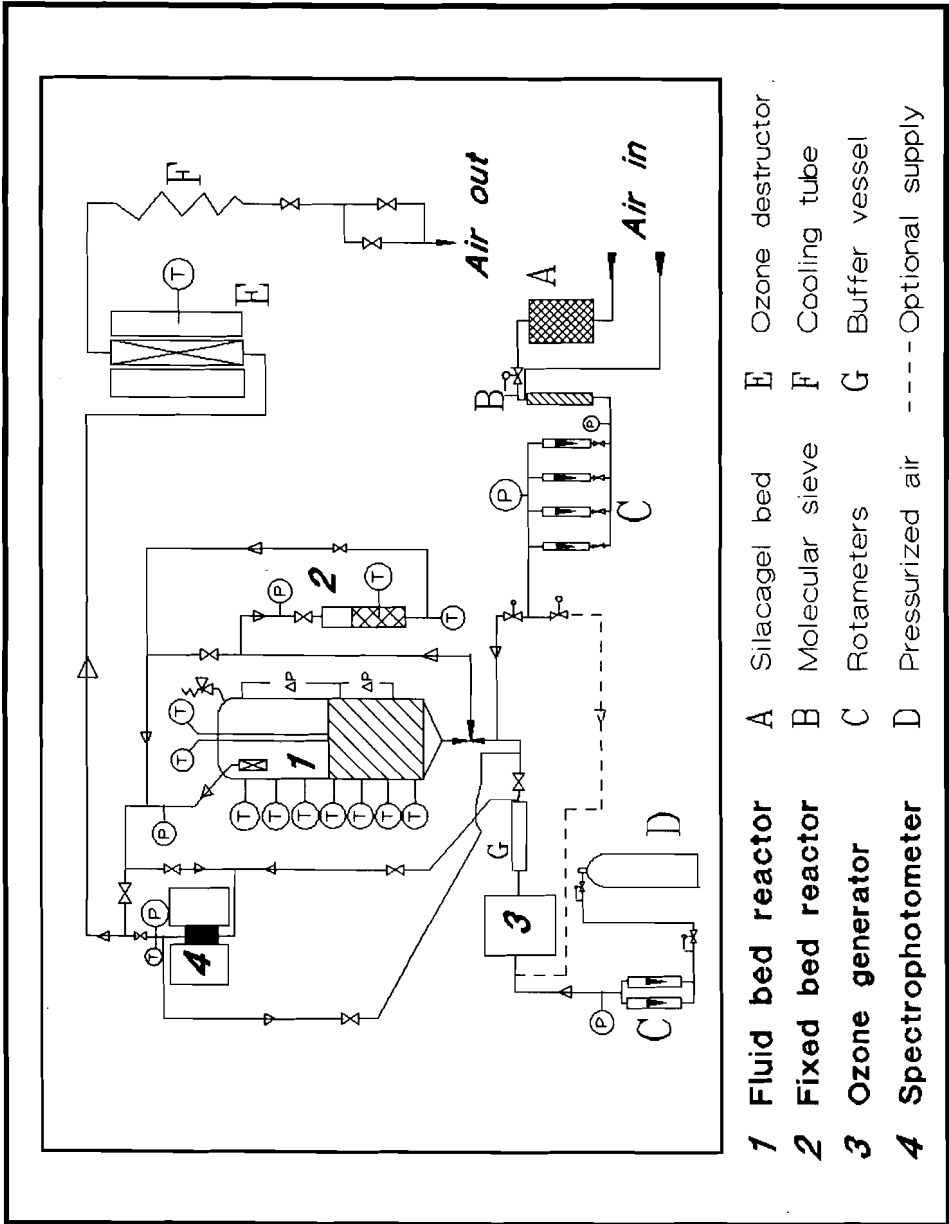
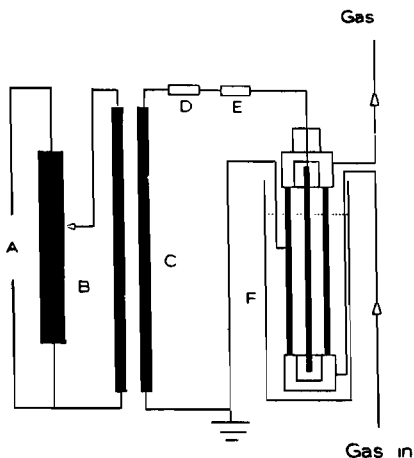


Figure 3.1 Schematic drawing of equipment for ozone decomposition.





- A** = Alternating current ( $\sim 220\text{ V}$ )
- B** = Regulator
- C** = Transformer
- D** = Resistance ( $120\text{ k}\Omega$ )
- E** = 20 melt securities ( $32\text{ mA}$ )
- F** = Ozone generator in water

**Figure 3.2** Schematic drawing of ozone generator.

A buffer vessel was placed between the ozone generator and the reactors to minimize pressure fluctuations. For the same reasons pressurized air was used to feed the generator. Furthermore this had the advantage that high volumetric flow rates through the fluid bed reactor could be used and small flow rates through the generator. This way sufficient ozone could be produced with a stable concentration.

Frye et al. (1958) showed that water poisons the catalyst. Therefore the air was dried ( $< 2\%$  water) by leading it through a packed bed of silicagel and then through a molecular sieve. Ozone rich air and ozone free air were mixed and led to the fluid bed or the fixed bed.

### 3.2.2. Experiments

The catalyst was quartz sand, impregnated with iron oxide. This was done by dripping a solution of  $\text{Fe}(\text{NO}_3)_3$  on a heterogeneously fluidized bed of quartz sand, with a bed temperature of  $80\text{ }^\circ\text{C}$ . The impregnated sand was heated during 24 hours at  $450\text{ }^\circ\text{C}$ , so that the iron oxide was formed. All experiments were performed under atmospheric conditions.

Reaction rate constants for the ozone decomposition were determined in the fixed bed with a 67  $\mu\text{m}$  catalyst and a 25  $\mu\text{m}$  catalyst. Experiments with the 25  $\mu\text{m}$  cat. and varying inlet concentration, catalyst mass and volumetric flow rate, showed that the reaction was indeed first order.

The activation energy for the 25  $\mu\text{m}$  cat. was found to be 147 kJ/mole and for the 67  $\mu\text{m}$  cat. 109 kJ/mole (fig. 3.3). Both values were of the same order as those reported in literature (Van Swaij and Zuiderweg (1972), Fryer and Potter (1976) and Bauer (1980)).

In the fluid bed the 25  $\mu\text{m}$  catalyst showed a great tendency of cohesion, leading to practical problems. For instance, due to the channeling an "extra by-passing phase" occurs, which also leads to a considerable lowering of the conversion (or to put it otherwise: the effective height of a mass transfer unit  $H_k$  increases considerably). This powder was therefore not used in the fluid bed experiments.

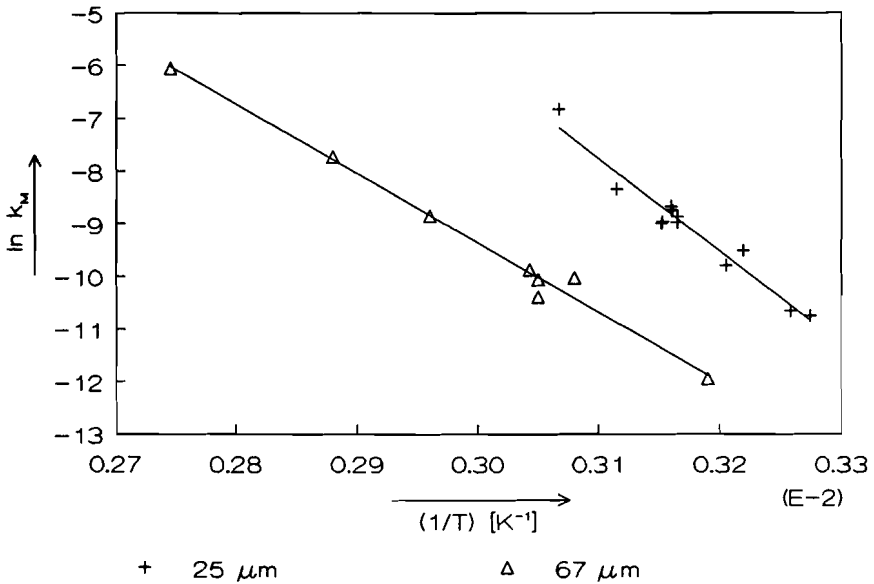


Figure 3.3 Arrhenius plot for 67  $\mu\text{m}$  and 25  $\mu\text{m}$  catalyst.

The properties of the catalyst used in the fluid bed experiments are listed in table 3.1.

mean sieve particle size	$d_{32}$	67 $\mu\text{m}$
particle density	$\rho_p$	2590 $\text{kg}/\text{m}^3$
minimum fluidization velocity	$U_{mf}$	0.6 $\text{cm}/\text{s}$
bed porosity	$\epsilon_{mf}$	0.55
wt % Fe		0.33

Table 3.1 Properties of catalyst used with fluid bed experiments.

To determine the bubble holdup and dense phase gas velocity as a function of the superficial gas velocity, collapse experiments were performed. The bed height was monitored with a video camera and recorder. The reactor vessel was a perspex cylindrical column with a diameter of 11 cm and a porous plate. For an example of such a collapse experiment see fig. 3.4. Bubble hold up and dense phase porosity were calculated from equation 1.7. The results as a function of superficial velocity are given in fig. 3.5.

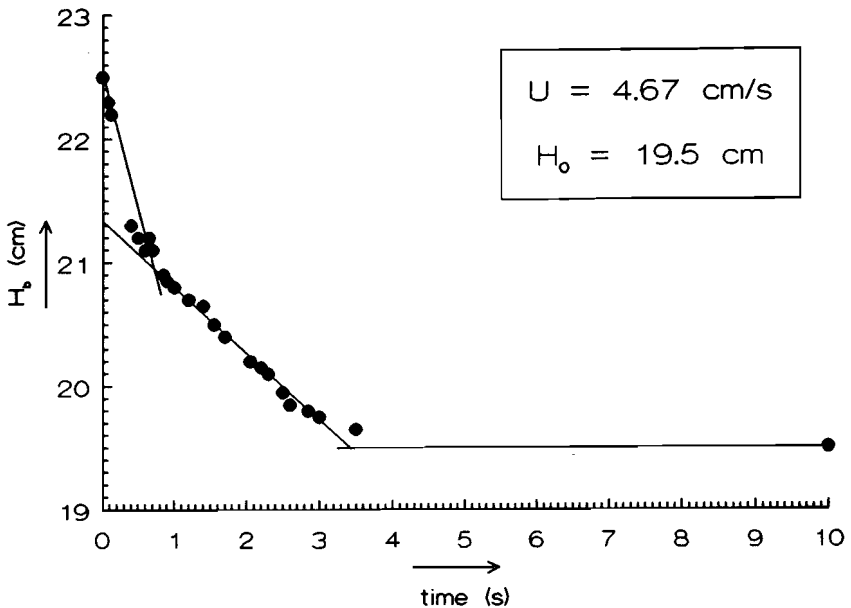
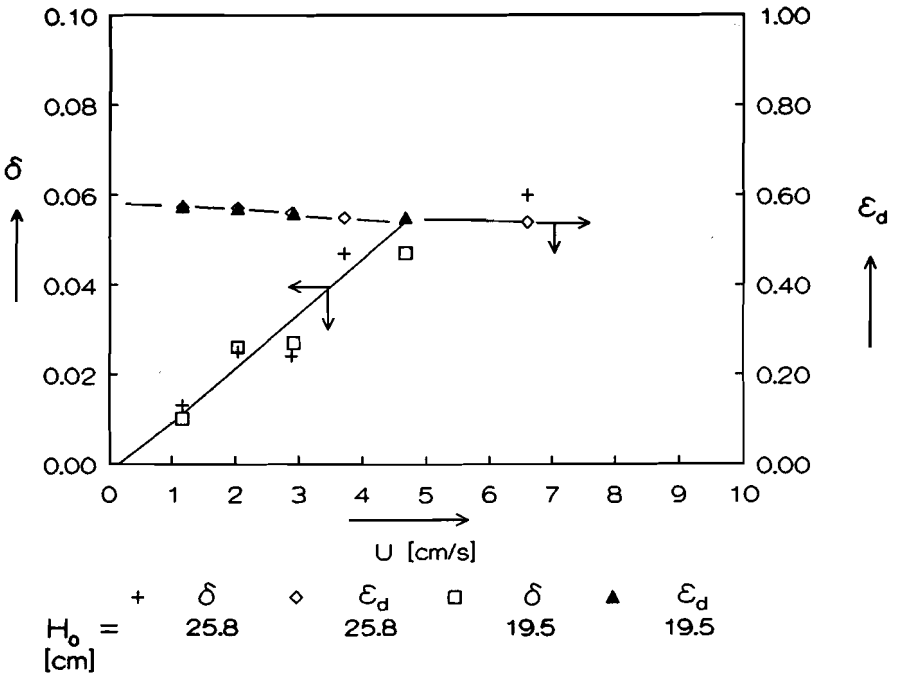


Figure 3.4 Bed height as a function of time during a collapse experiment.



**Figure 3.5** Bubble hold up and dense phase porosity as a function of superficial velocity for the 67  $\mu\text{m}$  catalyst.

The fluid bed was filled with 3.73 kg 67  $\mu\text{m}$  catalyst and was fluidized for several days. Bauer (1980) showed that this was necessary to obtain a constant catalyst activity. A small amount of catalyst was taken from the fluid bed reactor and about 10 g was used to determine the rate constant in the fixed bed. This was repeated after a few weeks for one temperature. Exactly the same  $k_m$  values were found, indicating that the catalyst was not deactivated.

Conversion, bed temperature and wall temperature of the several sections were measured. After these series of experiments, conversion in the empty reactor was measured. The same superficial velocity and wall temperatures, as during the previous experiments, were used. This way a correction for reaction at the wall was determined. The conversions in the empty reactor were between 1 - 10 %.

### 3.3 Results and discussion

Results for the height of a mass transfer unit  $H_k$  with variable superficial velocity  $U$  and reaction rate constant  $k_m$  (by changing the bed temperature) are shown in fig. 3.6. Equation 3.9 was used to calculate  $H_k$ .

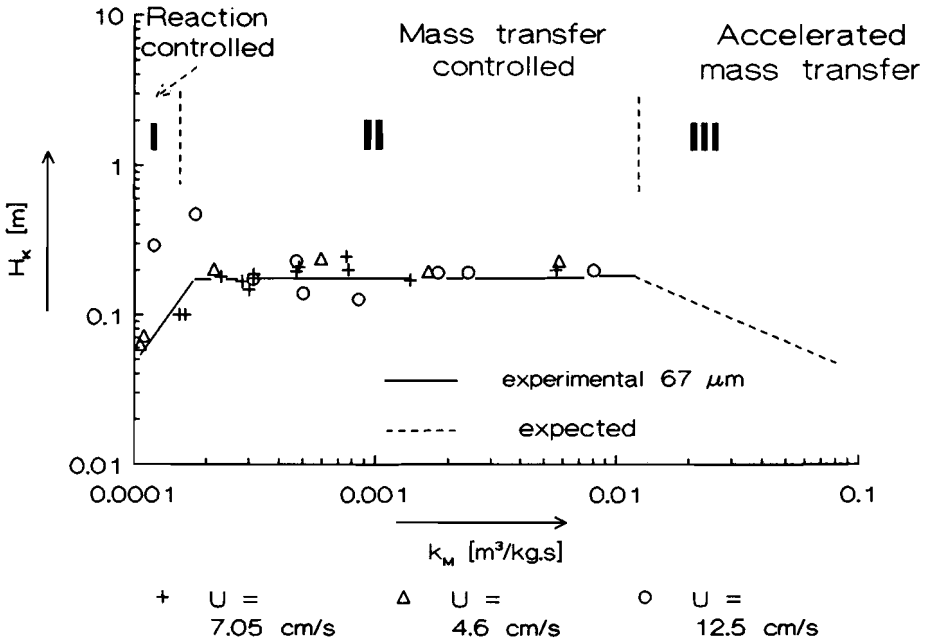


Figure 3.6 Theoretical and experimental relation between  $H_k$  and  $k_m$ .

At low  $k_m$  values the system is reaction controlled (I) (see fig. 3.6) which means that  $N_t \approx N_r$ . This implies that large  $N_k$  and small  $H_k$  values will be found (see equation 3.9). In this region it is also difficult to obtain accurate  $H_k$  values due to experimental error. Once the mass transfer controlled region is reached (II),  $H_k$  will become constant, until accelerated mass transfer occurs (III). Indeed we found this trend (fig. 3.6), but we did not reach region (III).

From literature it is known that region III indeed occurs (Van Swaij and

Zuiderweg (1972)). Accurate calculation of  $H_k$  is only possible in regions II and III, meaning that  $k_m$  (and therefore the number of reaction units  $N_r$ ) must be sufficiently high. From fig. 3.6 it can also be seen that the influence of the superficial velocity is rather small for these particles, probably due to the relatively large  $U/U_{mf}$  values. A  $H_k$  value of about 18 cm was found.

### 3.4 Concluding Remarks

The height of a mass transfer unit was determined using a chemical model reaction. It was found that for the "small" 67  $\mu\text{m}$  particles,  $H_k$  remains virtually constant (about 18 cm) and that the region with accelerated mass transfer was not reached.

Experiments with pressure higher than 1 atm. can only be performed when a pump is placed directly behind the ozone generator. The generator itself has to operate at atmospheric pressure, since at higher pressures the ozone production is reduced.

Coarse powders could not be used in the described equipment, because wall effects would occur (such as slugging). Furthermore the  $U_{mf}$  values are so large so that superficial velocities would have to be used, leading to problems concerning ozone analysis. For the coarse particles a new apparatus was designed for measuring the mass transfer but also for determining the hydrodynamic properties (especially the  $\varphi$  factor). This equipment and the results will be shown in the chapters 5 and 6.

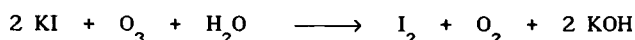
Data analysis of our own experiments and a lot of literature data, concerning chemical model reactions, will be discussed in chapter 4.

### Appendix 3.A

#### *Iodometric Method for calibration of ozone generator.*

An iodide solution was prepared by dissolving 2.5 g KI and 1 g NaOH in 250 ml water. The solution had to be placed after the U.V. spectrophotometer and the ozone rich air was led through it once a stable transmission value was reached. The ozone generator required a certain time to produce a constant concentration. Leading air through the iodide solution had to be done only then when this stable concentration was reached (this time was of the order of 30 seconds, but was of course strongly dependent on volumetric air flow rate).

The following reaction occurred:



To make sure that other gases like  $\text{SO}_2$  and/or  $\text{NO}_2$  did not influence the results of the measurements, 5 drops of 1 vol%  $\text{H}_2\text{O}_2$  were added and the solution was heated until it boiled. After the solution had cooled down, the pH was lowered to 3.8 with 20 % acetic acid and the solution became deep brown. Back titration with 0.01 M  $\text{Na}_2\text{S}_2\text{O}_3$  gave the ozone concentration (1 mole  $\text{S}_2\text{O}_3^{2-} \equiv 1/2$  mole  $\text{O}_3$ ) of the solution through which the ozone rich gas had been led.

### Appendix 3.B.

#### *Detailed information on equipment*

##### The U.V. spectrophotometer

The U.V. spectrophotometer was calibrated by an iodometric method, using a normal procedure and the Low Absorbance Method (LAM) (Skoog and West (1982)). With the LAM the zero level was adjusted to a transmission of say 0.90. Concentrations leading to a normal transmission between 0.90 and 1.0 were upgraded to a transmission between 0.0 and 1.0. Results of the calibration are shown in fig. 3B.1.

The spectrophotometer gave a transmission with a variation of  $\pm 0.003$ . An error in the concentration was calculated using this value and the measured

correlation. Results are shown in fig. 3B.2. This shows that accurate measurements (error less than about 10 %) are only possible in the transmission range of about 0.01 to about 0.96. Therefore the LAM had to be used when the measurement got out of this range, because this way a much higher accuracy was obtained.

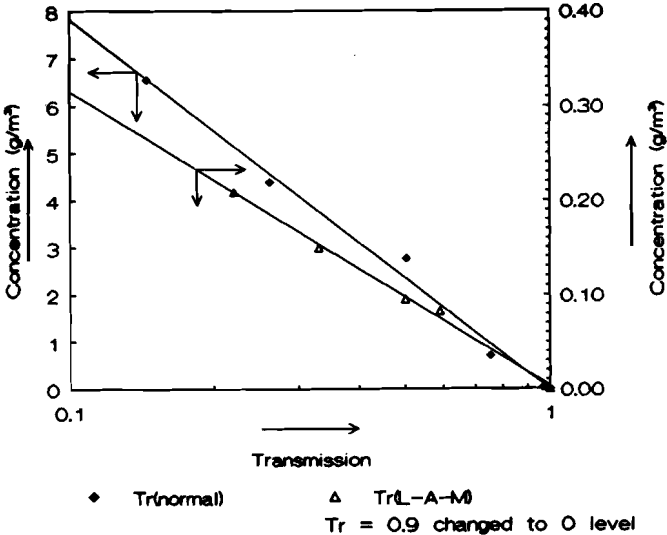


Figure 3B.1 Results of calibration with iodometric method.

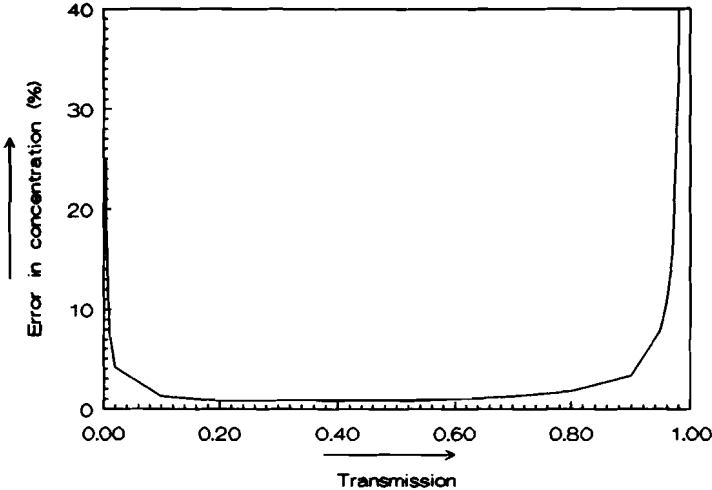


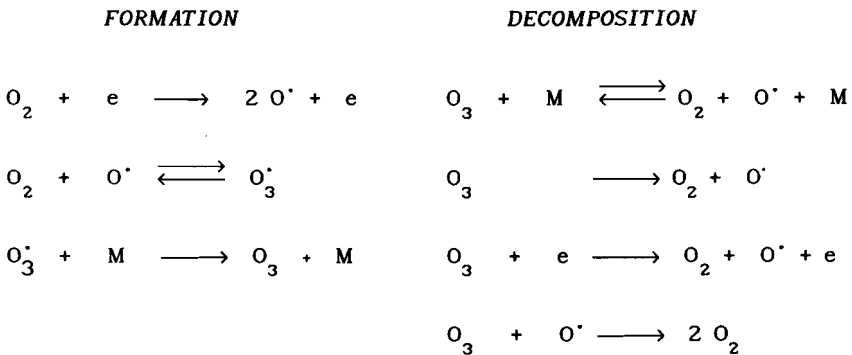
Figure 3B.2 Analysis of error for U.V. spectrophotometer.



The ozone generator

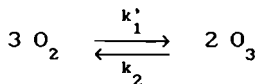
Experiments were performed to determine the ozone outlet concentration of the generator as a function of the superficial velocity and the pressure. It was found that small variations in these two process conditions could have a large influence on the amount of ozone produced (see fig. 3B.3)

The fact that the ozone generator produces a negligible amount of ozone above a certain pressure was also observed by Edelman (1967). This effect is due to the numerous reactions that occur during the electrical discharge in the generator. Edelman argued that the following reactions take place in the reactor:



*(all decomposition reactions are first order in  $O_3$ ).*

The overall reaction can be regarded to be:



Because we operate with an excess in oxygen, we can write for the reaction velocity  $r_{O_3}$  (first order in ozone) (Edelman (1967)):

$$r_{O_3} = \frac{dC_{O_3}}{dt} = k_1 - k_2 \cdot C_{O_3} \tag{B.3.1}$$

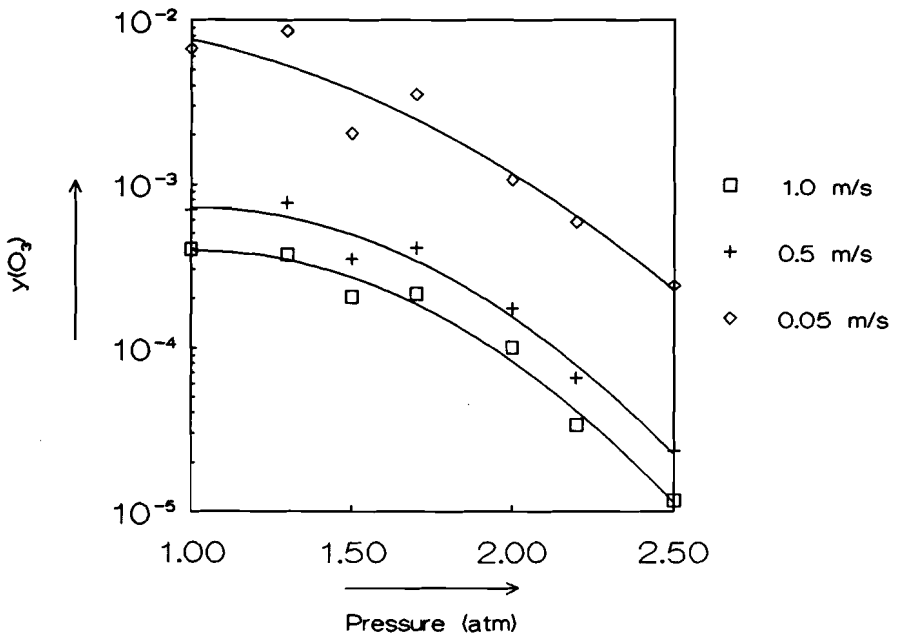
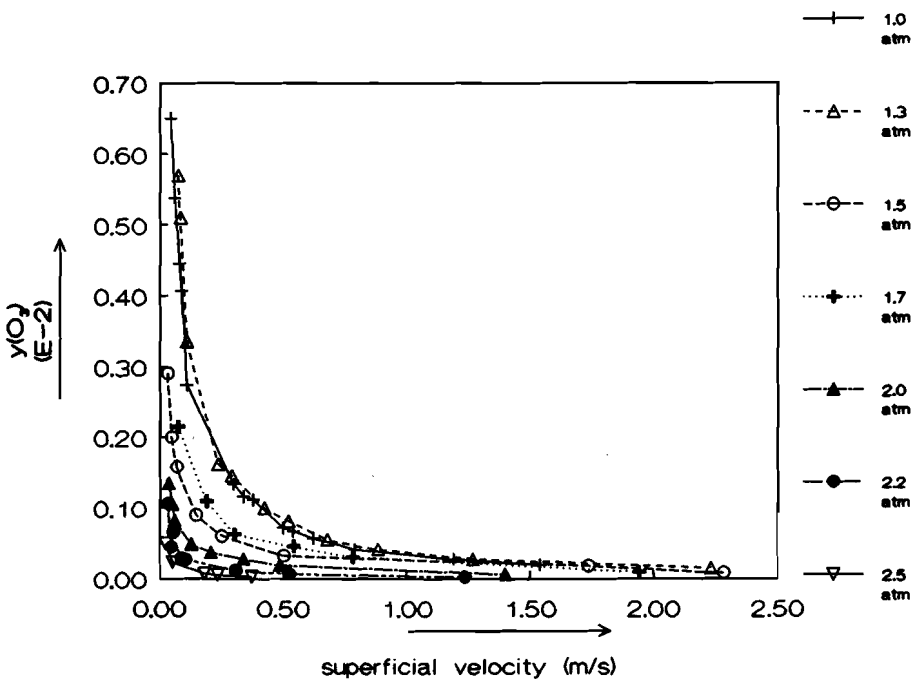


**Figure 3B.3** Ozone production of generator as a function of pressure and superficial gas velocity between the generator tubes.

When equilibrium is reached the following holds:

$$C_{O_3, \max} = \frac{k_1}{k_2} \quad (r_{O_3} = 0 \text{ !}) \quad (\text{B.3.2})$$

Assuming that the air flows through the ozone generator in plug flow gives:

$$\frac{\partial C_{O_3}}{\partial t} = -u \cdot \frac{\partial C_{O_3}}{\partial h} + k_1 - k_2 \cdot C_{O_3} \quad (\text{B.3.3})$$

Assuming steady state, substituting  $k_1 = k_2 \cdot C_{O_3, \max}$  and taking  $C_{O_3}|_{h=0} = 0$  leads to :

$$\zeta = 1 - e^{-k_2 \tau} \quad \text{where } \zeta = \frac{C_{O_3}}{C_{O_3, \max}} = \frac{y}{y_{\max}} \quad (\text{B.3.4})$$

and  $\tau$  is the residence time of the gas in the generator.

Hence

$$\ln y = \ln y_{\max} + \ln (1 - e^{-k_2 \tau}) \quad (\text{B.3.5})$$

Exit mole fractions were found that were in agreement with this correlation as is shown in fig. 3B.4.

It was tried to fit these data points to find  $y_{\max}$  and  $k_2$  (and consequently  $k_1$ ) as a function of pressure and superficial gas velocity in the generator. This, however, could not be done with sufficient accuracy, probably because there were not enough data points.

Figure 3B.4 shows that the pressure has a considerable effect on  $y_{\max}$  (asymptotic value of  $y$ ). This was also found and explained by Edelman (1967). It furthermore shows that in practice superficial velocity is never that low that the maximum obtainable  $O_3$  concentration is reached.

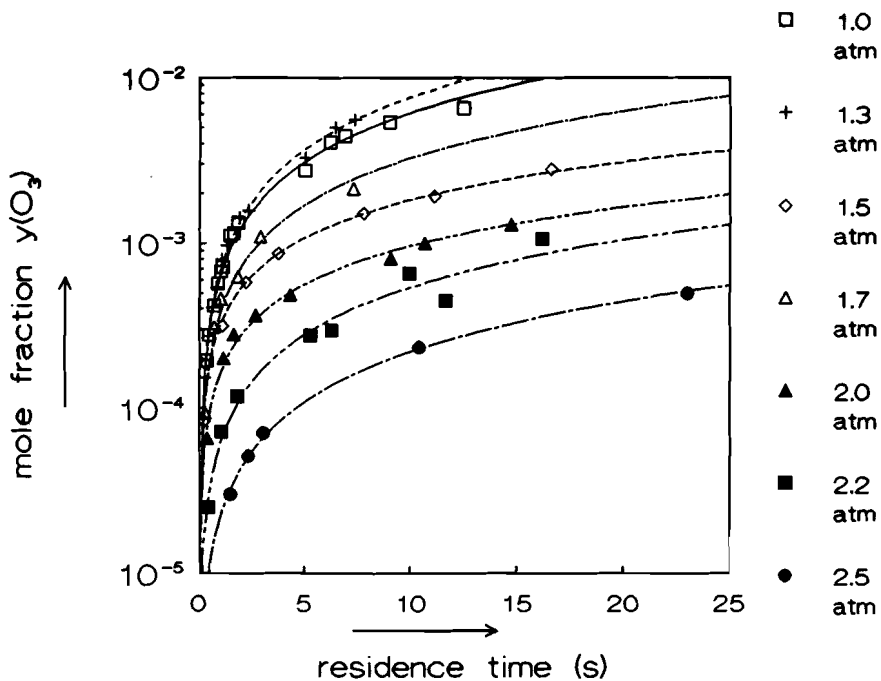


**Figure 3B.4** Exit mole fractions as a function of residence time  $\tau$  in generator.

#### 4.1. Introduction

Scale up is the target of a great number of investigations concerning gas fluidized beds: a method has to be found for predicting the conversion of a gas fluidized bed, under given circumstances. A very important factor that determines the conversion, is the mass transfer from the bubble phase to the dense phase. This thesis is concerned with the influence of the particle size on this mass transfer.

The height of a mass transfer unit  $H_k$  can be determined as a function of particle size  $d_p$  and superficial velocity  $U$ , but these parameters cannot be varied completely independently, because larger particles require a larger gas flowrate. Furthermore other independent variables, describing gas and particle properties and bed dimensions, have also an influence on  $H_k$ . To compare different systems, a factor is needed that contains these variables. With this factor it is then possible to determine the influence of particle size on the height of a mass transfer unit. To obtain this parameter, a lot of literature data and our own experimental work, discussed in chapter 3, were analyzed with the Van Deemter model (1961).

With  $N_r$  known and conversions measured,  $N_k$  (and therefore  $H_k$ ) can be calculated from equation 3.9.

#### 4.2 Data analysis

The process parameters, that were taken into account, were divided into three main groups:

- a) particle properties
- b) gas properties
- c) reactor dimensions and external influences.

A list of the parameters under consideration is given in table 4.1.

particle	gas	external/ reactor	
$d_p$	$\mu_g$	U	} independent variables
$\rho_p$	$D_g$	H	
	$\rho_g$	D internals, distributor, etc.	
			} dependent variables
		$H_k$	
$\epsilon_{mf}$		$N_k$ $N_r$	

**Table 4.1** List of parameters taken into consideration for analysis.

A list of the papers used and some relevant information is given in table 4.2.

The values for  $H_k$  were calculated from the given data (and from the figures presented) in the papers. If not given  $\mu_g$ ,  $D_g$ ,  $\rho_g$  were estimated from Perry's Handbook (Perry and Chilton, 1973). Occasionally some particle properties had to be estimated also. This was done using the relation of Wen and Yu (eq. 1.1).

Although  $d_p$  and U are independent variables, they cannot be varied completely independently, because large particles requires a large gas flow rate. Therefore  $U/U_{mf}$  was used, because this parameter describes the relative amount of gas in the bubble and dense phase.

Statistical analysis did not give a practical relation when using all the parameters given in table 4.1., but some trends did show. Based on these results a Scaling parameter S was defined, that contains the reactor dimensions and the ratio  $U/U_{mf}$ . For relatively rapid reactions it contains also  $N_r$ , accounting for accelerated mass transfer (region III, fig. 3.6).

Table 4.2 Listing of papers used for data analysis.

Author	Type of reaction	Bedproperties	External	Catalyst	Gasvelocity	$N_r$	$k_d' \cdot k_m$
Shen and Johnstone (1955)	decomposition $NO_x$	D = 11.4 cm H = 26 - 32 cm 220 - 250 °C, 1 atm.	Porous plate	alumina $d_p = 103 \mu m$ $U_{mf} = 0.21 \text{ cm/s}$	1.3 - 4.6 cm/s	0.08 - 0.35	$1.53 \cdot 10^{-2} - 9.25 \cdot 10^{-3} \text{ s}^{-1}$
Lewis et al. (1959)	dehydrogenation of ethylene	D = 5.2 cm H = 25 cm 113 °C, 1 atm.	Fixed bed distr., with/without baffles.	microspherical $d_p = 122 \mu m$ $U_{mf} = 0.73 \text{ cm/s}$	4.57 - 34.3 cm/s	6 - 48	$8.7 \text{ s}^{-1}$
Massimilla and Johnstone (1961)	oxidation of ammonia	D = 11.4 cm H = 19 - 60 cm 250 °C, 1.1 atm.	Porous plate distributor	alumina $d_p = 105 \mu m$ $U_{mf} = 0.27 \text{ cm/s}$	0.7 - 9 cm/s	0.19 - 2.4	$0.086 \text{ s}^{-1}$ (from Kunii and Levenspiel (1969)) $0.0446 \text{ s}^{-1}$ (from Werther and Hegner (1980))
Orcutt et al. (1962)	decomposition of ozone	D = 10.2, 15.3 cm H = 29.5 - 71 cm 27 - 88 °C	Porous plate	Alumina, $Fe_2O_3$ $d_p = 39 \mu m$ $U_{mf} = 0.43 \text{ cm/s}$	3.66 - 14.6 cm/s	0.2 - 60	
Kobayashi and Arai (1966)	decomposition of ozone	D = 0.2 m H = 0.34 m	Porous and perforated plate	Silica $d_p = 194 \mu m$ $U_{mf} = 2.1 \text{ cm/s}$	6.6 and 9.9 cm/s	0.89-7.5	* Remark: Data taken from Kunii and Levenspiel (1969).
de Groot (1967)	RTD-measurements $H_2$ - tracer	D = 0.1 - 1.5 m H = 1 - 4.9 m 25 °C	Porous and perforated plate	Silica $d_p = 96 \mu m$ $U_{mf} = 1.5 \text{ cm/s}$	0.1 - 0.2 m/s	0	0
Caiderbank et al. (1967)	decomposition of ozone	D = 0.15, 0.457 m H = 0.5 and 1 m	25 $\mu m$ bronze porous plate	Alumina-fresh-cat. $d_p = 192, 100, 83 \mu m$ $U_{mf} = 3.73, 1.07, 0.86 \text{ cm/s}$	1.6 - 8.6 cm/s	0.2 - 20	
van Swaaij and Zuiderweg (1972)	a) decomposition of ozone	D = 0.1 - 0.3 m H = 1 - 1.22 m 60 - 80 °C, 1 atm.	Porous plate	Quartz/ $Fe_2O_3$ $d_p = 147 \mu m$ $U_{mf} = 1 \text{ cm/s}$	1.8 - 20 cm/s	1 - 133	$1 \cdot 10^{-4} - 1 \cdot 10^{-2} \frac{\text{kg}}{\text{m}^3 \cdot \text{s}}$
	b) RTD-measurements He-tracer	D = 0.1 - 0.6 m H = 0.9 - 2.35 m	Porous plate	Quartz $d_p = 147 \mu m - ?$ $U_{mf} = 1 - ? \text{ cm/s}$	9.4 - 88 cm/s	0	0
Fryer and Potter (1976)	decomposition of ozone	D = 0.229 m H = 11.5 - 66 cm	Perforated plate $A_0 = 675 \text{ mm}^2$	Quartz/ $Fe_2O_3$ $d_p = 117 \mu m$ $U_{mf} = 1.7 \text{ cm/s}$	2 - 16 cm/s	0.2 - 110	$0.049 - 7.75 \text{ s}^{-1}$
Bauer (1980)	decomposition of ozone	D = 0.2 and 1 m H = 0.6 m	Porous and perforated plate	Quartz/ $Fe_2O_3$ $d_p = 108 \mu m$ $U_{mf} = 1.6 \text{ cm/s}$	10 - 25 cm/s	0.1 - 2.6	$0.06 - 0.9 \text{ s}^{-1}$
Boonstra (1983)	RTD-measurements $CH_4$ -tracer	D = 45.7 cm H = 0.41 and 0.82 m	Perforated plate $A_0 = 0.013$	Spent crack-cat. $d = 69 \mu m$	1.25 - 12.5 cm/s	0	0

$$S = \sqrt{H \cdot D \cdot (U/U_{mf})} / \sqrt{N_r} \quad \text{for a chemical reaction and } N_r \geq 1 \quad (4.1)$$

$$S = \sqrt{H \cdot D \cdot (U/U_{mf})} \quad \text{for RTD measurements } \rightarrow N_r = 0 \quad (4.2)$$

As was shown in chapter 3 too low a  $N_r$  value gave some inaccuracies in calculating  $H_k$ . Based on the data a minimum value  $N_r = 1$  was estimated. For the residence time distribution (RTD) measurements ( $N_r = 0$ ), the  $N_r$  value was simply left out. This means that the  $S$  values for reaction data are smaller than those calculated from RTD data.

### 4.3. Results and Discussion

Plots of  $H_k$  versus  $S$  for the several experiments are given in fig 4.1 - 4.11. They show that, in all cases,  $H_k$  could be correlated by:

$$H_k = c_1 + c_2 \cdot S \quad (4.3)$$

In equation 4.3 the constants  $c_1$  and  $c_2$  are dependent on the physical properties of the solid and gas phases and of the distributor type and internals. Equation 4.3 holds for all experiments, even for those where internals or perforated plates were used. Also for experiments with a wide range in  $H$ ,  $D$  and  $U/U_{mf}$  (see table 4.2),  $H_k$  could be correlated with  $S$  by equation 4.3, indicating the applicability of the equation for given physical properties of gas and solids. Van Swaij and Zuiderweg (1972) found that  $H_k \sim H^{0.5} \cdot D^{0.42}$ . We found virtually the same dependency, as is expressed by equations 4.1 to 4.3.

If all gas properties, the particle properties  $\rho_p$  and  $\epsilon_{mf}$  and the type of distributor and internals are known, it can be seen from table 4.1 that  $H_k$  depends on  $H$ ,  $D$ ,  $U$ ,  $U_{mf}$ ,  $N_r$  and  $d_p$ . The scaling parameter  $S$  can be used as a reference to determine the influence of  $d_p$  on  $H_k$ , since  $S$  contains  $H$ ,  $D$ ,  $U$ ,



$U_{mf}$  and  $N_r$ . At a given particle size,  $S$  can also be used as a tool in scale up.

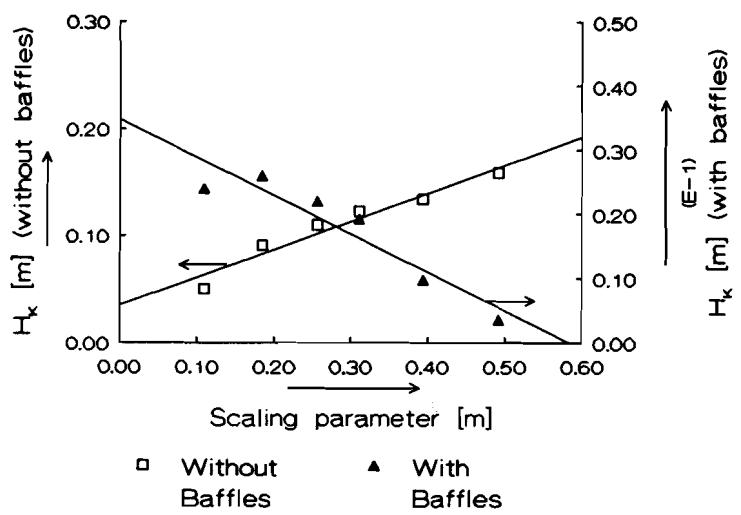


Figure 4.1  $H_k$  vs.  $S$  from Lewis et al. (1955).

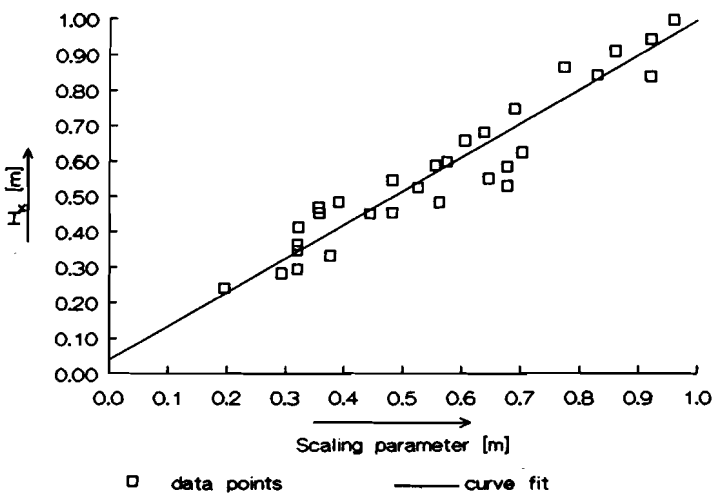


Figure 4.2  $H_k$  vs.  $S$  from Massimilla and Johnstone (1961). The data points have to be considered with an appropriate reserve. See text.

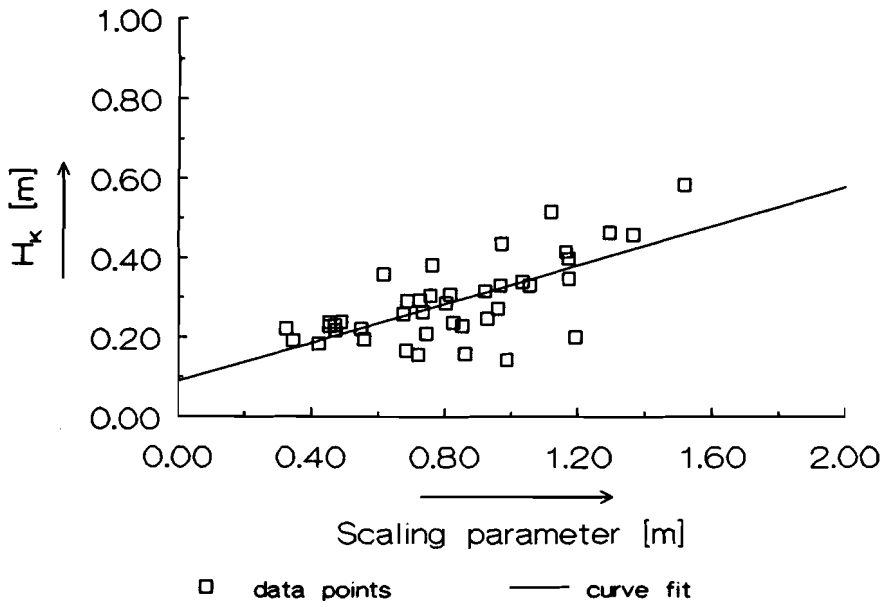


Figure 4.3  $H_k$  vs.  $S$  from Orcutt et al. (1962).

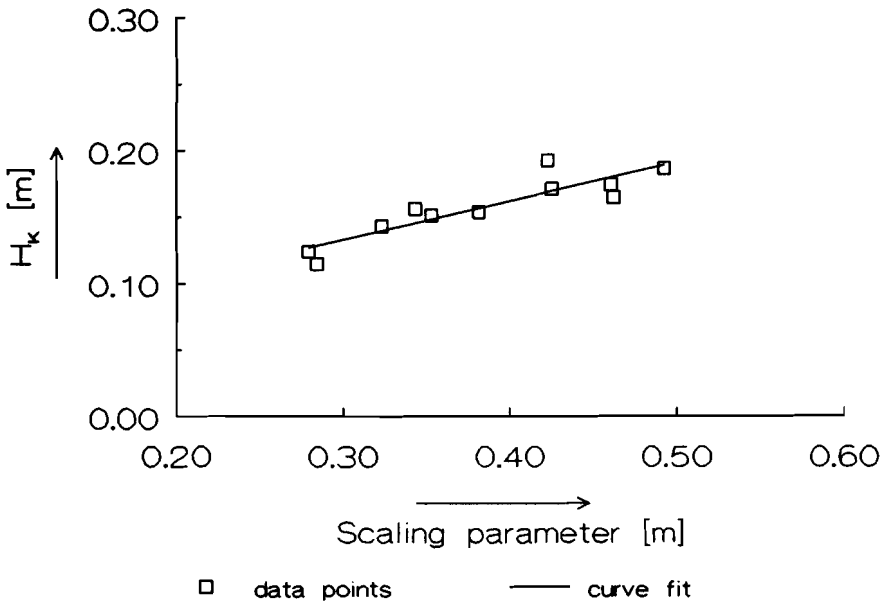


Figure 4.4  $H_k$  vs.  $S$  from Kobayashi and Arai (1966).

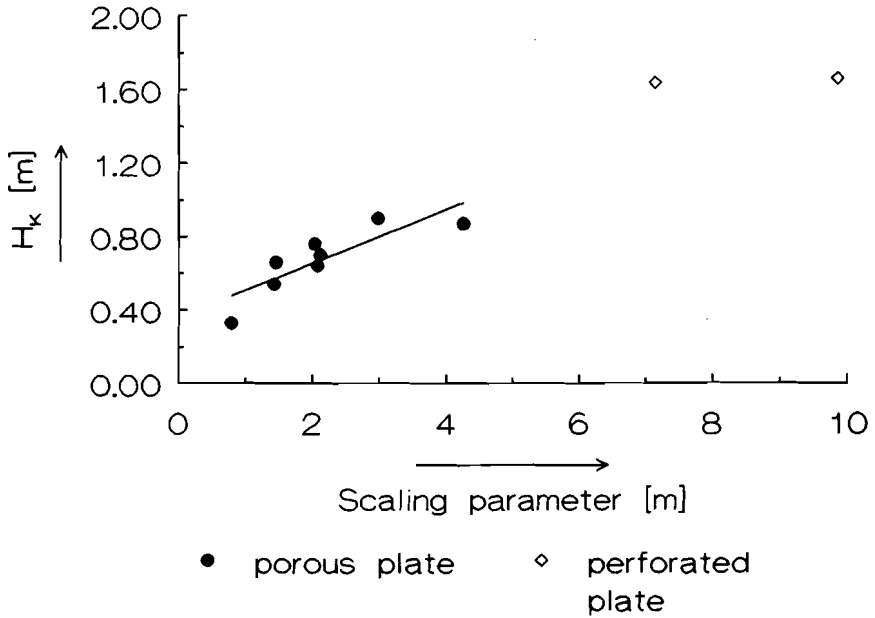


Figure 4.5  $H_k$  vs.  $S$  from de Groot (1967).

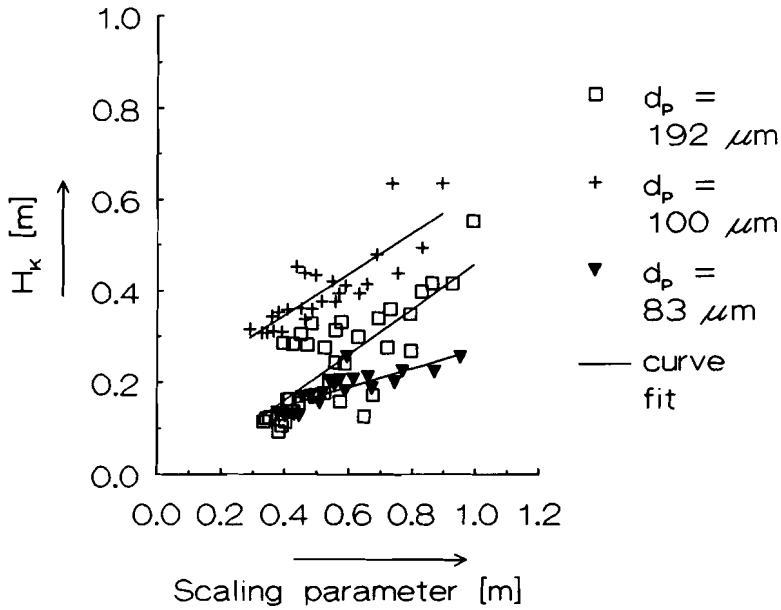
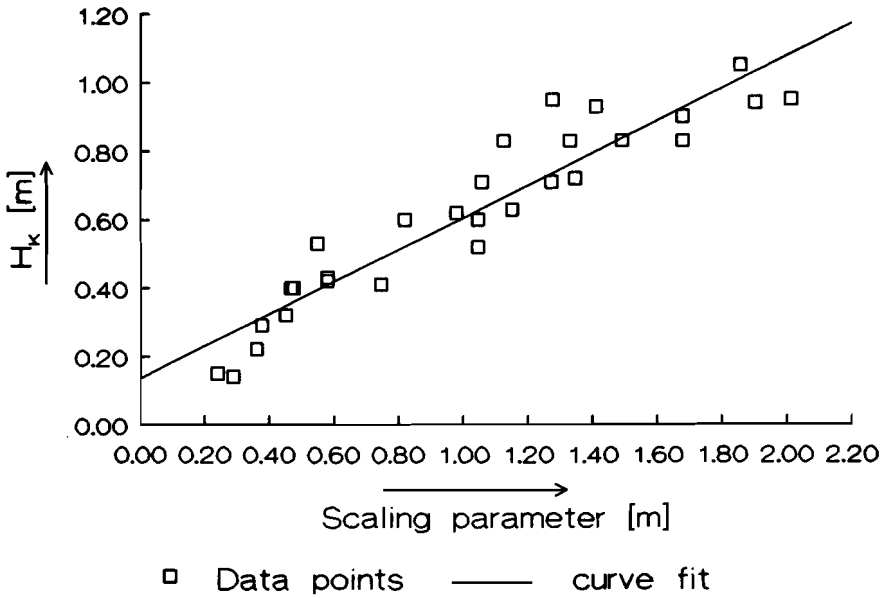
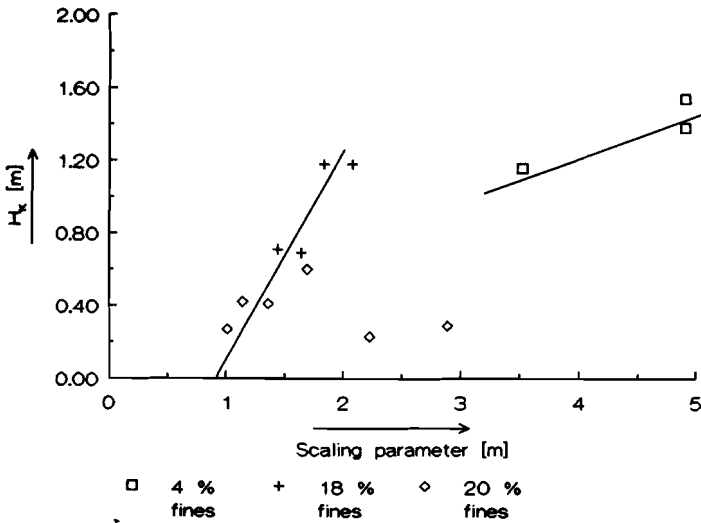


Figure 4.6  $H_k$  vs.  $S$  from Calderbank et al. (1967).



**Figure 4.7**  $H_k$  vs.  $S$  from van Swaaij and Zuiderweg (1972);  
ozone decomposition



**Figure 4.8**  $H_k$  vs.  $S$  from van Swaaij and Zuiderweg (1972);  
RTD measurements.

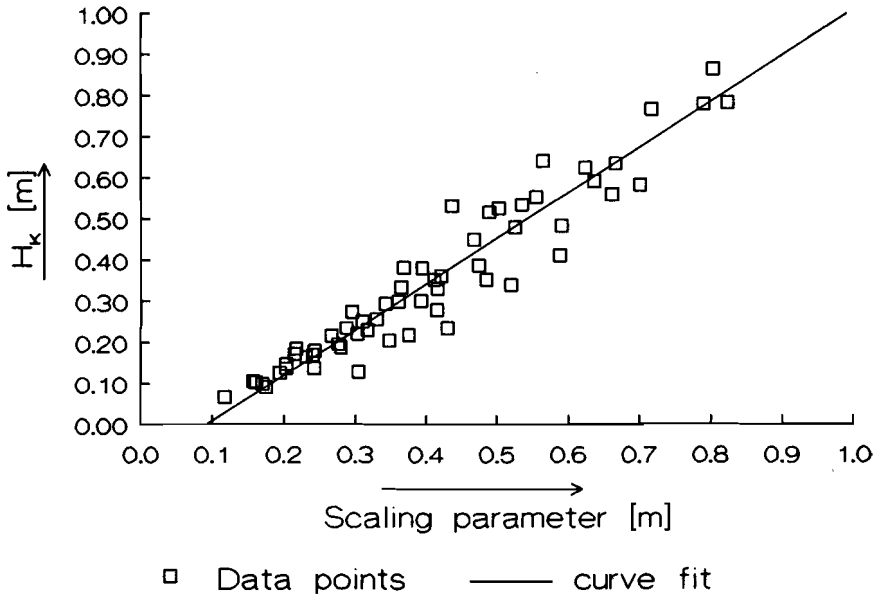


**Figure 4.9**  $H_k$  vs.  $S$  from Fryer and Potter (1976).

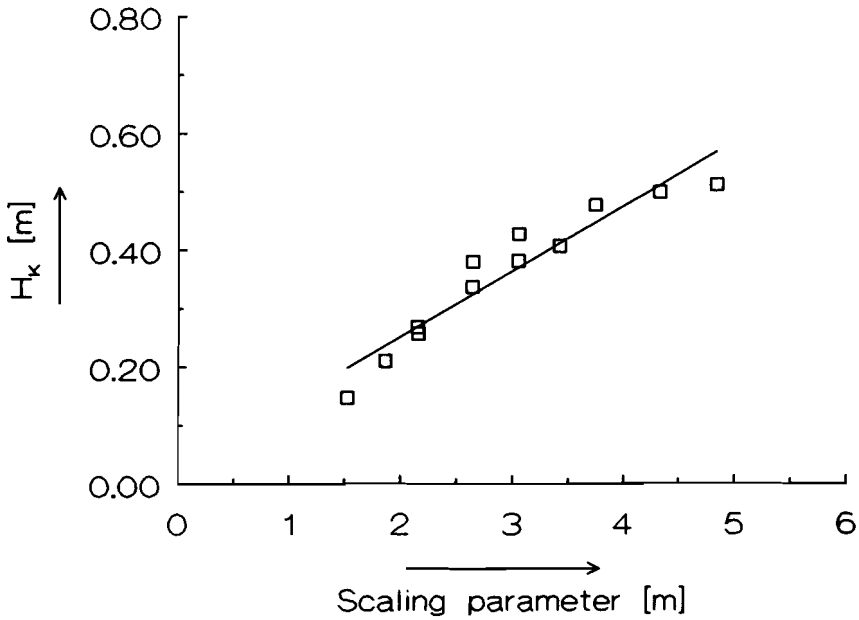


**Figure 4.10**  $H_k$  vs.  $S$  from Boonstra (1983).

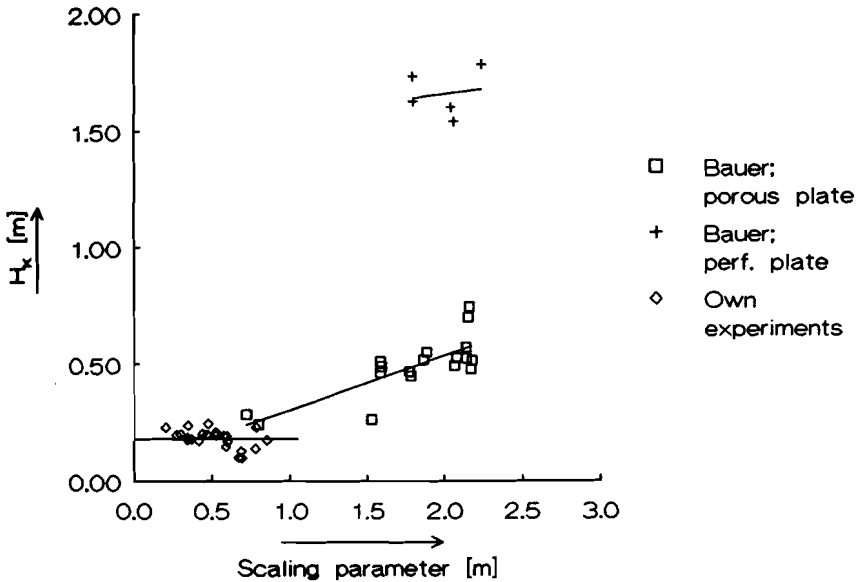


**Figure 4.11**  $H_k$  vs.  $S$  from Bauer (1980) and our own experimental work (see chapter 3).

Distributor (porous plate), catalyst (quartz sand) and reaction type (ozone decomposition) were only the same for the experiments of van Swaij and Zuiderweg (1972), Bauer (1980) and ourselves. Plotting  $H_k$ , from these experiments, as a function of  $d_p$  with constant Scaling parameter  $S$ , confirmed our calculations for A and fine B powders described in chapter 1. From fig. 4.12 it can be seen that  $H_k$  indeed rises with increasing particle size. A relatively small  $S$  value corresponds to a small reactor, a small  $U/U_{mf}$  value and a large  $N_r$  value. Therefore fig. 4.12 also shows that very small scale experiments (with reasonable  $U/U_{mf}$  and  $N_r$  values) are not suited for investigating the influence of  $d_p$  on  $H_k$ . This was also found by de Groot (1967).

Data from Calderbank et al. (1967) and Orcutt et al. (1962) have to be considered with a great reserve, because they used an alumina catalyst. This catalyst shows a great tendency of adsorption, which can influence the measurements of mass transfer rates considerably (Bohle and Van Swaij

(1978)). However, the tendency of increasing  $H_k$  with increasing particle size is also found from these experiments (fig. 4.6).

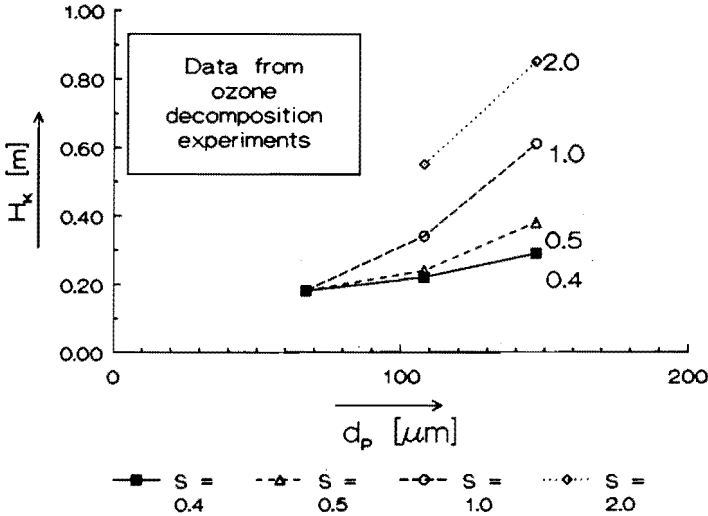


Figure 4.12 Height of a mass transfer unit versus mean particle size, with constant Scaling parameter. From various authors. See text.

Massimilla and Johnstone (1952) did not report sufficiently on the experimental conditions they used. The data from fig. 4.2 have all been calculated from their original given flows. The reaction rate constant was taken from Kunii and Levenspiel (1969). Later, Werther and Hegner (1980) recalculated the flow and reaction data. When using this approach, virtually all the  $N_r$  values became less than 1, which means that these data can not be used. Therefore fig. 4.2 has to be considered with some reservation.

Figure 4.1 shows results from Lewis et al. (1955). They used a cylindrical reactor with a diameter of only 5 cm, with and without baffles. This reactor seems to be so small that slugging must have occurred regarding the velocities they used. Certainly the reactor with baffles must have been in a slugging regime. This may be the reason for the negative slope of the curve

for the reactor with baffles.

Results from de Groot (1967) (fig. 4.5) indicate that for a sufficiently large scale the influence of the distributor plate becomes negligible. Extrapolation of the curve fit for the porous plate data appears to fit the data for the perforated plate. This is not surprising, because after a certain rising time the influence of the initial bubble size will be insignificant. The smaller the height at which the stable bubble diameter is reached, the smaller the influence of bed height will be. Then again the results from Bauer (1980) (fig. 4.11) show that, when the scale is not that large, the influence of the initial bubble size (dominated by the distributor type) can have a large influence.

Data from Van Den Aarsen (1985) and Roes and Garnier (1986) were originally not used for the statistical analysis. Plots of  $H_k$  versus  $S$  calculated from data of these publications are shown in the figures 4.13 and 4.14.

Van Den Aarsen (1985) used the oxidation of carbon monoxide as a first order chemical model reaction. Experiments were performed in a bench scale 3 cm diameter reactor and a reactor with a diameter of 30 cm. Four particle sizes were used:  $d_p = 55 \mu\text{m}$ ,  $U_{mf} = 0.0016 \text{ m/s}$  (in the 3 cm bed);  $d_p = 250 \mu\text{m}$ ,  $U_{mf} = 0.085 \text{ m/s}$  (in the 3 cm bed);  $d_p = 80 \mu\text{m}$ ,  $U_{mf} = 0.018 \text{ m/s}$  (in the 30 cm bed);  $d_p = 325 \mu\text{m}$ ,  $U_{mf} = 0.21 \text{ m/s}$  (in the 30 cm bed). The number of reaction units were calculated from the given bed heights and not from the minimum fluidization bed height, because this was not given. The difference will not be very great. Bed heights were  $\sim 5.5 \text{ cm}$  in the 3 cm reactor and  $0.24 \text{ m}$  and  $0.55 \text{ m}$  for the  $80 \mu\text{m}$  particles in the 30 cm bed and  $\sim 0.4 \text{ m}$  and  $\sim 0.85 \text{ m}$  for the  $325 \mu\text{m}$  particles in the 30 cm bed. Fig 4.13 shows that  $H_k$  for the  $325 \mu\text{m}$  particles was almost equal to those of the  $80 \mu\text{m}$  particles at a given scaling parameter. Combined with fig. 4.12 this indicates that the height of a mass transfer unit decreases with increasing particle size after passing through a maximum.

Roes and Garnier (1986) did residence time distribution measurements with Helium as tracer and nitrogen as fluidizing gas. They used two limestone powders of  $102 \mu\text{m}$  (A powder) and  $14 \mu\text{m}$  (C powder). The bed heights were  $1.17 \text{ m}$  and  $1.78 \text{ m}$  respectively. The minimum fluidization velocities were not given but were estimated from their data to be  $0.008 \text{ m/s}$  and  $\sim 0.007 \text{ m/s}$  respectively. Results of the cohesive powder have to be considered with some



reservation. Because of its cohesiveness strange (and unknown) phenomena may occur. Especially the cracks occurring in this type of powder seem to introduce a second short cut for the gas (beside the bubbles). The results for the 102  $\mu\text{m}$  can be fitted very well by equation 4.3.

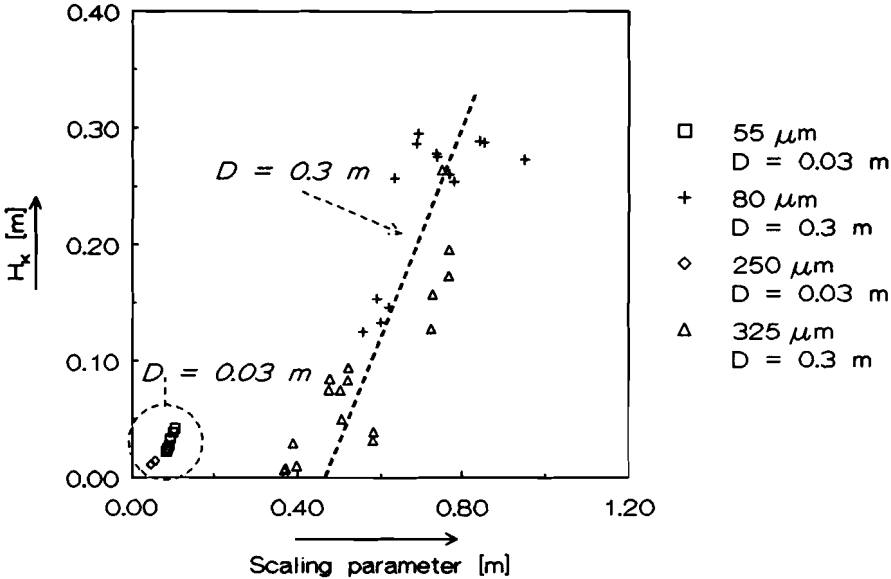


Figure 4.13  $H_k$  vs.  $S$  from Van Den Aarsen (1985). Four different particle sizes were used. Bed diameter  $D$  is given in the figure.

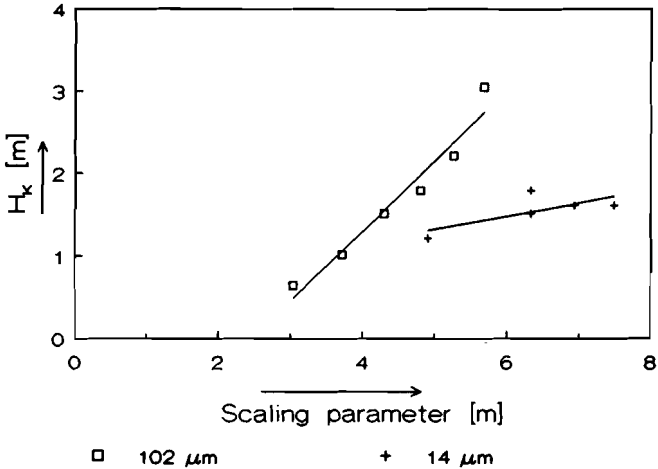


Figure 4.14  $H_k$  vs.  $S$  from Roes and Garnier (1986). See text.

#### 4.4. Conclusions

Values for the height of a mass transfer unit ( $H_k$ ) obtained from our experiments and a large number of literature data were analyzed. All these data could be correlated with the scaling parameter  $S$ .

The constants  $c_1$  and  $c_2$  can be obtained from small scale experiments, provided the scale is not too small. Therefore we believe that equations 4.1 to 4.3 can be useful in the scale up of fluidized beds. But the range in which equations 4.1 to 4.3 were tested has to be considered:  $0.03 \text{ m} < D < 1.5 \text{ m}$ ,  $0.055 \text{ m} < H < 4.9 \text{ m}$ ,  $1.2 < U/U_{mf} < \sim 35$  and  $1 < N_r < 133$ .

It was shown that for A/B type powders  $H_k$  increases with increasing particle size, which was in agreement with the theoretical considerations discussed in chapter 1. This shows that particle size selection is an important factor for improving the conversion in a fluidized bed. The particle size distribution also can have an effect on conversion (Sun and Grace (1990)). In this thesis only the average particle size are considered.

To determine whether the theoretical trend discussed in chapter 1 is confirmed for larger particles, experiments were performed with a residence time distribution method. The Scaling parameter can now be used for evaluating these experiments. This will be discussed in the next chapter.

### 5.1 Introduction

As was described in chapter 2, residence time distribution (RTD) measurement is an experimentally relatively simple method for determining the mass transfer and gas flow division. An amount of tracer is injected into the reactor, in such a way that the tracer is distributed evenly below the bottom plate and the response is measured in the exit flow.

The measured RTD curves were described with the model given in chapter 1. To solve the time dependent model equations, the numerical technique discussed in chapter 2 was used.

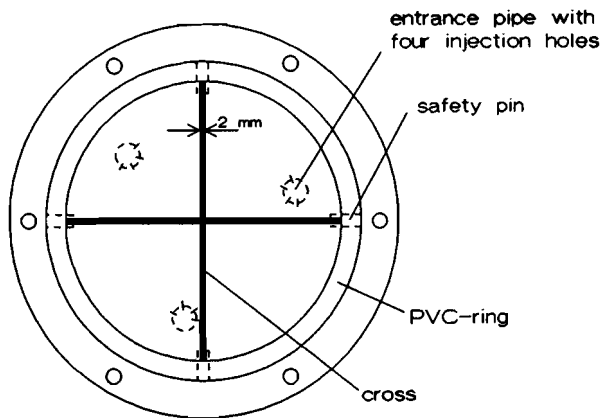
First the equipment will be discussed, followed by the measuring and analysis technique. Finally the results and conclusions will be presented.

### 5.2 Experimental

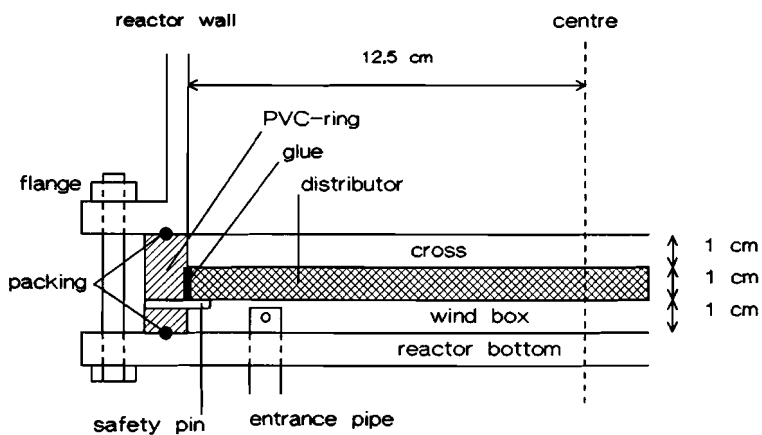
#### 5.2.1. The fluid bed reactor.

All experiments that will be discussed in chapters 5 and 6 were performed in a stainless steel cylindrical column with a diameter of 25 cm and a length of 160 cm. The fluidizing air was obtained from the 7 atm central air distribution system.

The distributor section was constructed in such a way that a homogeneous distribution of fluidizing air and tracer was ensured (fig. 5.1). The distributor was a porous polyethylene plate (Flexolith H) with a thickness of 10 mm. The windbox had a diameter of 25 cm and a height of 1 cm. This height was chosen to make sure that the residence time in the windbox was that small that this would not influence the measurements. The air entering the windbox was divided over three single tubes, at the end provided with 4 radial holes, each of 5 mm diameter. The tubes were placed so that the air was distributed evenly in the windbox (fig. 5.1).



**upper view**



**side view**

**Figure 5.1** *Construction of the distributor section.*

The distributor plate was glued in a PVC ring. To obtain a rigid construction a stainless steel cross with a height of 10 mm and a thickness of 2 mm was placed above the distributor plate and 4 supporting pins were mounted under it.

A general schematic drawing of the equipment is given in fig. 5.2.

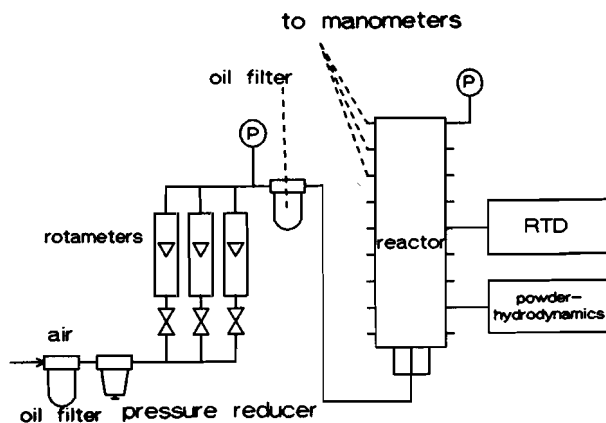


**Figure 5.2** Schematic drawing of the equipment used for RTD and for hydrodynamic measurements.

The bed pressure was measured using a water filled manometer system connected to a row of pressure taps. A row of measuring points could be used for a probe. In each row the distance between the taps (holes) was 10 cm.

The fluidizing air was led through two oil filters and through rotameters for measuring the gas flow. The maximum obtainable superficial gas velocity was about 65 cm/s, which was more than sufficient for all experiments. The air left the bed through a dust filter mounted in the top of the reactor. Although this filter gave a small pressure drop, all experiments that will be described were performed under virtual atmospheric conditions.

### 5.2.2. Measuring equipment

A Flame Ionisation Detector (FID) was used to measure the residence time distribution of the methane tracer. Methane was used as a tracer, because it can be detected easily by the FID. Adsorption of methane on the quartz sand particles, used as fluidizing powder, was neglected, based on the work of Drinkenburg (1970) and Cottaar (1985). Air and tracer gas were sucked through a capillary into the FID, which was held at a constant low pressure. This was accomplished by using an aspirator pump and a buffer vessel (fig. 5.3). An I.R. heating was used to avoid condensation of the water formed in the FID. The capillary was constructed so that it could be put horizontally in the bed, just above the bed surface (fig. 5.3b).

The residence time of the gas in the FID was so small that the influence on the overall RTD curve could be neglected. The signal of the FID was amplified and sampled by a computer every 0.09 seconds. If the noise/signal ratio was too high, the measured curve could also be smoothed by the program. The computer was also used to trigger the magnetic valves for the tracer injection.

A rapid mixing of the tracer with the fluidizing air was accomplished by injecting the methane in counter current with the air (fig. 5.3c)

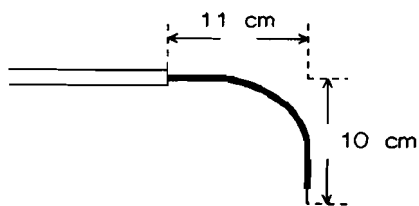
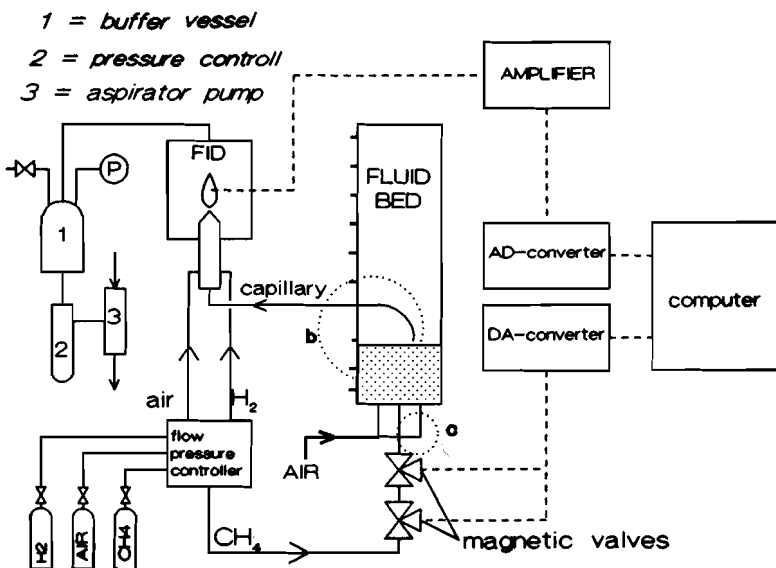


Fig. 5.3b Capillary leading to FID

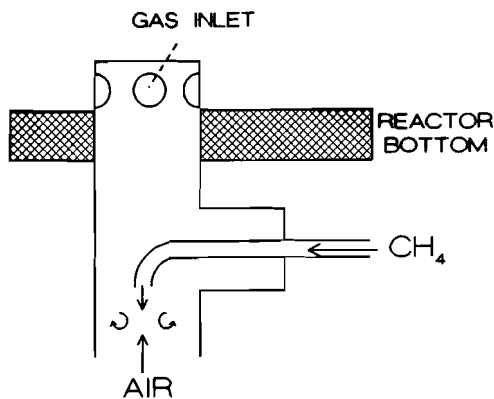


Fig. 5.3c Tracer injection system.

Figure 5.3 Experimental set-up for the RTD measurements.

### 5.2.3. The measurements

The properties of the quartz sand powders used are given in table 5.1. The minimum fluidization velocities and the dense phase porosities were experimentally determined. Particle size distributions can be found in appendix 5.A.

$d_p$ [ $\mu\text{m}$ ]	106	165	230	316	398	587
$U_{mf}$ [cm/s]	1.4	2.3	5.1	6.1	11.2	21.3
$\epsilon_{mf}$ [ - ]	0.54	0.47	0.43	0.42	0.45	0.43

**Table 5.1** *Properties of the quartz sand powders ( $\rho_p = 2650 \text{ kg/m}^3$ ).*

Measurements with all powders were done as a function of bed height and superficial gas velocity. The superficial gas velocity was always larger than the minimum fluidization velocity and was varied between 4 and about 30 cm/s. A superficial velocity smaller than 4 cm/s could not be used, because then the mixing of the tracer in the distributor section was not sufficient. Velocities larger than about 30 cm/s could not be used, because then slugging would set in. Furthermore the gas velocity had to be so high, that the fraction of gas in the bubble phase  $f_b$  was sufficiently large. This meant that for the two largest powders the experimentally possible  $U/U_{mf}$  range was rather small.

The bed height was always adjusted until the capillary was just above the bed surface when fluidizing the powder. If this distance was too large an extra gas mixing would occur due to the erupting bubbles, which would disturb the measurements. During fluidization the bed height of course fluctuated, so that the probe was sometimes just in the bed and sometimes above the bed surface. However, by varying the bed height somewhat, it was found that the residence time distribution curve was not affected by this.

The RTD curves were measured at seven radial positions ( $r = 0, 2, 4, 6, 8, 10$  and  $12$  cm, with  $r = 0$  being the bed centre). An example of differences that could occur at three radial positions is shown in fig. 5.4. As can be



seen from this figure, there can be considerable differences at the various positions. It is therefore essential that measurements are performed as a function of radius  $r$  and not only in just one radial position. Three to five experiments were performed in every radial position. The data were averaged to obtain the average RTD.

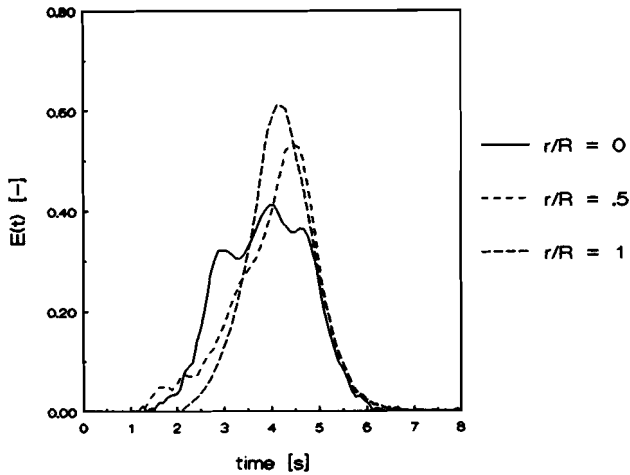


Figure 5.4 RTD for 230  $\mu\text{m}$ ;  $U = 11 \text{ cm/s}$  and  $H = 55 \text{ cm}$ .

To perform computations on mass transfer, the injection pulse has to be known. From experiments performed at various radial positions just above the porous plate, it was found that the distribution of the tracer was indeed uniform (fig. 5.5). Even the amount of tracer was found to be equal at all single radial positions. The injection pulse was measured for every powder and for every condition. The data were then fed to the numerical program and used for computation of the RTD curves.

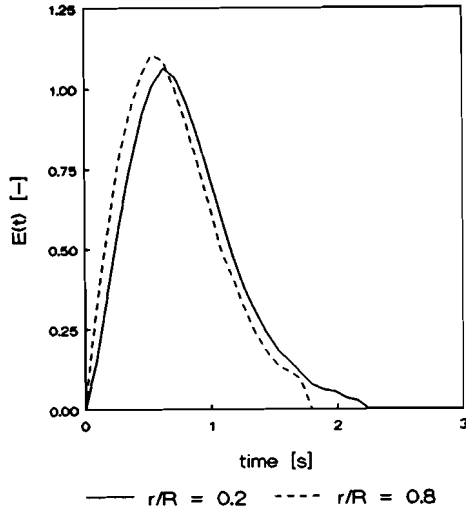


Figure 5.5 Injection pulse at two radial points.

#### 5.2.4. Data processing

The average concentration  $\bar{c}(t)$  has to be calculated by (Westerterp, Van Swaij and Beenackers (1984)):

$$\bar{c}(t) = \frac{\iint_{\partial A} c_1(t) \cdot u_1 \cdot \partial A}{\iint_{\partial A} u_1 \cdot \partial A} \quad (5.1)$$

where  $u_1$  is the local gas velocity,  $c_1$  the local concentration and  $\partial A$  a surface area segment. The average  $E(t)$  curve is defined by (also chapter 2):

$$E(t) = \frac{\bar{c}(t)}{\int \bar{c}(t) \cdot dt} = \frac{\frac{\iint_{\partial A} c_1(t) \cdot u_1 \cdot \partial A}{\iint_{\partial A} u_1 \cdot \partial A}}{\iint_{\partial A} \frac{\int c_1(t) \cdot u_1 \cdot \partial A \cdot dt}{\int u_1 \cdot \partial A \cdot dt}} = \frac{\int N_1(t)}{\int N_1(t) \cdot dt} \quad (5.2)$$

The local gas throughflow (in  $[m^3/s]$ ) is given by  $u_1 \cdot \partial A$  and therefore  $\iint_{\partial A} c_1 \cdot u_1 \cdot \partial A$  is the number of moles passing per unit of time ( $N_1$ ). Because the FID measures an amount of tracer, the average RTD value at a given time was

determined by adding all measured values and normalizing by the total amount of values:

$$E(t) = \frac{M_1(t) + M_2(t) + \dots + M_n(t)}{\sum_{i=1}^n M_i(t) \cdot \Delta t} \quad (5.3)$$

(In our case  $n = 7$  in equation 5.3)  $M_i(t)$  gives the response (measured in real time) at radial position  $i$ .

The average residence time was calculated by:

$$\tau = \int_0^{\infty} t \cdot E(t) \cdot \Delta t \quad (5.4)$$

The equations described in chapter 2 were used to compute a RTD curve with given parameter values. The dispersion terms were neglected ( $Pe_b$  and  $Pe_d$  were taken to be infinite: ideal plug flow). The reason for this has been discussed extensively in chapters 2 and 3.

For the minimization it was essential that the average residence times of the computed and measured curve were identical, because otherwise it was not possible to compare both curves. This was more practical if the computations were performed in real time. In practice the two average residence times were never exactly the same, due to inaccuracies in measured parameter values and in the measured RTD curves. The time difference was in most cases  $\pm 0.5$  second. With the computations the time difference was subtracted (or added) from (to) the computed curve. This of course also can be done with the measured curve.

The least squares minimization was performed with two degrees of freedom: the  $\phi$  factor (to draw more conclusions on the gas flow division) and the number of mass transfer units. More degrees of freedom would cause insufficient accuracy. A simulated curve was minimized and it was found that the error the minimization returned was about 20 %. This means that the error in the number of mass transfer units and  $\phi$  were about 20 %. All computations were performed on a VAX/VMS main frame computer.

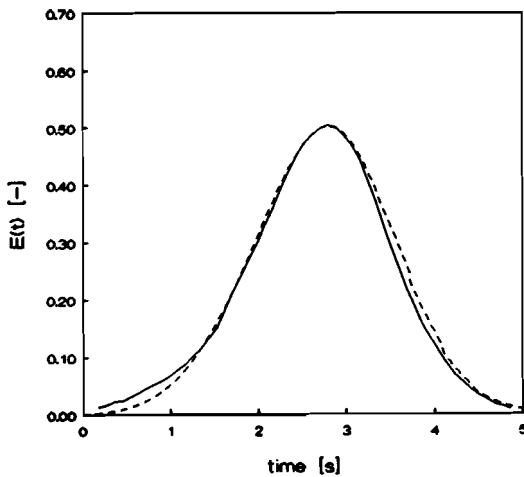
Some computations were also performed with the Crank-Nicholson technique and the resulting  $E(t)$  curves were identical.

### 5.3. Results and discussion.

The boundaries for the minimization were  $0.01 \leq N_k \leq 20$  and  $1 \leq \varphi \leq U/U_{mf}$ . The starting values were  $N_k \sim 1-5$  and  $\varphi = 1$ . The dense phase porosity at minimum fluidization velocity was used for  $\epsilon_d$ . The bubble hold up  $\delta$  was measured from the bed expansion. The accuracy of the minimization was expressed in terms of the sum of squares, which is the sum of the squares of the difference between computed and measured curves at a given time  $t$ .

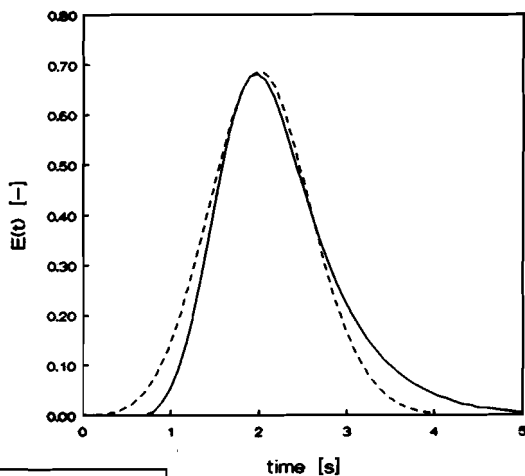
In general it was found that for larger particles it became more difficult to obtain accurate results, due to the constraints on bed height and superficial velocity.

Examples of measured and calculated curves are shown in the figures 5.6a to 5.6c. From these figures it can be seen that for our computations a sum of squares value of about 0.15 still is acceptable. Although the sum of squares value of 0.21 (fig. 5.6c) appears to be relatively high, it can be seen that the tail of the curve is fitted rather well and that only the fit at the top is not good. It was therefore decided to take computations that returned a sum of squares of about 0.2 - 0.25 into consideration with an appropriate reserve. This occurred, however, only twice for the 106  $\mu\text{m}$  particles. The returned values, however, fitted very well in the overall picture and therefore these computations were used. The same holds for two results for the 165  $\mu\text{m}$  particles, where sum of squares of 0.35 and 0.39 were returned. Although this appears to be relatively high, again the returned mass transfer values fitted well in the general picture for these particles. Again these results were used but they should be considered with some scepticism. A summary of the experiments performed and the results are shown in table 5.2a - 5.2e.



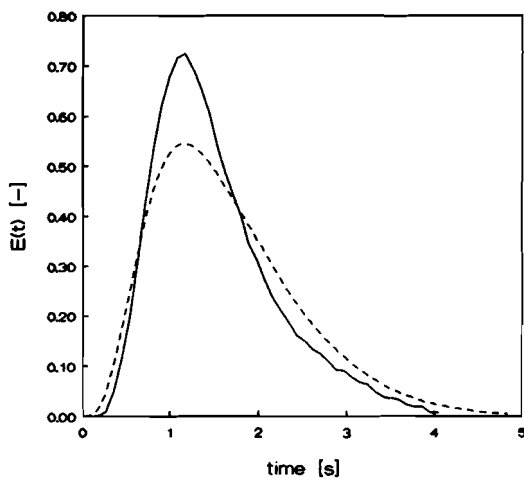
←

**5.6a** Sum of squares = 0.01  
 (230  $\mu\text{m}$ ,  $U = 7.5$  cm/s,  
 $H = 55$  cm)



→

**5.6b** Sum of squares = 0.11  
 (230  $\mu\text{m}$ ,  $U = 7.8$  cm/s,  
 $H = 25$  cm)



←

**5.6c** Sum of squares = 0.21  
 (165  $\mu\text{m}$ ,  $U = 14.6$   
 cm/s,  $H = 25$  cm)

**Figure 5.6** Comparison of some calculated and measured curves.

H [cm]	U [cm/s]	$\delta$ [-]	$N_k$	$\varphi$	sum of squares	$H_k$ [cm]	S [cm]
25	4.20	0.082	2.14	1.00	0.222	11.68	43.30
	5.70	0.089	2.33	1.00	0.200	10.73	50.44
	8.69	0.090	2.33	1.00	0.0321	10.73	62.29
	10.60	0.093	2.36	1.00	0.0369	10.59	68.79
55	5.55	0.052	5.85	1.00	0.109	9.40	73.83
	14.6	0.116	5.77	1.00	0.032	9.53	119.7
95	5.35	0.05	8.16	1.00*	0.0273	11.64	95.27
	14.2	0.09	12.6	1.00*	0.0657	7.54	155.21

**Table 5.2a** Results for quartz sand 106  $\mu\text{m}$ .  $U_{mf} = 1.4 \text{ cm/s}$ ,  $\epsilon_d = 0.54$ .

\* means that minimization was done with  $\varphi$  fixed to 1. See text.

H [cm]	U [cm/s]	$\delta$ [-]	$N_k$	$\varphi$	sum of squares	$H_k$ [cm]	S [cm]
25	4.9	0.053	4.80	1.00	0.030	5.2	36.5
	9.8	0.093	2.53	1.00	0.39 (!)	9.9	51.6
	14.0	0.128	1.18	1.00	0.21	21.2	61.7
	19.4	0.164	0.80	1.00	0.020	31.3	72.6
55	4.7	0.053	1.65	1.00	0.090	33.3	53.0
	5.7	0.057	2.13	1.01	0.022	25.8	58.4
	9.3	0.096	1.45	1.00	0.35 (!)	37.9	75.8
	9.9	0.111	1.22	1.00	0.0085	45.1	76.9
	14.0	0.118	1.18	1.00	0.06	46.6	93.4
75	8.6	0.096	1.36	1.01	0.049	55.15	83.4
	10.9	0.114	1.80	1.00	0.091	41.67	94.4
115	4.15	0.052	2.90	1.00	0.067	39.7	72.0
120	6.0	0.083	2.60	1.05	0.064	46.0	88.5
125	8.0	0.106	2.04	1.20	0.104	61.0	104.45

Table 5.2b Results for quartz sand 165  $\mu\text{m}$ .  $U_{mf} = 2.3 \text{ cm/s}$ .  $\epsilon_d = 0.47$ .

H [cm]	U [cm/s]	$\delta$ [-]	$N_k$	$\varphi$	sum of squares	$H_k$ [cm]	S [cm]
25	7.8	0.027	1.59	1.07	0.11	15.7	30.9
	11.2	0.083	1.17	1.00	0.16	21.4	37.0
	14.1	0.109	1.29	1.00	0.11	19.4	41.6
55	7.5	0.057	1.64	1.05	0.01	33.5	45.0
	11.0	0.096	1.19	1.00	0.02	46.2	54.5
	14.6	0.113	0.76	1.00	0.04	72.4	62.7

Table 5.2c Results for quartz sand 230  $\mu\text{m}$ .  $U_{mf} = 5.1 \text{ cm/s}$ .  $\epsilon_d = 0.43$ .

H [cm]	U [cm/s]	$\delta$ [-]	$N_k$	$\varphi$	sum of squares	$H_k$ [cm]	S [cm]
24	12.1	0.050	1.14	1.28	0.017	21.05	35.7]*
			2.59	1.00	0.025	9.27	
25	15.2	0.081	4.12	1.00	0.108	29.96	59.06
55	11.5	0.068	1.90	1.04	0.022	28.95	52.67
			17.0	0.109	0.89	1.14	
			1.05	1.00	0.028	52.38	
	14.5	0.094	0.73	1.20	0.049	74.93	59.14]*
			1.15	1.00	0.079	47.83	
	20.5	0.128	1.20	1.02	0.0052	45.83	70.32
72	14.1	0.067	1.47	1.02	0.040	48.98	66.73
74	16.6	0.092	1.82	1.07	0.060	40.66	73.40

**Table 5.2d** Results for quartz sand 316  $\mu\text{m}$ .  $U_{mf} = 6.1 \text{ cm/s}$ .  $\epsilon_d = 0.42$ .

] \* means that the minimization has also been performed with  $\varphi$  fixed to 1 and only  $N_k$  has been used as degree of freedom. See text.

H [cm]	U [cm/s]	$\delta$ [-]	$N_k$	$\varphi$	sum of squares	$H_k$ [cm]	S [cm]
65	22.5	0.093	1.10	1.00	0.017	59.0	57.2
			1.66	1.03	0.060	39.2	57.2
75	22.4	0.105	2.67	1.04	0.013	28.1	61.2

**Table 5.2e** Results for quartz sand 398  $\mu\text{m}$ .  $U_{mf} = 11.2 \text{ cm/s}$ .  $\epsilon_d = 0.45$ .  
See text.



Table 5.2a. shows that for the 106  $\mu\text{m}$  the fit in general was quite good (most sum of squares  $\leq 0.1$ ). The returned  $\phi$  values were  $\sim 1$ , which would imply that the two phase theory of Toomey and Johnstone (1952) applies in this case. However, the computational error is about 20 % which means that this can not be concluded with sufficient accuracy. Two results were obtained with  $\phi$  fixed at 1 and only leaving  $N_k$  as a degree of freedom, because minimization with two degrees of freedom took an extensively long time. The minimization with  $\phi$  fixed at 1 returned a very good sum of squares so that the fit was satisfactory. Also all other returned  $\phi$  values were equal to one.

With regard to the 230 and 165  $\mu\text{m}$  particles it can be concluded that the results were quite satisfactory. There were only two relatively high sums of squares for the 165  $\mu\text{m}$  particles and one minimization returned a  $\phi$  value of 1.2. Again the mass transfer results fitted well in the overall picture. However, a certain scepticism seems appropriate concerning these data points. It can be seen that these strange results were found with relatively high bed heights. The larger fluctuations that occur at these bed heights can be an explanation for the reason why so different values were returned, regarding the problems described above.

With the 316  $\mu\text{m}$  powder three dubious ( $N_k, \phi$ ) combinations returned, certainly when compared to the other results. Therefore new minimizations were performed with  $\phi$  set to 1 and leaving  $N_k$  as the only fitting parameter. From the other powders and from the 316  $\mu\text{m}$  powder itself, it could be seen that  $\phi$  had to be in the order of 1. From the returned sum of squares (table 5.2d) it can be seen that this way the computed curves also led to good fits. But even if the dubious data are left out the general picture is not changed.

Due to the constraints on bed height and superficial velocity only a few experiments could be performed with the 398  $\mu\text{m}$  powder. With this powder large bubbles were formed, that gave large fluctuations in bed height, which led to fluctuations in the measured RTD curves and lowered the experimental accuracy.

With the 587  $\mu\text{m}$  powder the fraction of gas in the bubbles ( $f_b \sim 0.15 - 0.25$ ) was too small to determine the number of mass transfer units. Due to this there were no detectable differences between the experiments, although bed heights of 55 and 95 cm and superficial velocities between 22.9 and 29 cm/s were used. The computed and measured curves were identical. Even a variation of  $N_k$  from 0.05 to 10 gave no difference in the computed curves.

The height of a mass transfer unit versus the scaling parameter S for the different particle sizes are shown in fig. 5.7.

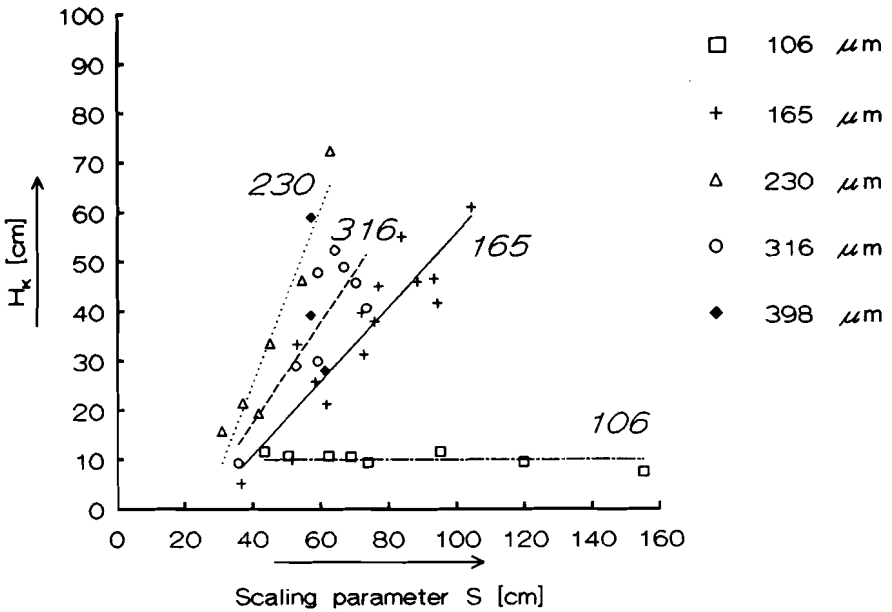


**Figure 5.7**  $H_k$  versus S determined from the RTD measurements. Results for all particles used are shown.

From fig. 5.7 it can be seen that the height of a mass transfer unit  $H_k$  again is linearly dependent on S. A plot of  $H_k$  versus  $d_p$  at a given scaling parameter (fig. 5.8) confirms our initial computations discussed in chapter 1. With increasing particle size the height of a mass transfer unit increases up to a maximum at about 200 - 250  $\mu\text{m}$ . After that  $H_k$  decreases with increasing particle size. Although the results of the 398  $\mu\text{m}$  particles are not very accurate, it can be seen that the average  $H_k$  value of these particles is in the order of the value found for the 316  $\mu\text{m}$  particles. Even when this point is left out, the overall effect appears to be in agreement with the expected trend.

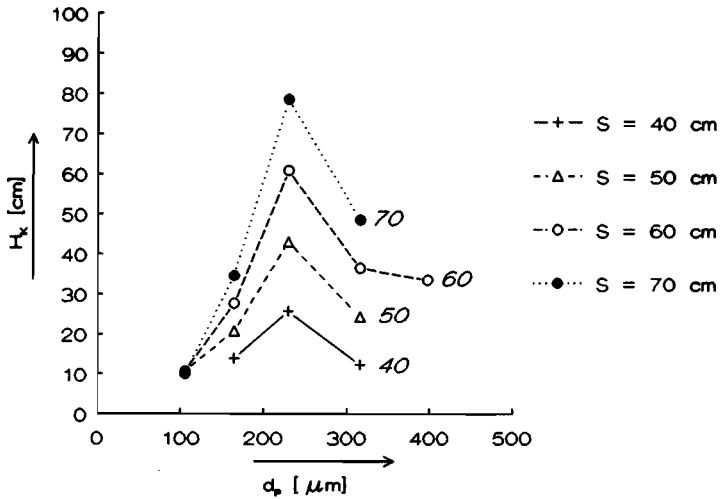


**Figure 5.8**  $H_k$  as a function of particle size  $d_p$ , with constant scaling parameter  $S$ .

#### 5.4. Concluding remarks

To obtain a good tracer distribution a special distributor design was built and tested and it was shown to distribute the tracer uniformly below the porous plate.

One overall RTD curve was obtained from 21 - 35 measurements and a least square minimization was performed with  $N_k$  and  $\varphi$  as the fitting parameters. It was found that the decoupling method could fit the experimental curves. A few computed curves were compared with curves computed with the Crank-Nicholson method and it was found that the results were identical.

More difficulties occurred with increasing particle size, probably due to

the more vehement motion of the bed surface. The results showed clearly that the theoretical predicted trend was correct: with  $H_k$  as a function of particle size  $d_p$ , a maximum in  $H_k$  was found at about 200 - 250  $\mu\text{m}$ . This implies that the theory discussed in chapter 1 can be used for describing the mass transfer from the bubble phase to the dense phase. A problem that remains is the theoretical quantification of the height of a mass transfer unit. For this reason more information is needed concerning the stable bubble diameter, because this determines in a great extent the average specific mass transfer surface. The hydrodynamic measurements performed to obtain this information, are discussed in the next chapter.

**Appendix 5.A.** *The particle size distributions of the powders used.  
From sieve analysis.*

For the 106  $\mu\text{m}$  particles:

Range ( $\mu\text{m}$ )	Weight percentage
< 56	2
56 - 71	4.22
71 - 80	4.38
80 - 90	9.26
90 - 100	7.36
100 - 125	37.06
125 - 160	34.03
160 - 200	1.41
> 200	0.26

For the 165  $\mu\text{m}$  particles:

Range ( $\mu\text{m}$ )	Weight percentage
< 100	0.5
100 - 160	39
160 - 200	49
200 - 315	11
315 - 400	0.5

For the 230  $\mu\text{m}$  particles:

Range ( $\mu\text{m}$ )	Weight percentage
< 100	0
100 - 160	5
160 - 200	22
200 - 315	66
315 - 400	6
400 - 630	1

For the 316  $\mu\text{m}$  particles:

Range ( $\mu\text{m}$ )	Weight percentage
< 125	0.42
125 - 200	6.90
200 - 250	11.3
250 - 300	30.1
300 - 400	40.1
400 - 500	8.22
> 500	3.0

For the 398  $\mu\text{m}$  particles:

Range ( $\mu\text{m}$ )	Weight percentage
< 125	0.4
125 - 200	1.0
200 - 250	2.7
250 - 315	8.9
315 - 400	27.0
400 - 500	42.8
500 - 630	16.0
> 630	1.2

For the 587  $\mu\text{m}$  particles:

Range ( $\mu\text{m}$ )	Weight percentage
< 400	1.4
400 - 450	5.5
450 - 500	5.2
500 - 630	43.2
630 - 710	25.8
800 - 1000	3.0
> 1000	0.2

## CHAPTER 6

### INVESTIGATION ON BUBBLE CHARACTERISTICS AND STABLE BUBBLE HEIGHT

---

#### 6.1. Introduction

As the bubbles rise in the gas fluidized bed, they grow due to coalescence and split due to instabilities at the bubble boundary. At the stable bubble height  $h^*$  there is an equilibrium between these two processes and the maximum stable bubble diameter is reached. This stable bubble diameter determines the average bubble diameter and hence the average specific surface, which is an important factor that influences the overall mass transfer (e.g. Van Swaaij, 1985).

Experimental evidence that a maximum stable bubble diameter appears in fluidized beds was found by Matsen (1973). Several theories were proposed to explain and quantify this phenomenon. Some workers proposed that bubble splitting occurs when particles fall through the bubble roof, others believe that particles are taken upwards from the bubble wake (e.g. Yates, 1983). A qualitative theory has been proposed by Clift et al. (1974), based on Taylor disturbances at the bubble boundary. They showed that if these disturbances increased to a certain limit a bubble would split. It was indeed possible to explain some phenomena qualitatively, but it was not possible to predict the maximum stable bubble diameter. Several authors (e.g. Clift and Grace, 1985) correlated the stable bubble diameter with the terminal settling velocity of the particles, but this correlation has no theoretical background and experimental evidence for this procedure is not available. Quantitative data on the stable bubble height have mostly been based on conversion data combined with a model description (Werther, 1978). It therefore appears that more experimental data are needed.

There have been numerous investigations on the bubble gas flow in a two dimensional gas fluidized bed (Pyle and Harrison (1969), Grace and Harrison (1969), Geldart (1967) and Geldart and Cranfield (1972)). However, wall effects can usually not be neglected and therefore results from these experiments can not simply be extrapolated to three dimensional beds.

The use of visual methods in three dimensional beds is limited. Rowe et al. (1979) used a X-ray method with which it was possible to analyze the

behavior of one or few bubbles in a three dimensional bed. However, hydrodynamics are different in freely bubbling fluidized beds (Clift and Grace (1985)). For these types of beds several methods have been used, such as observation of the bubble eruption diameter (e.g. Argyriou et al., 1971). There is however not a unique relation between the bubble eruption diameter and the actual bubble diameter when the bubble shape is not known. Also this technique only gives information on the bubbles leaving the bed and not on the bubbles still in the bed. Light probes that were put in the bed have been used by Whitehead and Young (1967) and Glicksman and McAndrews (1985).

Another more direct method has been used first by Werther (1972) and later by Fan et al. (1983) and is based on electrical capacity differences between the bubble phase and the dense phase. With this method a small capacitance probe is put in the fluidized bed. Rowe and Masson (1981) did an extensive investigation on the effect of the probe on the bubble shape. They showed that some probes can have a considerable effect on the bubble shape and they suggested that probe and tip should be aligned in the same vertical axis and that the probe should be as small as possible. Clift and Grace (1985) proposed that the use of probes gives information on the flow pattern and the bubble coalescence rate (Fan et al., 1983). We selected the capacitance probe method for obtaining obtain information on the visible bubble gas flow. (Due to the finite size of the probe not all bubbles are detectable and therefore the term visible is used).

## **6.2. Experimental method**

A small capacitive double needle probe (fig. 6.1) was used as the basis of the measurement technique. The probe was shaped so that it was possible to put it horizontally in the bed (which is more stable than vertical) and still have a vertical alignment with a rising bubble (fig. 6.1). A somewhat larger probe than the one used by Werther (1972) was designed, because in our investigations larger particles were used.

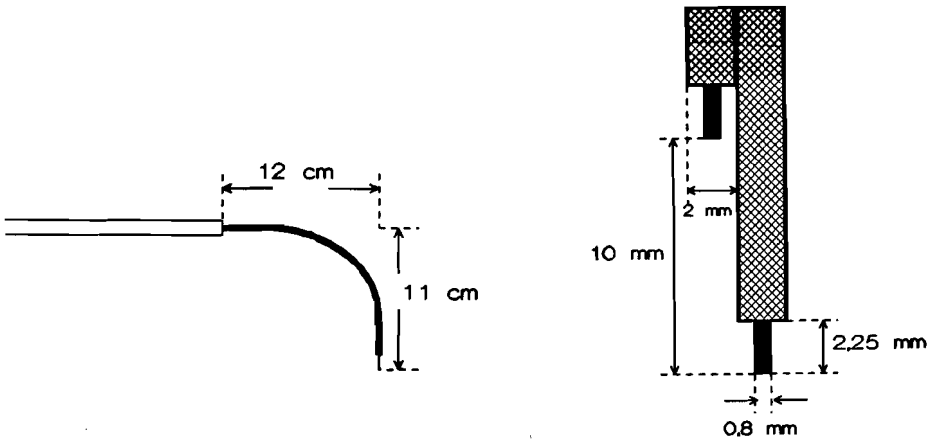


**Figure 6.1** *The capacity probe used in the experiments. A side view (left) and the probe tip (right) are shown.*

In the fluid bed the probe responds to porosity variations in the measuring volume as a function of time. Bubbles striking the probe as they rise cause an electric pulse (fig. 6.2).

When two probes are used with a known vertical distance between the needle tips, the bubble velocity  $u_b$  can be measured. The duration of the bubble signal gives information on the time the probe has been immersed in the bubble (the so called bubble contact time  $t_b$ ). Although the bubble can be pierced in an arbitrary place, the average bubble contact time (combined with the bubble velocity) gives a measure for the bubble size when the shape of the bubble is known.

All experiments were performed in the 25 cm diameter stainless steel bed, described in chapter 5. The solids fluidized were quartz sand powders having an average mean sieve particle size of 106, 165, 230 and 587  $\mu\text{m}$  and a particle density of 2650  $\text{kg}/\text{m}^3$  (see also chapter 5). The experimentally determined minimum fluidization velocities were 1.4, 2.3, 5.1 and 21.3  $\text{cm}/\text{s}$  respectively. The powders were fluidized with air ( $U/U_{mf} \cong 1.08 - 8.4$ ) and at varying bed heights. Measurements were performed at seven radial positions ( $r = 0, 2, 4, 6, 8, 10$  and 12 cm, with  $r = 0$  being the centre of the bed).



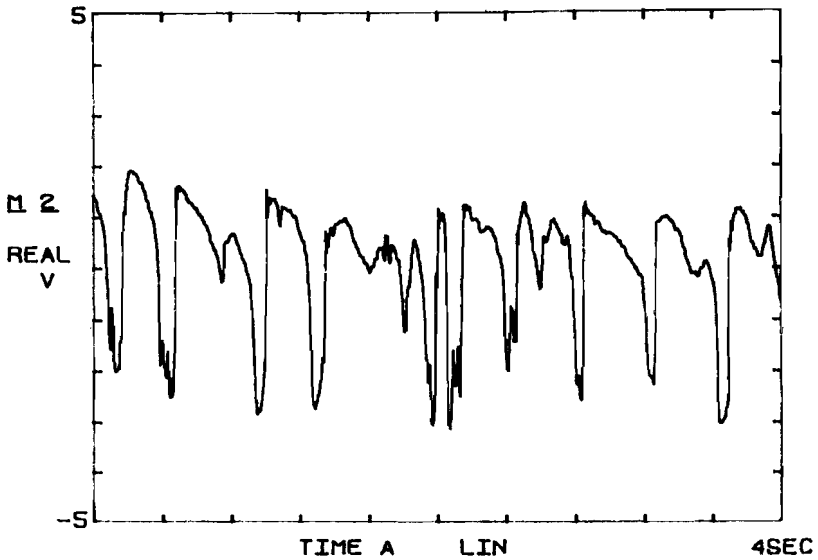


**Figure 6.2** *Example of bubble signal in a heterogeneously fluidized bed.*

A schematic diagram of the equipment is shown in fig. 6.3. The probe was connected to two displacement meters (A and B). The signals were transferred to a Fast Fourier Transform (FFT) analyzer. In order to measure the bubble frequency  $k$  one of the signals was also transferred to a comparator and a pulse counter. This comparator generates a block pulse when the incoming signal exceeds a pre-set level. The pulse duration is as long as the signal exceeds this level. The counter counts the number of block pulses  $n$  in a time  $T$ . The ideal working pre-set level for the comparator was found by using a method developed by Werther (1972) (fig. 6.4): when the level is too low the random noise of the signal generates non-wanted pulses and the measured bubble frequency is too high. When the level is too high none or very few pulses were generated and the measured bubble frequency was too low. In between these two areas there was a region where the frequency was independent of the level. This was the desired pre-set level.

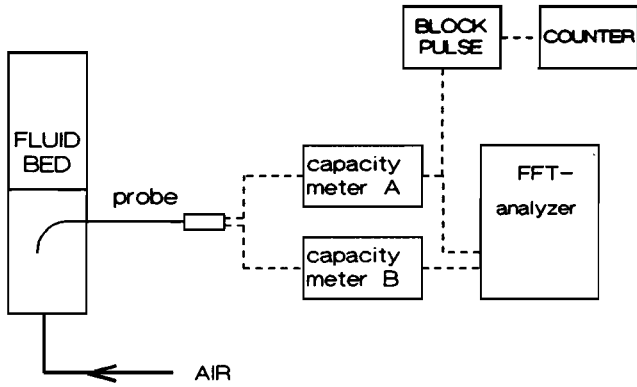


**Figure 6.3** Schematic diagram of the equipment used for hydrodynamic measurements.

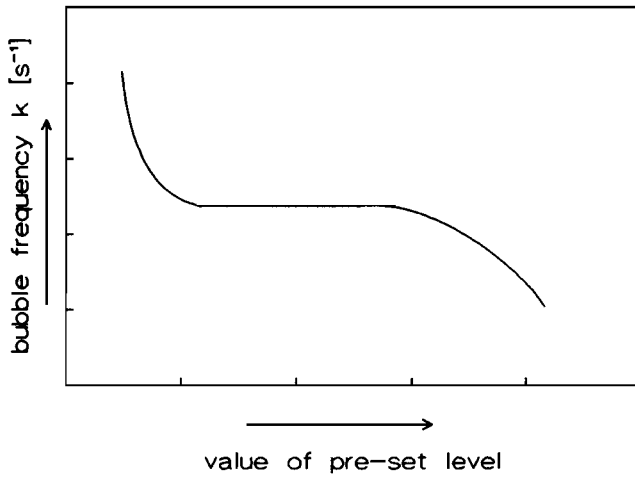


**Figure 6.4** Determination of pre-set level for bubble frequency measurements with comparator.

In a bubbling bed the capacitance probe gave signals as shown in fig. 6.2. For determining the bubble velocity the time difference between the signals of the two probes had to be measured. In principle this can be done by using the cross correlation function  $\varphi_{xy}$ . This function is defined in the following way (e.g. Werther, 1972):

$$\varphi_{xy} = \lim_{T \rightarrow \infty} \frac{1}{2 \cdot T} \int_{-T}^{+T} x(t) \cdot y(t+\tau) \cdot d\tau \quad (6.1)$$

with T being the total measuring time and t the real time. The  $\tau$  value at which the  $\varphi_{xy}$  function shows its maximum is the time difference  $t_a$  between the two signals x and y. The FFT-analyzer had the possibility of measuring this time difference  $t_a$ . A trigger level had to be defined. When a bubble signal passed this level, the total signal was measured during a user defined time (fig. 6.5). It was found that  $t_a$  was strongly dependent on the shape of the signal and that many signals had to be used to obtain an accurate average  $t_a$ .

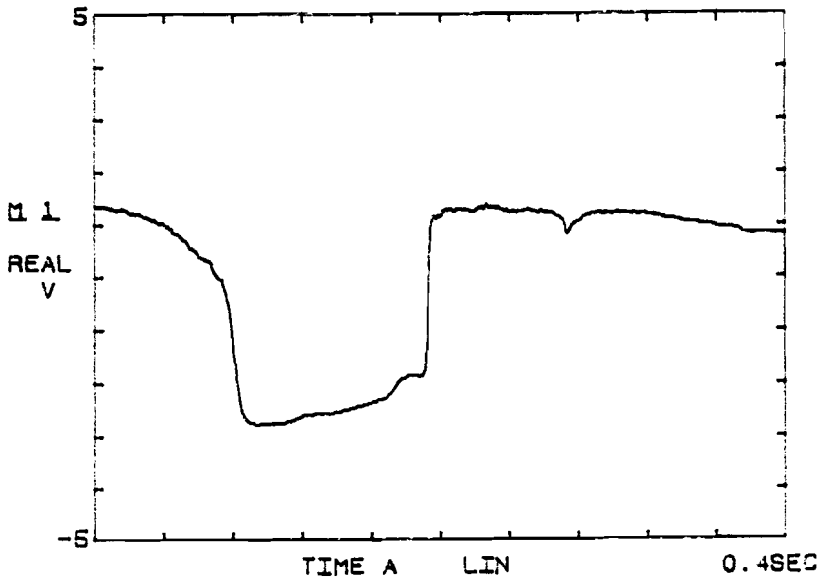


Figure 6.5 Example of a signal of one bubble, after passing the trigger level.

The FFT-analyzer also had the possibility of time averaging the signal. This means that occasional signal fluctuations could be averaged out. Therefore a certain trigger level had to be defined. When the signal from the lower probe (channel A) exceeded this level the averaging of the two bubble signals started. We measured as many bubbles as were needed to obtain an averaged time signal that was stable (which could be monitored constantly). It was found that 128 or 256 bubble pairs were sufficient (the number of bubbles could only be measured in powers of two).

### 6.3. Statistical Signal Analysis

If we consider block pulses it can readily be seen that the time averaged signal is a cumulative pierced length distribution. All bubbles contribute to the averaged signal of probe A at the trigger time  $t_{\text{trig}}$  (fig. 6.6). The bubbles strike the second probe (B) later than the first probe (A). Because the averaging of the two time signals is triggered by the signal of probe A, this means that the time averaged signal of probe B contains a bubble size distribution as well as a bubble velocity distribution (fig. 6.6). To describe both signals, the following assumptions were made:

1) *The bubble size and velocity were both described with a log-normal distribution, defined by (Pollard, 1977):*

$$f(x) = \frac{1}{(x - \theta) \cdot \sigma \cdot \sqrt{2\pi}} \cdot \exp \left[ - \frac{(\ln(x - \theta) - \mu)^2}{2 \cdot \sigma^2} \right] \quad (6.2)$$

$\mu$  = average value of log-normal distribution

$\sigma$  = deviation of log-normal distribution

$\theta$   $\left\{ \begin{array}{l} = \text{starting value of the distribution for which } f(x) > 0 \\ = 0 \text{ in many cases} \end{array} \right.$

with  $f(x)$  being the possibility of finding a value  $x$ . In this case  $\theta = 0$ , because it is impossible to find velocities and sizes that are smaller than zero.

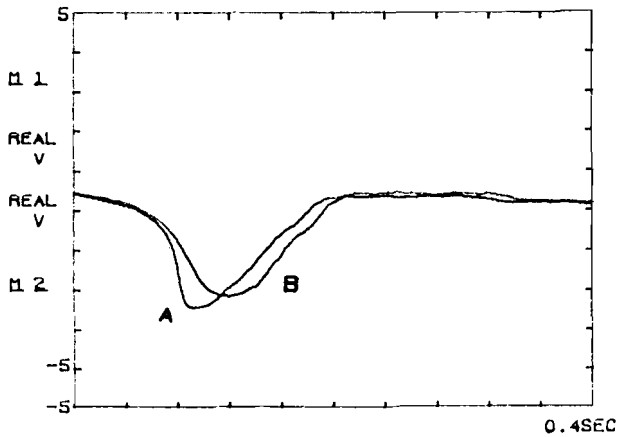
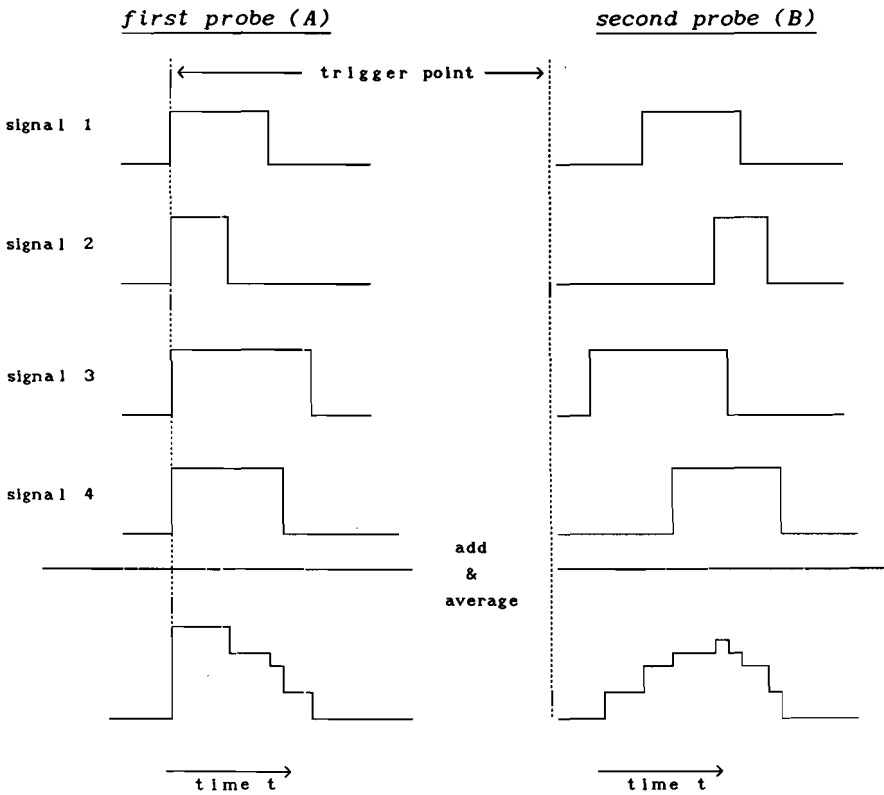


Figure 6.6 Schematic presentation of how the time averaged signal is determined. Experimentally determined curves are shown below.

Werther (1972) found a log-normal distribution in rising velocities for the bubbles. We measured  $t_b$  values by analyzing signals of many individual bubbles. Figure 6.7 shows that the found probability curve can also be described by a log-normal distribution. The real average  $M$  and deviation  $S_a$  can be found from (Pollard, 1977):

$$M = \theta + \exp \left\{ \mu + \frac{1}{2} \cdot \sigma^2 \right\} \Rightarrow$$

$$M = \exp \left\{ \mu + \frac{1}{2} \cdot \sigma^2 \right\} , \quad \text{because in this case } \theta = 0. \quad (6.3)$$

$$S_a^2 = \exp(2\mu) \cdot \exp(\sigma^2) \cdot [\exp(\sigma^2) - 1] \quad (6.4)$$

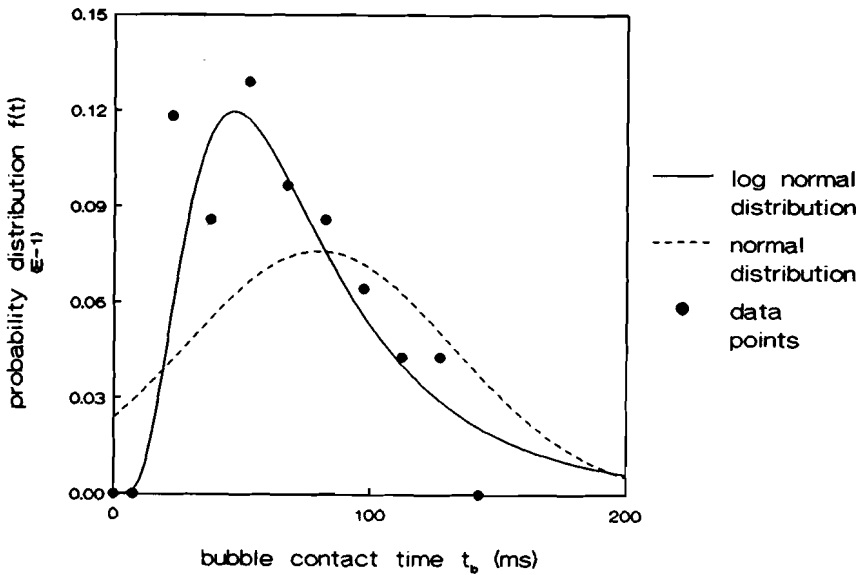


**Figure 6.7** Experimentally determined probability distributions for bubble contact time  $t_b$ . Both distributions were calculated from the average and standard deviation of the data points.

2) Rising time  $t_a$  and bubble contact time  $t_b$  were taken to be stochastically independent. Although bubble diameter and rising time are interdependent, rising time and bubble contact time are not because a bubble is pierced in an arbitrary place.

3) The average bubble time signal of the lower and upper probes were equal. This is of course essential, because if this was not the case it would mean that something happened between the two probe points and the second signal could not be analyzed using the first signal. For an individual bubble the two signals do not have to be equal because each probe can pierce the bubble at a slightly different place. It was indeed found by observing the probe signal that the two individual signals were not always the same, but that the averaged signals were virtually the same as is shown in fig. 6.8. This was checked for several conditions.

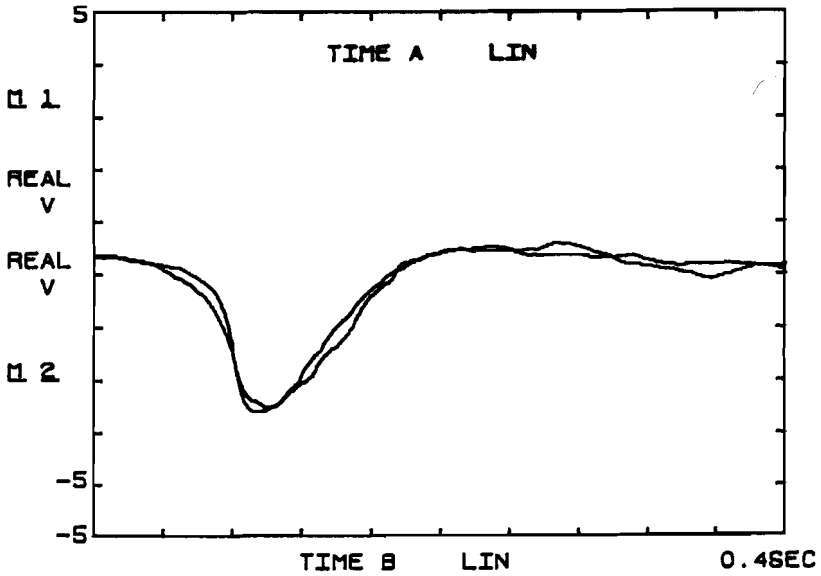
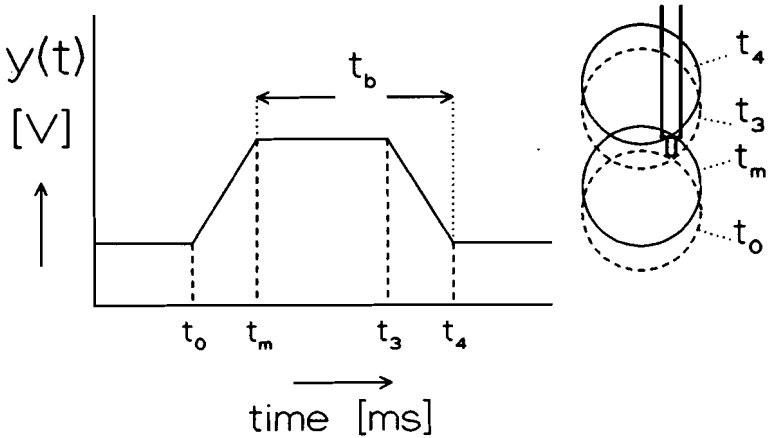


Figure 6.8 Comparison of time averaged signals for the two probes.

4) The signal was assumed to be trapezium shaped. The same description was used as the one given by Werther (1972) (fig. 6.9). He argued that  $\alpha = \ell/u_b$ , where  $\alpha$  is the trapezium slope and  $\ell$  is the probe length. This is

only true for a sudden change from the bubble to the dense phase. In reality this change will be more gradual, hence the slope will indicate an underestimated bubble velocity. That the signal was indeed trapeziumlike is shown in fig. 6.5.



**Figure 6.9** Schematic presentation of trapezium and the corresponding bubble.

The time at which the bubble first reached the lower probe is called  $t_0$  (fig. 6.9). As the bubble rose the amplitude of the signal became larger, until a maximum value was reached at  $t_m$ . When the probe reached the "bottom" of the bubble at  $t_3$ , the signal started to descend, until the bubble had passed the probe completely at  $t_4$ . The bubble contact time  $t_b$  is the time the bubble needs to pass the probe tip completely, being  $t_3 - t_0$  (or  $t_4 - t_m$ ). The process was described mathematically by the following equations:

$$y(t) = 0 \qquad (t < t_0 \text{ and } t > t_4) \qquad (6.5a)$$



$$y(t) = \frac{(t - t_0)}{(t_m - t_0)} \cdot y_{\max} \quad (t_0 \leq t \leq t_m) \quad (6.5b)$$

$$y(t) = y_{\max} \quad (t_m \leq t \leq t_3) \quad (6.5c)$$

$$y(t) = \frac{(t - t_4)}{(t_3 - t_4)} \cdot y_{\max} \quad (t_3 \leq t \leq t_4) \quad (6.5d)$$

The FFT-analyzer determined the average signal by adding the individual signals and dividing the sum by the total number of signals:

$$\overline{y(t)} = \frac{\sum_{i=1}^n y_i(t)}{n} \quad (6.6)$$

with  $n$  being the number of signals and  $\overline{y(t)}$  the averaged time signal.

The signals of the lower probe were all triggered at  $t_0$ , so the first slope is the averaged slope of the signal. All bubbles made contact with the probe at  $t_m$ , giving a maximum  $y$  value of  $y_{\max}$  at this time value. The probability that a bubble hits the probe at  $t_m$  is therefore equal to one. When a bubble with the largest contact time had passed the probe the time averaged signal would of course be equal to zero, meaning that the probability of finding bubbles with an even larger time was also equal to zero. The time averaged signal is therefore related to a cumulative distribution function of the bubble contact times. This can be shown by:

$$P(t_b \leq t) = F(t) = \int_0^t f(t)dt =$$

$$= \frac{\text{number of signal values corresponding to a bubble contact time } \leq t}{\text{total number of measured signals}} \quad (6.7a)$$

$$= \frac{\sum_{i=1}^n y_i(t_b \leq t)}{n} \quad (6.7b)$$

with  $P(t_b \leq t)$  being the probability of finding  $t_b$  values less than or equal to a given  $t$  value and  $F(t)$  the cumulative distribution function. If we put the zero-point of the curve at  $t_m$ , the cumulative distribution function was given by the following equation:

$$F(t) = 1 - \frac{y(t)}{y_{\max}} \quad (6.8)$$

$F(t)$  could also be calculated by numerical integration of  $f(t)$  (eq. 6.2). Average and deviation of the bubble contact time were found by fitting several points of the averaged curve, using equations 6.3 and 6.4.

The signal of the second probe tip (B) was determined after the rising time  $t_a$ : at a time  $(t_0 + t_a)$  the signal of the second probe started to change. Because there is a probability distribution for the rising velocity, this means that not all bubbles hit the probe at a certain time, hence there is no point on the averaged curve of the second probe that gives a "hit-probability" of one. The curve is however related to the cumulative distribution function of bubble contact time and rising time, but these distributions could not be determined directly from the curve as was the case for the first probe (A).

This problem was solved by simulating the averaged signal of the second probe with a computer program. The bubble contact time distribution determined from the first probe was used to generate simulated signals. The average and deviation in the rising time  $t_a$  were varied and the signal of the second probe was simulated by adding the signals and dividing by the total number of generated signals.

The complete scheme for obtaining the average and the standard deviation of the bubble contact time  $t_b$  and rising time  $t_a$  was:

i) The measured signals on the FFT-analyzer were described by taking several points of the curves.

ii)  $t_0$ ,  $t_m$  and the slope of the trapezium were determined from the averaged signal of the first probe (A). By extrapolating the first slope to zero,  $t_0$  was determined. Extrapolating to  $y_{\max}$  (that was measured directly) gave  $t_m$ .

iii) For  $t \geq t_m$  the curve was equal to  $1 - F(t)$ . Six to nine points were taken to describe the curve for  $t > t_m$ . Using equation 6.5 the curve was fitted with a least square method. Figure 6.10a shows the difference between computed and measured signal.

iv) The averaged signal of the second probe was simulated by assuming a trapeziumlike signal (eq. 6.5). Slope of the left and right side of the trapezium were taken to be equal to the slope determined from the first signal (step ii). A total number of 600 bubbles were "generated" and an average signal was determined in the same way the FFT analyzer does. The curve was again fitted using a least squares method. The maximum of the curve was not known before (as was explained earlier). Therefore bubble signals were generated with an arbitrary height. The maximum of the simulated curve was taken equal to the maximum of the measured curve. All other points of the calculated curve were also corrected with this ratio. In this way measured and simulated curve could be compared. Measured and computed curves are shown in fig. 6.10b.

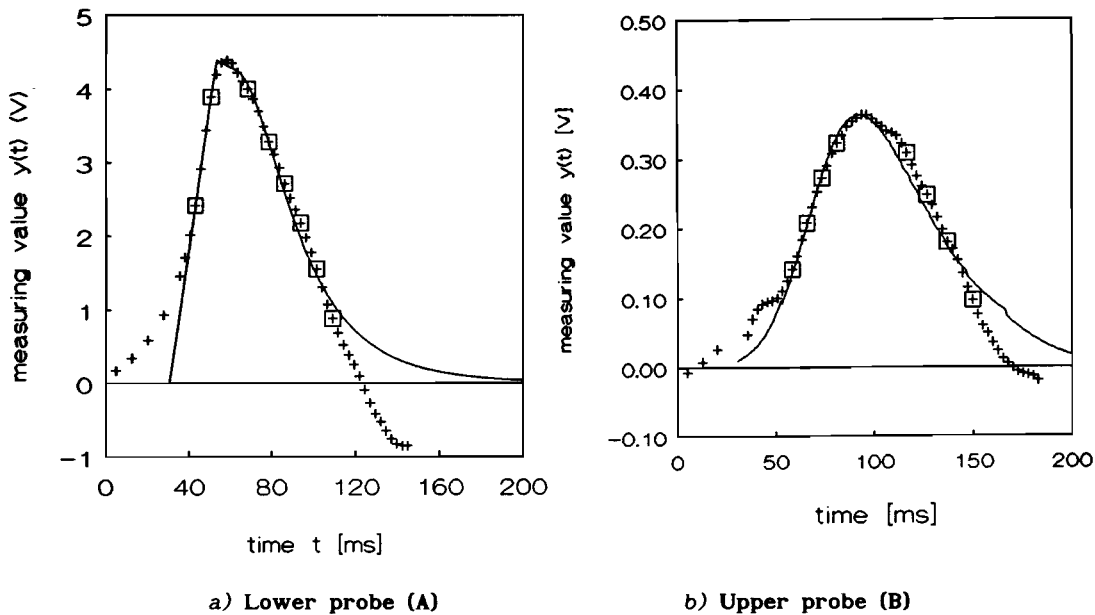


Figure 6.10 Calculated and measured average bubble signals.  
 (—): calculated curves; (+): measured points;  
 (□): data points used for simulation.

From the figures 6.10a and 6.10b it can be seen that it is possible to describe the time averaged signals with this method. Discrepancies between measured and calculated curves occur because the actual signal is more gradual and not an exact trapezium with its sudden changes.

Cross correlations could not be used to determine  $t_a$  as can be shown mathematically. The time averaged signal is defined by equation 6.6. We use  $\overline{\varphi_{xy}}$  for denoting the cross correlation function of the two time averaged signals. Hence (the notation  $\lim_{T \rightarrow \infty}$  has been left out):

$$\overline{\varphi_{xy}} = \frac{1}{2 \cdot T} \int_{-T}^{+T} \overline{x(t) \cdot y(t+\tau)} \cdot d\tau \quad (6.9)$$

Here  $\overline{x(t)}$  and  $\overline{y(t+\tau)}$  denote the time averaged signals of the two different probes. Substitution of eq. 6.6 in eq. 6.9 leads to:

$$\overline{\varphi_{xy}} = \frac{1}{2 \cdot T \cdot n^2} \int_{-T}^{+T} \sum_{i=1}^n x_i(t) \cdot \sum_{j=1}^n y_j(t+\tau) \cdot d\tau \quad (6.10)$$

$$= \frac{1}{2 \cdot T \cdot n^2} \int_{-T}^{+T} (x_1 + x_2 + \dots + x_n) \cdot (y_1 + y_2 + \dots + y_n) \cdot d\tau \quad (6.11)$$

(Note: the notations  $(t)$  and  $(t+\tau)$  have been left out for simplicity)

$$= \frac{1}{2 \cdot T \cdot n^2} \left\{ \int_{-T}^{+T} x_1 \cdot y_1 \cdot d\tau + \int_{-T}^{+T} x_1 \cdot y_2 \cdot d\tau + \dots + \int_{-T}^{+T} x_n \cdot y_n \cdot d\tau \right\} \quad (6.12)$$

$$= \frac{1}{2 \cdot T \cdot n^2} \sum_{i=1}^n \sum_{j=1}^n \int_{-T}^{+T} x_i \cdot y_j \cdot d\tau \quad (6.13)$$

$$\Rightarrow \overline{\varphi_{xy}} = \varphi_{11} + \varphi_{12} + \varphi_{13} + \dots + \varphi_{nn} = \sum_{i=1}^n \sum_{j=1}^n \varphi_{ij} \quad (6.14)$$

This shows that signals are correlated that are not obtained from the same bubble. If the distributions had been normal distributions it would not make any difference. But the  $t_a$  with the highest probability is not the average  $t_a$ , since the probability distribution is log-normal. With the average cross correlation  $\overline{\varphi_{xy}}$  there is in general a larger probability of finding a time difference that is smaller than the average time difference. A larger time difference is of course also possible depending on the skewness of the distribution. But in general smaller values will be found. The errors will become larger with larger deviations, because then the log-normal distribution differs more from the normal distribution. When the deviation is small enough the difference disappears. The experimentally measured ratio of the rising time  $t_a$  determined by the statistical method and by the cross correlation is shown in fig 6.11. This shows that the expected trend indeed was found, though the deviations from the mean values are considerable.

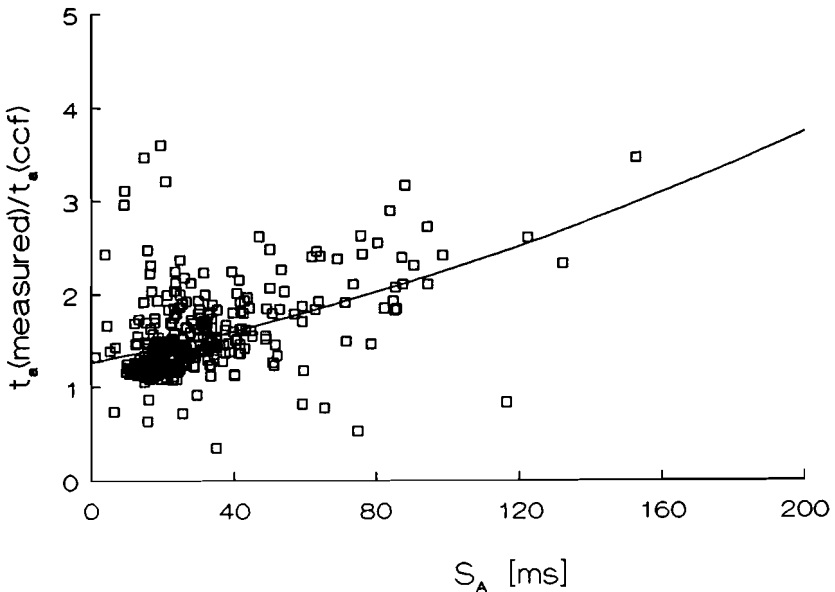


**Figure 6.11**  $t_a$  values experimentally determined by statistical method and by cross correlation as a function of determined deviation  $S_A$ . ( $\square$ : measured data points; (—): curve fit).

#### 6.4. Determination of local fluidizing state

The equations for calculating all necessary local parameters have all been described extensively by Werther (1972).

The pierced lengths and bubble velocities are stochastic variables. Average values will be used in our calculations.

The pierced length  $l_1$  of one bubble is given by its velocity  $u_{b,1}$  and pierced time  $t_{b,1}$  :

$$l_1 = u_{b,1} \cdot t_{b,1} \quad (6.15)$$

Since the pierced length and bubble velocity are stochastically independent, the mean pierced length  $E[l]$  can be calculated by:

$$E[l] = u_b \cdot t_b \quad (6.16)$$

The average bubble velocity  $u_b$  can be calculated from:

$$u_b = \frac{s}{t_a} \quad (6.17)$$

with  $s$  being the distance between the two probe points (for the probes we used  $s = 10$  mm).

The bubble hold up  $\delta$  can be determined from the total time the probe is immersed in bubbles ( $n \cdot t_b$ ) compared to the total measuring time  $T$ :

$$\delta = \frac{n \cdot t_b}{T} = k \cdot t_b \quad (\text{with } k = n/T) \quad (6.18)$$

where  $k$  is the bubble frequency.

The local visible bubble gas flow is given by the measured total amount of gas in the bubbles (with the probe surface  $\partial A$  as reference) per square cm per second:

$$\dot{V}_b \left[ \frac{\text{cm}^3}{\text{cm}^2 \cdot \text{s}} \right] = \frac{n \cdot l \cdot \partial A}{T \cdot \partial A} = k \cdot t_b \cdot u_b \quad (6.19)$$

The dense phase through flow factor  $\varphi$  is defined by (see chapter 1):

$$\varphi = \frac{U - \dot{V}_b}{U_{mf}} \quad (6.20)$$

This factor gives the extra flow through the dense phase compared to the two phase theory of Toomey and Johnstone (1952). When  $\varphi = 1$  the two phase theory applies.

The average values of these parameters were calculated by the "cup mixing" principle:

$$\bar{v} = \frac{\int_0^R r \cdot v(r) \cdot dr}{\int_0^R r \cdot dr} \cong \frac{2 \cdot \sum_{j=1}^7 r_j \cdot v_j(r) \cdot \Delta r_j}{R^2} \quad (6.21)$$

## 6.5. Results and Discussion

It occurred occasionally that a measured time averaged signal could not be fitted accurately (about 5 %). This occurred more often for the larger particle powders (230  $\mu\text{m}$  and 587  $\mu\text{m}$ ) than for the smaller particle powders (106  $\mu\text{m}$  and 165  $\mu\text{m}$ ). There are two reasons for this: the change from the dense phase to the bubble phase is more gradual for the larger particle powders and the probe size - particle size ratio is smaller for the larger particles. The average values were then calculated by extrapolation of the other radial values obtained at one height.

Measuring conditions and results obtained for the several powders are given in the tables 6.1a to 6.1d. Here only the radial averaged values at one height are given. Most values were obtained from the seven radial positions. Some parameters will be discussed individually.

### Bubble frequency

In general the bubble frequency decreased with increasing height, due to coalescence, and increased with increasing superficial velocity.

H [cm]	U [cm/s]	h [cm]	k [s <sup>-1</sup> ]	$\bar{E}[1]$ [cm]	$u_b$ [m/s]	$\delta$ [-]	bed expansion [-]	$\varphi$ [-]
95	5.4	24	1.78	1.43	0.34	0.08	~ 0.05	2.01
		34	1.60	1.70	0.33	0.08		1.84
		44	1.83	2.10	0.37	0.10		1.44
		54	1.52	1.62	0.31	0.09		1.97
		64	1.49	2.26	0.39	0.09		1.14
		74	1.70	2.08	0.36	0.10		0.92
		84	1.67	2.19	0.39	0.09		0.98
95	10.8	24	3.09	1.45	0.29	0.16	~ 0.11	4.46
		34	2.55	2.51	0.43	0.15		2.96
		44	1.61	3.17	0.49	0.11		2.83
		54	1.95	2.85	0.40	0.15		3.48
		64	2.46	3.66	0.43	0.21		0.76
		74	2.02	3.95	0.46	0.17		1.79
		84	2.20	3.66	0.38	0.20		1.30

Table 6.1a Results for the 106  $\mu\text{m}$  quartz sand powder ( $U_{mf} = 1.4 \text{ cm/s}$ )



H [cm]	U [cm/s]	h [cm]	k [s <sup>-1</sup> ]	$\overline{E[1]}$ [cm]	$u_b$ [m/s]	$\delta$ [-]	bed expansion [-]	$\phi$ [-]
55	4.7	14	1.28	0.68	0.34	0.03	~ 0.05	1.71
		24	1.01	0.53	0.21	0.03		1.83
		34	0.95	0.82	0.24	0.03		1.69
		44	1.13	0.86	0.23	0.04		1.56
	9.3	14	2.58	1.03	0.30	0.09	~ 0.10	2.87
		24	1.97	1.23	0.27	0.09		2.95
		34	1.49	1.50	0.28	0.08		3.03
		44	1.84	1.94	0.32	0.11		2.42
	14.0	14	1.18	1.06	0.28	0.04	~ 0.12	5.46
		24	1.46	1.71	0.29	0.09		4.91
		34	1.71	2.23	0.34	0.12		4.30
		44	1.55	3.28	0.44	0.11		3.72
35	4.9	14	1.46	0.59	0.19	0.05	~ 0.05	1.73
		24	1.25	0.71	0.21	0.04		1.69
	12.2	14	2.19	0.91	0.25	0.08	~ 0.11	4.42
		24	2.04	1.53	0.27	0.12		3.90
	19.4	14	1.09	1.22	0.26	0.05	~ 0.16	7.84
		24	1.73	2.12	0.32	0.11		6.73

Table 6.1b Results for the 165  $\mu\text{m}$  quartz sand powder ( $U_{mf} = 2.3 \text{ cm/s}$ )

H	U	h	k	$\overline{E[1]}$	$u_b$	$\delta$	bed expansion	$\phi$	
[cm]	[cm/s]	[cm]	[s <sup>-1</sup> ]	[cm]	[m/s]	[-]	[-]	[-]	
55	7.5	24	1.03	0.67	0.23	0.04	~ 0.06	1.33	
		34	1.00	0.76	0.22	0.03		1.32	
		44	0.76	0.94	0.24	0.03		1.33	
	11.0	24	1.85	0.92	0.25	0.25	0.07	~ 0.10	1.82
		34	1.61	0.87	0.19	0.19	0.07		1.88
		44	1.09	1.42	0.25	0.25	0.06		1.83
	14.6	14.6	14	2.48	1.17	0.28	0.10	~ 0.11	2.29
			24	1.49	1.34	0.23	0.09		2.46
			34	1.32	1.49	0.24	0.08		2.48
			44	0.73	1.12	0.19	0.04		2.69
	35	7.8	14	1.33	0.52	0.19	0.04	~ 0.03	1.39
			24	0.87	0.56	0.19	0.03		1.44
14			1.69	0.78	0.23	0.06	~ 0.08		1.94
24			1.20	0.94	0.22	0.051			1.98
14.1		14	3.63	1.72	0.26	0.24	~ 0.11	1.57	
		24	2.44	1.85	0.28	0.16		1.88	

Table 6.1c Results for the 230  $\mu\text{m}$  quartz sand powder ( $U_{mf} = 5.1 \text{ cm/s}$ )

H [cm]	U [cm/s]	h [cm]	k [s <sup>-1</sup> ]	$\bar{E}[I]$ [cm]	$u_b$ [m/s]	$\delta$ [-]	bed expansion [-]	$\varphi$ [-]
55	22.9	14	0.83	1.44	0.24	0.05	~ 0.03	1.02
		24	0.65	1.48	0.22	0.04		1.03
		34	0.47	1.47	0.22	0.03		1.04
		44	0.41	1.92	0.25	0.03		1.04
	26.1	14	0.79	1.13	0.20	0.05	~ 0.07	1.18
		24	0.43	1.73	0.25	0.03		1.19
		34	0.50	1.91	0.26	0.03		1.18
		44	0.42	2.16	0.28	0.03		1.18
	29.0	14	1.00	0.83	0.14	0.06	~ 0.07	1.32
		24	0.82	2.06	0.30	0.06		1.28
		34	0.61	1.83	0.23	0.05		1.31
		44	0.57	2.58	0.30	0.05		1.29
95	25.2	54	0.32	2.18	0.26	0.03	~ 0.07	1.16
		64	0.30	2.16	0.25	0.03		1.15
		74	0.36	1.60	0.20	0.03		1.15
		84	0.30	2.77	0.32	0.03		1.14

**Table 6.1d** Results for the 587  $\mu\text{m}$  quartz sand powder ( $U_{mf} = 21.3 \text{ cm/s}$ ).

Mean pierced length

The pierced length was calculated from  $t_a$  and  $t_b$  (eq. 6.16 and 6.17) and therefore the accuracy will be lower and the variance larger than for the bubble frequency (which is measured directly). As was expected  $\overline{E[I]}$  (the radially averaged mean pierced length) increased with increasing measuring height  $h$  and superficial gas velocity  $U$ . Particle size had a minor effect at a given  $U - U_{mf}$ .

According to Darton et al. (1977) the ratio between the equivalent bubble diameter and the maximum pierced length is about 1.6 for a spherical cap bubble. Because the bubbles are pierced in an arbitrary place the average  $\overline{E[I]}$  value will be smaller than the maximum  $E[I]$  value at one height and so the ratio of  $d_b(\text{Darton})/\overline{E[I]}$  has to be larger than 1.6. From fig. 6.12a it can be seen that this ratio is about 2.5 - 3. From fig. 6.12b (data for 106 and 165  $\mu\text{m}$ ) this ratio was estimated to be about 2.7. Again the deviation of the values was smaller for the smaller particles.

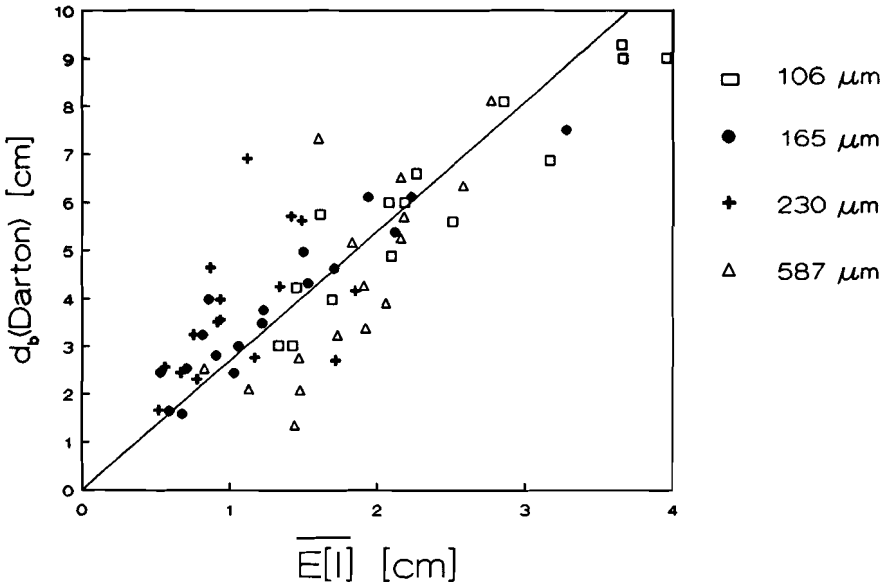
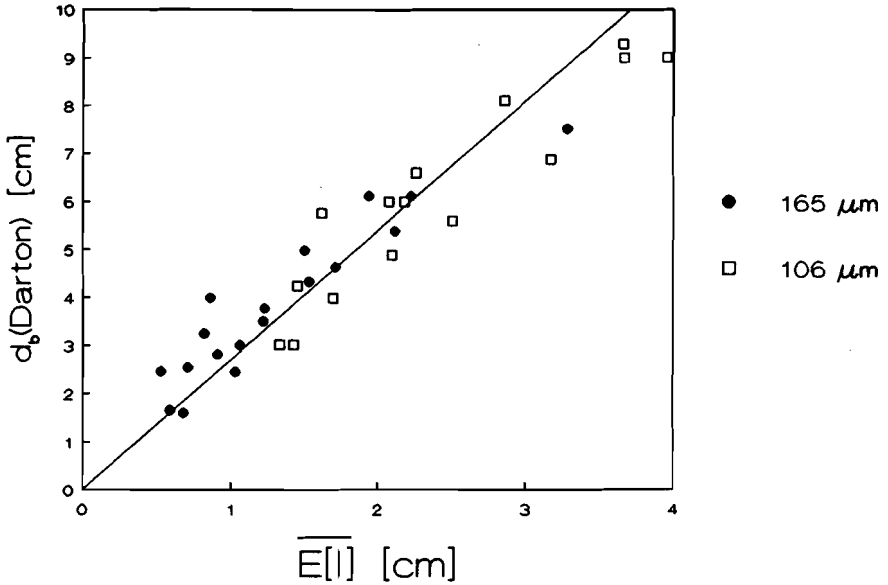


Figure 6.12a Radial averaged mean pierced length versus bubble diameter calculated from Darton et al. (1977). All particle sizes.  
 ( — ) :  $d_b(\text{Darton}) = 2.7 \cdot \overline{E[I]}$ .



**Figure 6.12b** Radial averaged mean pierced length versus bubble diameter, calculated from Darton et al. (1977). (106  $\mu\text{m}$  and 165  $\mu\text{m}$ ).  
 ( — ) :  $d_b(\text{Darton}) = 2.7 \cdot \overline{E[l]}$  ).

A plot of  $d_b(\text{Darton})$  versus  $\overline{E[l]}$  yielded a linear relation which implies that the measured  $\overline{E[l]}$  values are related to the process variables as predicted as by the relation given by Darton et al. (1977). Furthermore it implied that the  $\overline{E[l]}$  values could be used to investigate the bubble growth in height.

Plotting the  $\overline{E[l]}$  values for the 106  $\mu\text{m}$  powder versus the measuring height  $h$ , it can be seen that  $\overline{E[l]}$  appears to reach a maximum value at a given bed height of about 60 cm (fig. 6.13). This is the so called stable bubble height  $h^*$  beyond which bubbles do not grow further: an equilibrium between coalescence and splitting is reached. This height  $h^*$  has been introduced first by Werther (1978). For the other powders the bed height was not high enough to reach  $h^*$ , which indicates that there might be a particle size dependency of  $h^*$ .

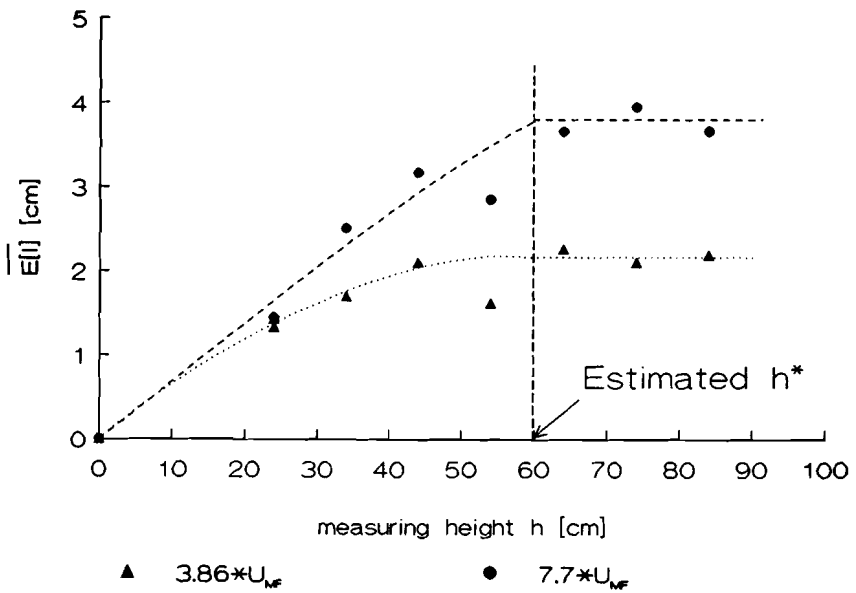
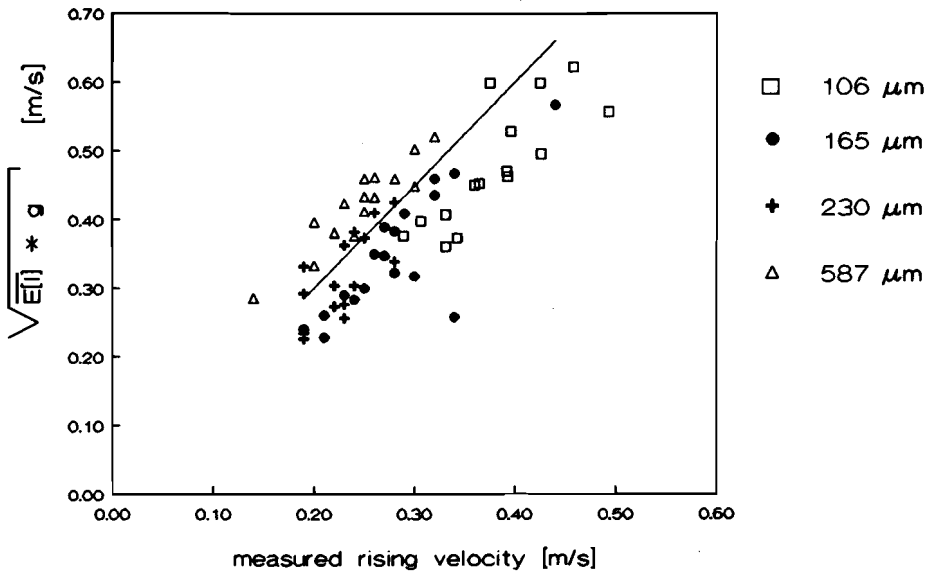


Figure 6.13. Radial averaged mean pierced length versus measuring height for the 106  $\mu\text{m}$  particles, for two flow rates.

### Bubble velocity

The bubble velocity  $u_b$  increased with increasing measuring height  $h$  and increasing superficial velocity  $U$ . This was in agreement with results of other authors (Clift and Grace, 1985). The total bed height appeared to be of no influence.

Figure 6.14 shows a plot of  $(\overline{E(I)} \cdot g)^{1/2}$  versus  $u_b$ , which could be described by  $u_b \sim 1.5 \cdot (\overline{E(I)} \cdot g)^{1/2}$ .



**Figure 6.14**  $(E[II] \cdot g)^{0.5}$  versus experimentally determined average bubble velocity  $u_b$ . (—) = eq. 6.22).

There appeared to be a minor particle size effect, which could be due to the fact that it is more difficult to determine a bubble boundary for the larger particles, because of the more gradual change discussed before. There is however an other effect: for the smaller particles the bubble frequency and therefore the probability of coalescence were larger at a given  $\overline{E[II]}$ . It is a well known effect that the bubble rise velocity is influenced when a bubble is in the vicinity of other bubbles (see for instance Clift and Grace, 1985). This again could be an explanation for the fact that the bubble rise velocity is somewhat larger for the smaller particles at a given  $\overline{E[II]}$ . Therefore a particle size effect can not be ruled out nor can it be confirmed.

The measured bubble velocity could be described by:

$$u_b \approx 1.5 \cdot \sqrt{E[II] \cdot g} \tag{6.22}$$

This relation can be compared to the relation of Werther (1978)

$$u_b = 1.6 \cdot D^{0.4} \cdot \sqrt{d_b \cdot g} \quad (\text{for } 0.1 \text{ m} < D < 1 \text{ m}) \quad (6.23)$$

$$= 0.92 \cdot \sqrt{d_b \cdot g} \quad (\text{with } D = 0.25 \text{ m}) \quad (6.24)$$

where D is the bed diameter. Equations 6.22 and 6.24 can be combined to give:

$$u_b \approx 0.92 \cdot \sqrt{2.7 \cdot \overline{E[1]} \cdot g} \quad (6.25)$$

The same ratio for  $d_b/\overline{E[1]}$  ( $\approx 2.7$ ) is found as from the comparison with the relation given by Darton et al. (1977).

#### The visible bubble gas flow $\dot{V}_b$

In general our measured values of the local visible bubble gas flow  $\dot{V}_b$  were the same as those obtained by Werther (1972). With increasing bed height bubbles moved towards the bed centre and away from the wall. This effect became more outspoken at larger  $U/U_{mf}$  ratios. The local maximum  $\dot{V}_b$  values were about 2 to 4 times the radial averaged  $V_b$  value. The bed height, the superficial gas velocity and the particle size had no effect on this ratio. At the reactor wall the visible bubble gas flow was virtually zero. This indicates a circulation of powder, which was generally observed by several investigators (e.g. Werther (1972)). Examples of  $\dot{V}_b$  versus  $r$  and  $h$  for the 106  $\mu\text{m}$  and 165  $\mu\text{m}$  powders are given in the figures 6.15 and 6.16.



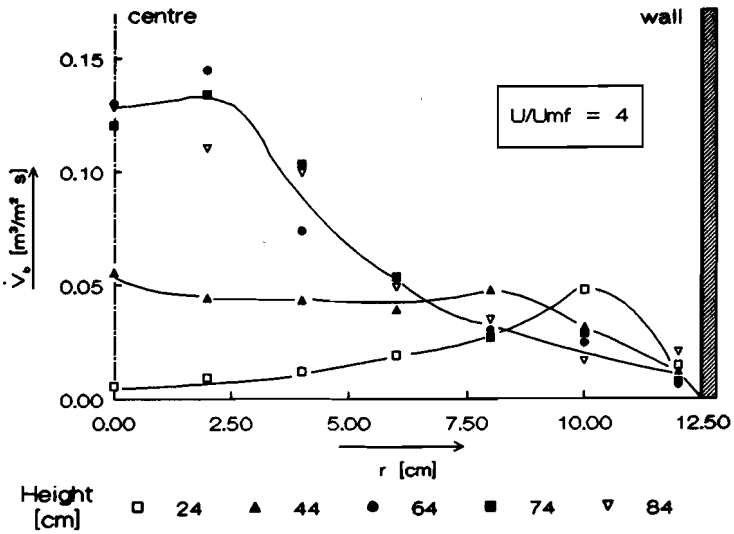


**Figure 6.15** Experimentally determined local visible bubble gas flow  $\dot{V}_b$  with variable radial position  $r$  and measuring height  $h$ . (106  $\mu\text{m}$  particles,  $H = 95 \text{ cm}$ ,  $U = 5.4 \text{ cm/s}$ ).

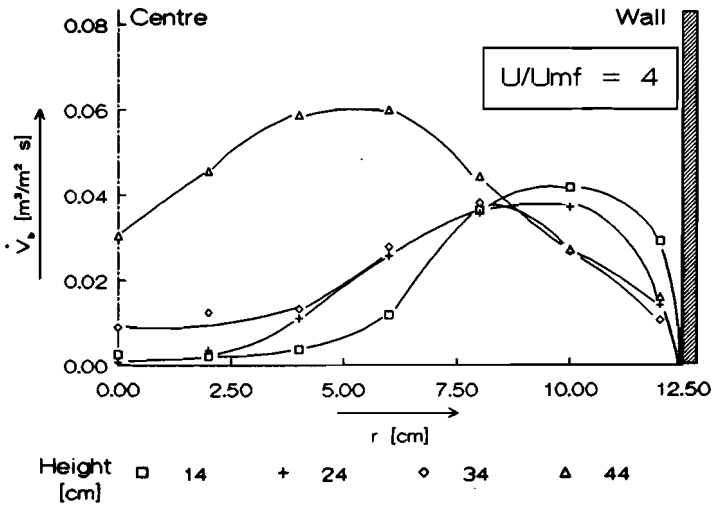


**Figure 6.16** Experimentally determined local visible bubble gas flow  $\dot{V}_b$  with variable radial position  $r$  and measuring height  $h$ . (165  $\mu\text{m}$  particles,  $H = 55 \text{ cm}$ ,  $U = 9.3 \text{ cm/s}$ ).

### The stable bubble height $h^*$

The bubbles grow with increasing height which means that the  $\varphi$  factor should decrease with increasing height. This was indeed the case (see the figures 6.17 to 6.21). The  $\varphi$  values obtained from measurements at different total bed heights but equal superficial velocities were virtually the same for the same particle size at equal measuring height. This indicated the negligible effect of total bed height on  $\varphi(h)$ .

For all powders there appeared to be a linear relation between height  $h$  and factor  $\varphi$ . Extrapolation to  $h = 0$  always gave  $\varphi \approx U/U_{mf}$ . This could be expected, because a porous plate was used as a gas distributor: the initial bubbles are that small that they can not be detected and therefore  $V_b$  will be equal to zero at  $h = 0$ . Equation 6.20 then shows that  $\varphi$  should indeed be equal to  $U/U_{mf}$  at  $h = 0$ .

The  $\varphi(h)$ -lines were extrapolated to  $\varphi = 1$  and it was found that all lines intersected at about the same  $h$  value. At  $\varphi = 1$  the two phase theory holds. Average  $\varphi$  values smaller than one are not possible, because this would mean that at that height the powder is not fluidized. According to the n-type theory the following equation holds (for instance Clift and Grace (1985) and chapter 1, equation 1.6):

$$\varphi = 1 + 2 \cdot \delta \quad (6.26)$$

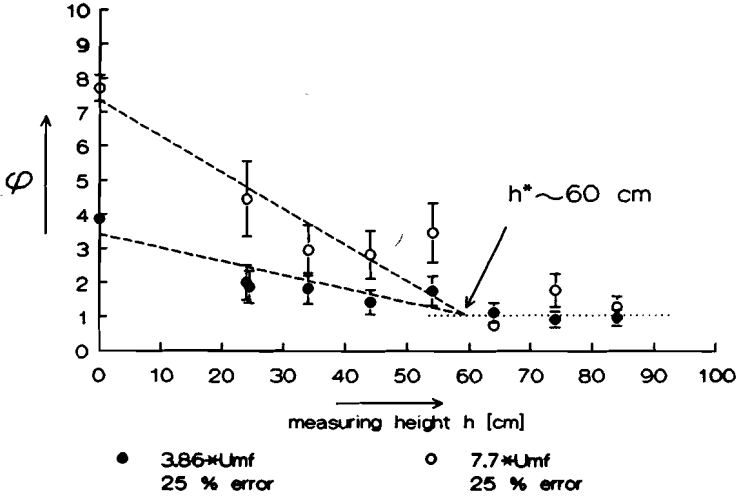
With a  $\delta$  value of about 0.1, the measuring accuracy is too small to decide whether an extrapolation line from the two phase theory or from the n-type theory applies. Therefore, for our analysis a value of  $\varphi = 1$  is adequate.

Figure 6.17 shows that for the 106  $\mu\text{m}$  particles the  $h$  value at which the lines intersect is equal to the height at which the mean pierced length did not increase anymore (fig. 6.14). This led to the idea that these points might give an indication for the stable bubble height  $h^*$ .

The  $V_b$  data from Werther (1972) for quartz sand powder of 83  $\mu\text{m}$ , were used to calculate  $\varphi(h)$  values. These values, given in fig 6.18 were also extrapolated to  $\varphi = 1$  and this yielded a stable bubble height  $h^* = 25 - 30$  cm. About the same value for  $h^*$  was estimated from his bubble pierce length measurements with the same powder in a 100 cm bed (Werther, 1974).

From experiments with spent cracking catalyst Werther (1983) measured a stable bubble size at a measuring height of 25 - 30 cm. Analysis of his

visible bubble gas flow measurements with the  $\phi(h)$ -extrapolation gave also a stable bubble height of about 30 cm.



**Figure 6.17** Dense phase through flow factor  $\phi$  with variable measuring height  $h$  and  $U/U_{mf}$ , for the 106  $\mu\text{m}$  particles.

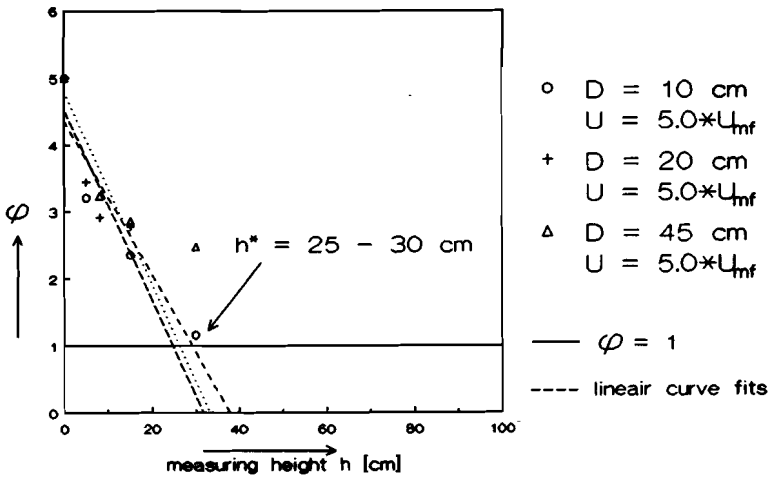


**Figure 6.18** Dense phase through flow factor  $\phi$  with variable measuring height  $h$ , calculated from Werther (1972).

Based on the results mentioned above it was concluded that extrapolation of  $\varphi(h)$  to  $\varphi = 1$  gives an estimate of the stable bubble height  $h^*$ . Therefore, the same procedure was used for the other quartz sand powders, giving  $h^*$  values of 100 cm, 130 cm and 300 - 400 (~ 350) cm for the 165  $\mu\text{m}$ , 230  $\mu\text{m}$  and 587  $\mu\text{m}$  powders respectively (see figures 6.19, 6.20 and 6.21).

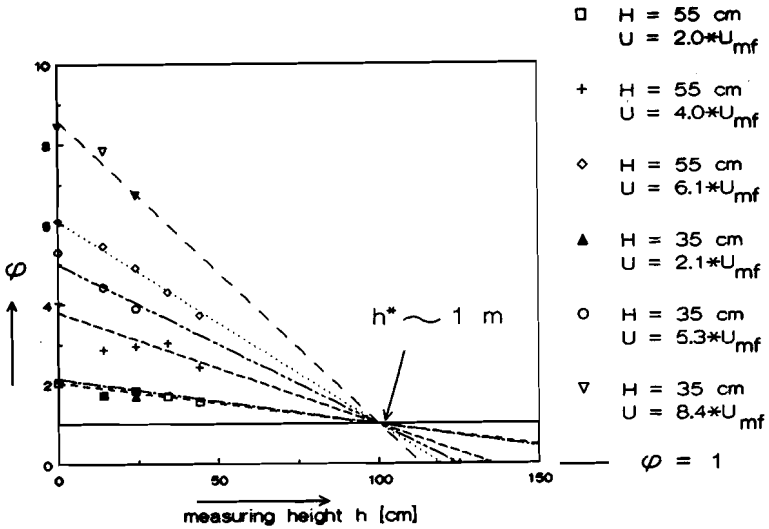


Figure 6.19 Dense phase through flow factor  $\varphi$  with variable measuring height  $h$  and  $U/U_{mf}$ , for the 165  $\mu\text{m}$  particles.

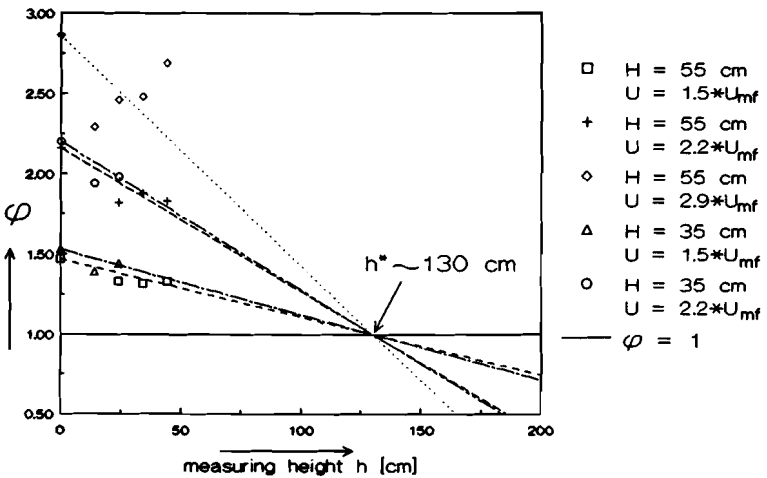


Figure 6.20 Dense phase through flow factor  $\varphi$  with variable measuring height  $h$  and  $U/U_{mf}$ , for the 230  $\mu\text{m}$  particles.

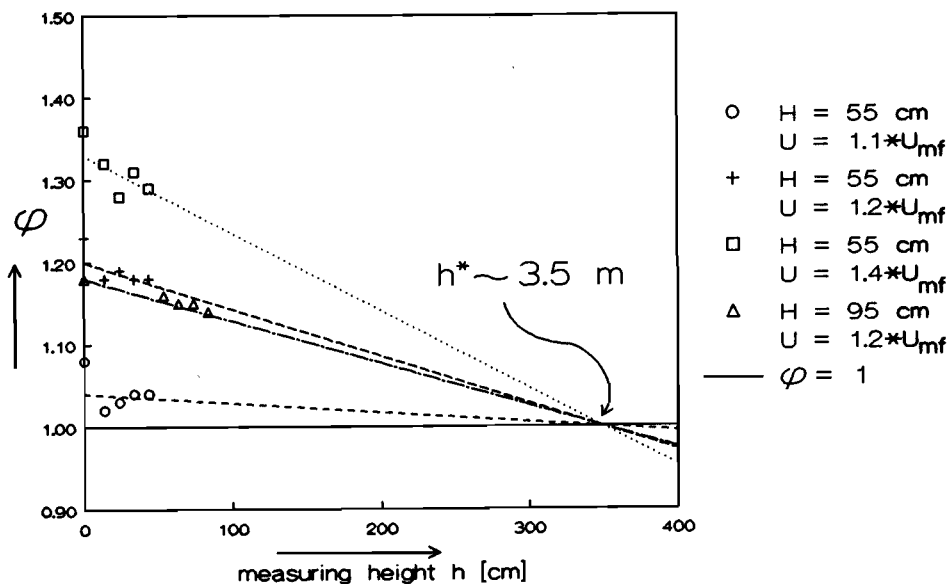


Figure 6.21 Dense phase through flow factor  $\phi$  with variable measuring height  $h$  and  $U/U_{mf}$ , for the  $587 \mu\text{m}$  particles.

Extrapolation of the lines gives of course only an estimate of  $h^*$ . Measurements for the larger particles were less accurate and extrapolation had to be done to larger heights. Therefore with increasing particle size the inaccuracy will become larger. However, the  $h^*$  values were of the same order as estimated by Werther (1978) from conversion and tracer experiments.

From fig. 6.15 it can also be seen that at  $h \geq h^*$  the location of the maximum in  $\dot{V}_b$  does not change. This means that at  $h \geq h^*$  not only the bubbles do not grow further (due to an equilibrium between coalescence and splitting) but that also the bubble tracks do not change. The fact that the bubbles rise in the centre of the bed, of course indicates that there is an overall particle circulation, which keeps the bubbles in the bed centre. Perhaps the observation of a constant bubble track might be another way to measure  $h^*$ , for instance by visual observation of the bed surface at different bed heights.

Plotting  $h^*$  values (obtained from the extrapolation) versus particle size shows that there is a linear relation between these two variables (fig. 6.22).

The linear curve fit gave the following relation:

$$h^* = -0.123 + 6.17 \cdot 10^{-3} \cdot d_p \quad (d \text{ in } \mu\text{m}, h^* \text{ in m}) \quad (6.27)$$

For  $h^* = 0$  this equation gave  $d_{p,0} \sim 20 \mu\text{m}$ . According to the Geldart classification (1973) this type of powder is then in the cohesive region where no stable bubbling occurs. For other particle types this equation does not have to be valid, but we think that it gives a reasonable indication for  $h^*$  values (see for instance fig. 6.22: the data point from Werther (1983) for spent FCC fits the data points for quartz sand).

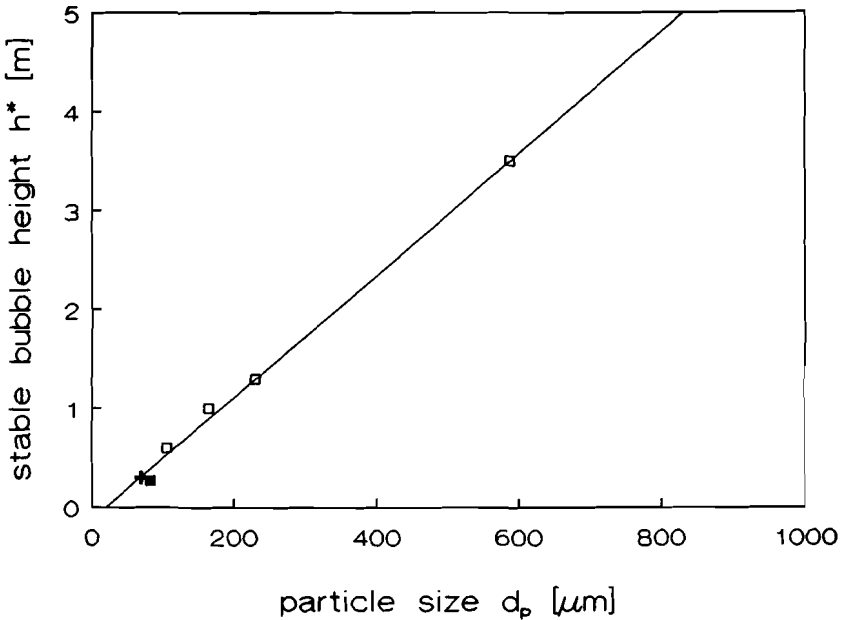


**Figure 6.22** Stable bubble height  $h^*$  as a function of particle size  $d_p$ .  
 ( $\square$  = own measurements,  $\blacksquare$  = calculated from Werther (1972),  
 + = taken from Werther (1983) for spent FCC ( $d_p \sim 70 \mu\text{m}$ ),  
 (—): eq. 6.27).

## 6.6 Concluding Remarks

Information on the bubble characteristics was obtained from measurements based on electrical capacity changes. Four different powders were used.

The time averaged signal could not be used to obtain all necessary parameters for calculating  $\dot{V}_b$ . Therefore a statistical method was developed which gave good, reproducible and consistent results. It was possible to obtain information on the deviation in rising time and bubble contact time, which can be helpful for a statistical description of a fluidized bed.

We estimated the bubble diameter to be about 2.7 times the mean pierced length  $E[1]$ .

A new method was used to estimate the maximum stable bubble height  $h^*$  and it was found that  $h^*$  was linearly dependent on  $d_p$  only. Our own measurements have shown that there is no influence of the bed height  $H$  and the superficial velocity  $U$  on the  $h^*$  value. From the data of Werther (1972, 1974) (see fig. 6.18) it appears that the bed diameter has also no influence on the  $h^*$  value. This implies that the stable bubble size can vary for different conditions, but that the height at which this diameter occurs is always the same for a given powder. There is still no physical explanation for this phenomenon and more investigation is needed in this area.

Due to experimental inaccuracy it was not possible to arrive at definite conclusions on the question whether the two phase theory or the n-type theory (with  $n = 2$ ) (see chapter 1) is applicable. However, based on the results of this chapter and chapter 5 it seems reasonable to conclude that the deviations from the two phase theory are not so large as is often assumed (e.g. Clift and Grace (1985) for a review). The conclusions reported in literature are often based on experimental techniques with which it is not possible to measure the total bubble (and therefore dense phase) gas flows. The real dense phase gas flow can only be measured with collapse experiments, and this is only possible with powders having a dense phase expansion (A-type powders). It is therefore suggested to use the two phase of Toomey and Johnstone (1952) or the n-type theory (discussed in chapter 1) to describe the gas flow division in a gas fluidized bed.

### 7.1 Introduction

In the chapters 4 and 5 we have shown that it is now possible to scale up a fluid bed reactor on the basis of a given number of a mass transfer units for first order reactions and tracer experiments. However, it would be much more practical if it was possible to predict (or estimate) the height of a mass transfer unit and/or the conversion of a fluidized bed, also for other types of reactions. For this purpose theoretical equations for the mass transfer coefficient and the specific mass transfer area have to be known.

For estimating the specific mass transfer area, the bubble growth has to be taken into consideration. For this reason Level III models were used (chapter 1 and Van Swaaij (1985)). An important parameter in these models is the stable bubble height  $h^*$ , discussed in chapter 6. The results of that chapter will be used to estimate  $h^*$ .

For predicting the mass transfer coefficient  $k_g$  various theories have been reported. As was shown in the chapters 1 and 5 the theory of Sit and Grace (1978) can explain the influences of process variables on the mass transfer and therefore it was used in our model description. However, other Level III models will also be tested to verify their usefulness. A summary of these Level III models and their differences has been given by van Swaaij (1985). Therefore only the necessary features of the models will be discussed.

All models take bubble growth as a function of height into consideration. The essential difference lies in the definition of the mass transfer coefficient. Van Swaaij (1985) assumes a constant mass transfer coefficient, only differing with the type of powder. Werther (1978) takes  $k_g$  to be a function of  $(U - U_{mf})$  and powder type only. The models of Davidson et al. (1977), Krishna (1981) (which uses the Davidson model) and Sit and Grace (1978) all contain a mass transfer coefficient with a convective and diffusional term.

These models will be discussed, finally leading to our model, which is based on theories of Werther (1978) and Sit and Grace (1978). With this model a simple design computation will be performed, showing that in some situations coarser particles than commonly used can be more efficient.



## 7.2. Modeling

### Basic concepts of our model

The theory of Sit and Grace (1978) has been discussed in chapter 1. This theory was adapted by proposing that the velocity difference ( $u_b - u_d$ ) should be used for estimating the contact time. However, computations have shown that for the considered conditions  $u_b \gg u_d$  and therefore the dense phase velocity  $u_d$  was neglected.

The mass transfer coefficient  $k_g$  and the specific surface  $a$  are essentially local parameters. Computing  $H_k$  values by using average  $k_g$  and  $a$  values will introduce an error. However, it has to be done this way, because the original equations, with which  $H_k$  was calculated, were also based on average values (chapter 1). Calculations showed that the height integrated  $\int (k_g \cdot a)$  values were larger than the average  $(\bar{k}_g \cdot \bar{a})$  values. This means that a correction factor in computing  $H_k$  is necessary. In our model  $H_k$  is defined in the following way (only average values are used):

$$H_k = \frac{U}{k_g \cdot a \cdot c} \quad (7.1)$$

Werther (1978) introduced a shape factor  $\psi$  for the bubbles, because in reality the bubbles are of course not completely spherical as is assumed in the models. In general the specific mass transfer area will become larger due to the the wake and/or ellipsoid shape of the bubbles. In our model the specific surface  $a$  is therefore also defined by:

$$a = \frac{6 \cdot \delta \cdot \psi}{d_b} \quad (7.2)$$

Werther (1978) gave a value of  $\sim 1.67$  for  $\psi$ , based on bubbles in a gas/liquid bubble column. This is also applicable for spherical cap bubbles that are

encountered in fluidized beds with small particle powders. Cranfield and Geldart (1974) showed that for coarse particle systems the bubbles tend to be of a spherical shape. Although they used particles of more than 1 mm this shows that the shape factor may very well decrease with increasing particle size. As a first approximation we used  $\psi = 1.67$  for the smaller particles and  $\psi = 1.0$  for the larger particles, thus introducing a discontinuity. In reality this will be a more gradual variation, but there are still no experimental data available about this parameter. More research is needed in this area. The constant  $c$  and the shape factor  $\psi$  can also be put together in one parameter  $c \cdot \psi$ . This parameter can then be used as the fitting parameter in explaining mass transfer data. At first  $\psi$  was taken to be 1.67 (or 1) and only  $c$  was used as the variable parameter.

The bubble hold up  $\delta$  is found from:

$$\delta = \frac{U - U_{mf}}{u_b} \quad (7.3)$$

The two phase theory of Toomey and Johnstone (1952) was used, because the results of chapters 5 and 6 have shown that this is a reasonable approximation.

For  $u_b$  the relation given by Werther (1978) is used, because this relation was in agreement with our hydrodynamic measurements (chapter 6):

$$u_b = \phi \cdot \sqrt{g \cdot d_b} \quad \text{with} \quad \phi = \begin{cases} 0.64 & \text{if } D < 0.1 \text{ m} \\ 1.6 \cdot D^{0.4} & \text{if } 1 < D < 0.1 \text{ m} \\ 1.6 & \text{if } D > 1 \text{ m} \end{cases} \quad (7.4)$$

The  $\phi$  factor is an empirically determined parameter.

The average bubble diameter is obtained from the integrated relation of Darton et al. (1977) (eq. 1.3):

(7.5)

$$d_b = \frac{0.54 \cdot (U - U_{mf})^{0.4}}{1.8 \cdot g^{0.2} \cdot H} \cdot \left\{ \left[ H + 4 \cdot \sqrt{A_0} \right]^{1.8} - \left[ 4 \cdot \sqrt{A_0} \right]^{1.8} \right\} \quad \left( \text{for } H < h^* \right)$$

and

$$d_b = \frac{0.54 \cdot (U - U_{mf})^{0.4}}{g^{0.2} \cdot H} \left\{ \frac{(h^* + 4 \cdot \sqrt{A_0})^{1.8} - (4 \cdot \sqrt{A_0})^{1.8}}{1.8} + (h^* + 4 \cdot \sqrt{A_0})^{0.8} \cdot (H - h^*) \right\}$$

(for  
H ≥ h\*)

According to Sit and Grace (1978) (see also chapter 1) the following relation for  $k_g$  is applicable:

$$k_g = \frac{U_{mf}}{3} + \left[ \frac{4 \cdot D_g \cdot \epsilon_{mf} \cdot u_b}{\pi \cdot d_b} \right]^{1/2} \quad (7.6)$$

Substituting equations 7.2 to 7.6 in eq. 7.1 gives a value for the height of a mass transfer unit  $H_k$ , when the process conditions are known.

### Other models

#### Davidson et al. (1977)

Davidson et al. (1977) proposed the following relation for the mass transfer coefficient:

$$k_g = 1.19 \cdot U_{mf} + 0.91 \cdot D_g^{1/2} \cdot g^{1/4} \cdot d_b^{-1/4} \cdot \frac{\epsilon_{mf}}{1 + \epsilon_{mf}} \quad (7.7)$$

This equation was also used instead of eq. 7.6 for computing  $H_k$  from eq. 7.1.

Werther (1978)

The Werther model (1978) is based on his hydrodynamic measurements and analysis of literature data. In his definition of  $H_k$  he used  $(U - U_{mf})$  instead of just  $U$ , because this followed from the mass balances he drew up. The difference will be small because in general  $U \gg U_{mf}$ . The  $F$  factor given in equation (7.8) was obtained from his bubble size measurements.

(7.8)

$$H_k = \frac{U - U_{mf}}{k_g a} \quad a = 2910 \frac{U - U_{mf}}{\sqrt{1 + 27(U - U_{mf})}} [\phi \cdot F(H, h^*)]^{-1}$$

$$\phi = \begin{cases} 0.64 & D \leq 0.1 \text{ m} \\ 1.6 \cdot D^{0.4} & 0.1 < D < 1 \text{ m} \\ 1.6 & D \geq 1 \text{ m} \end{cases} \quad (\phi \text{ from eq. 7.4})$$

$$F = H / 0.18 [1 - (1 + 6.84H)^{-0.8}] \quad \text{for } H < h^*$$

$$F = H / \{0.18 [1 - (1 + 6.84h^*)^{-0.8}] + (1 + 6.84h^*)^{-1.8} (H - h^*)\} \quad \text{for } H \geq h^*$$

$$k_g = 3.44 \cdot 10^{-4} \cdot \frac{1}{K} \cdot \sqrt{1 + 27(U - U_{mf})} \quad \text{with } K = 0.15 \text{ for sand}$$

$K = 0.055 \text{ for porous silica}$

Krishna (1981) (From Roes and Garnier (1984) and Van Swaij (1985))

Krishna incorporated the theory of Davidson et al. (1977) for  $k_g$  and the theory of Darton et al. (1977) for the bubble diameter. He calculated the bubble velocity from the relation given by Werther (1978).

(7.9)

$$H_k = \int_0^H \frac{k_g \cdot a \cdot dh}{U} \quad u_b = \phi \cdot \sqrt{g \cdot d_b} \quad \text{definition of } \phi \text{ is taken from Werther (1977) (eq. 7.4)}$$

$$a = \frac{6 \cdot \delta}{d_b} \quad \delta = \frac{U - U_{mf}}{u_b} \quad k_g \text{ from eq. 7.7}$$

$$\left. \begin{aligned} d_b &= 0.54(U - U_{mf})^{2/5} \cdot (h + 4\sqrt{A_0})^{4/5} \cdot g^{-1/5} & \text{for } h < h^* \\ d_b &= 0.54(U - U_{mf})^{2/5} \cdot (h^* + 4\sqrt{A_0})^{4/5} \cdot g^{-1/5} & \text{for } h > h^* \end{aligned} \right\} \text{ taken from Darton et al. (1977)}$$

Elaborating this for ( $H > h^*$ ) leads to (Roes and Garnier, 1984): (7.10)  
( $H > h^*$ )

$$\frac{1}{H_k} = \frac{7.14 \cdot U_{mf} \cdot (U - U_{mf})^{0.4}}{U \cdot \phi \cdot g^{0.2} \cdot (0.54)^{1.5} \cdot H} \cdot \left[ \frac{5}{h_0^{0.2}} - \frac{5}{(h^* + h_0)^{0.2}} + \frac{H - h^*}{(h^* + h_0)^{1.2}} \right] + \frac{5.46 \cdot (U - U_{mf})^{0.3} \cdot g^{0.1} \cdot D_g^{0.5}}{U \cdot \phi \cdot (0.54)^{1.75} \cdot H} \cdot \frac{\epsilon_d}{1 + \epsilon_d} \cdot \left[ \frac{2.5}{h_0^{0.4}} - \frac{2.5}{(h^* + h_0)^{0.4}} + \frac{H - h^*}{(h^* + h_0)^{1.4}} \right]$$

with  $h_0 = 4 \cdot \sqrt{A_0}$  and  $\phi$  taken from Werther (1978). Van Swaij (1985) suggested that  $U_d (= \phi \cdot U_{mf})$  should be substituted for  $U_{mf}$ , which was done by Roes and Garnier (1984). Because we have no information on  $U_d$  we still used  $U_{mf}$ .

Simple model (Van Swaaij (1985))

Van Swaaij (1985) used a constant mass transfer coefficient  $k_g$  as an approximation, because he found  $k_g$  always to be in the same order of magnitude (that is why he called it "The Simple Model"). Combined with the average bubble diameter of Darton et al. (1977) (eq. 7.5) and a fit parameter (15.12) he derived the following equations:

(7.11)

$$H_k = \frac{H}{N_k} \quad N_k = \text{number of mass transfer units.}$$

$$N_k = \frac{15.12 \cdot k_g \cdot (U - U_{mf})^{0.4}}{U \cdot \Phi \cdot g^{0.2}} \{5(4\sqrt{A_0})^{-0.2} - 5(H + 4\sqrt{A_0})^{-0.2}\} \text{ for } H < h^*$$

$$N_k = \frac{15.12 \cdot k_g \cdot (U - U_{mf})^{0.4}}{U \cdot \Phi \cdot g^{0.2}} \{5(4\sqrt{A_0})^{-0.2} - 5(h^* + 4\sqrt{A_0})^{-0.2} + \dots$$

$$\dots + (H - h^*)(h^* + 4\sqrt{A_0})^{-1.2}\} \text{ for } H \geq h^*$$

$k_g = 0.008$  m/s for sand

$k_g = 0.017$  m/s for porous silica

definition of  $\Phi$  is taken from Werther (1977)

Mass transfer with chemical reaction

For chemical reacting systems Werther (1978) suggested that an enhanced mass transfer occurred, in analogy with gas/liquid systems. Mass transfer occurs from the bubble to the film (with thickness  $\delta_f$ ) defined by a mass transfer coefficient (fig 7.1). Mass transfer from the film to the dense phase bulk occurs by diffusion. This means the dense phase of the fluid bed is now regarded as pseudo-homogeneous.

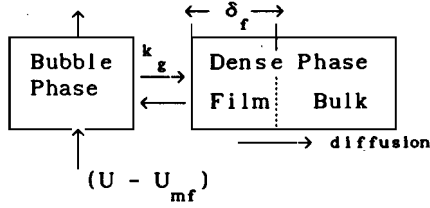


Figure 7.1 Schematic presentation of Werther model for fluidized bed with chemical reaction

Based on partial differential equations for each phase Werther (1978) derived the following equations for a first order reaction:

$$X_a = 1 - \exp \left\{ - \left[ \frac{(\Phi_H^{-1} - 1)Ha + \tanh(Ha)}{(\Phi_H^{-1} - 1)Ha \cdot \tanh(Ha) + 1} \right] \cdot Ha \cdot N_k \right\} \quad (7.12a)$$

with:

$$Ha = \frac{\sqrt{k_d \cdot D_g}}{k_g} \quad (7.12b)$$

$$N_k = \frac{k_g \cdot a \cdot H}{(U - U_{mf})}, \quad \delta_f = \frac{D_g}{k_g} \quad \text{and} \quad \Phi_H = \frac{a \cdot \delta_f}{(1 - \delta)} \quad (7.12c)$$

The factor  $\Phi_H$  is the ratio of film volume and total dense phase volume. The Hatta number  $Ha$  defines the ratio between chemical reaction and diffusion in the film. The number of mass transfer units  $N_k$  is defined somewhat differently compared to our definition, however the difference will be small, because in general  $U \gg U_{mf}$ . As can be seen this is completely comparable to gas/liquid reacting systems (e.g. Thoenes (1972) and Baerns, Hofmann and Renken (1987)). Werther (1978) and Werther and Hegner (1980) showed that this model could explain measured conversion data. Their definitions of  $k_g$  and  $a$  might not be

correct for larger particles, because their analysis that led to the semi-empirical equations for  $k_g$  and  $a$  was based on small particle systems. However, we accept the essential idea of a pseudo homogeneous phase and in analogy with these systems an enhancement factor  $E$  for a first order reaction is defined and the height of a mass transfer unit in our model is redefined by:

$$H_k = \frac{U}{k_g \cdot a \cdot c \cdot E} \quad (7.13a)$$

with (7.13b)

$$E = 1 \quad \text{for} \quad Ha < 0.3$$

$$E = \sqrt{1 + Ha^2} \quad \text{for} \quad 0.3 < Ha < 3$$

$$E = Ha \quad \text{for} \quad Ha > 3$$

$Ha$  is calculated from eq. 7.12b.

### 7.3 Model Computations

Our RTD experiments were analyzed with all the models described, to estimate the value of the constant  $c$  and the particle size at which the shape factor  $\psi$  changes. For the stable bubble height  $h^*$  the results from the hydrodynamic measurements were used (equation 6.27). In most cases  $H < h^*$  which means that the validity of this equation can not be fully tested. The results of the calculations are shown in fig. 7.2.

For the calculation of the bubble diameter for reactors with porous distributor plates  $A_0$  was taken to be 0. If it was necessary for the model to use  $A_0 \neq 0$  we used  $A_0 \sim 10^{-4} \cdot D$ , based on the work of Darton et al. (1977). Fryer and Potter (1976) used a distributor plate with multiple tuyeres. Probably due to interacting bubbles the initial bubble diameter was larger than calculated from the hole sizes. The relation of Darton et al. (1977) was fitted with their measurements and a value of  $0.006 \text{ m}^2$  was found for  $A_0$  for their distributor plate.

Based on our RTD results we estimated  $c \sim 0.6$  for our model (fig. 7.2). For  $d_p < \sim 200 \text{ } \mu\text{m}$   $\psi$  was taken to be 1.67 and for  $d_p > \sim 200 \text{ } \mu\text{m}$   $\psi \sim 1$ , meaning



that the discontinuity was at about 200  $\mu\text{m}$ . For other particles and reactor conditions (e.g. elevated temperatures) this discontinuity may very well be at another particle size, because the bubble shape may be influenced by these conditions.

For the Davidson model the same particle size ( $\sim 200 \mu\text{m}$ ) was taken for the discontinuity in  $\psi$ . The best value for the constant  $c$  was found to be about 0.3. This shows that the  $k_g$  values from Sit and Grace (1978) are about 2 times smaller than the  $k_g$  values from Davidson et al. (1977), because the only difference between these two models is the definition of  $k_g$ .

The models of Krishna (1981) (eq. 7.10), Werther (1978) (eq. 7.8) and Van Swaij (1985) (Simple model, eq. 7.11) were also used to calculate  $H_k$ .

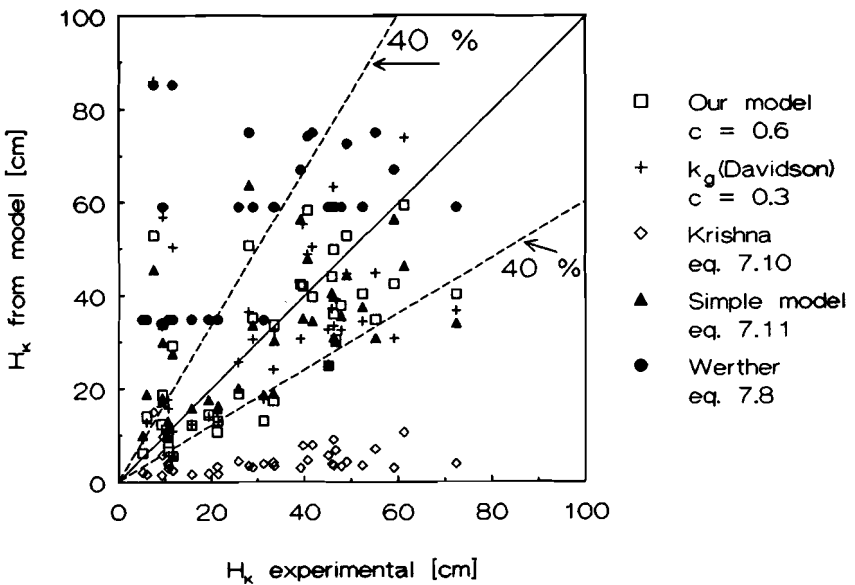


**Figure 7.2** *Model computations for various descriptions, based on our own RTD experiments.*

Figure 7.2. shows that the Werther model (1978) leads to various levels for the computed value of  $H_k$ . This can be explained from equation (7.8). Substituting the relations for  $a$  and  $k_g$  in  $H_k$  leads to the following equation (also Werther and Hegner (1980)):

$$H_k \sim [\Phi \cdot F(h, h^*)] \cdot \kappa \quad (7.14)$$

According to equation 7.14 and 7.8  $H_k$  is, at a given bed height and bed diameter, a function of  $h^*$  only. This means that Werther and Hegner (1980) use  $h^*$  to account for the dependency of  $H_k$  on the superficial velocity  $U$ . This implies that in their approach  $h^*$  is also a function of the superficial velocity, which is in contradiction with our results, where  $h^*$  is a function of particle size only (chapter 6).

Figure 7.2. shows that the best fits were obtained with our model and with "the simple model" of Van Swaaij (1985). That the "simple model" fits that well means that it is a good approximation to use a constant  $k_g$  in this situation.

For clarity we have shown the results for the "simple model" and our model in fig. 7.3.

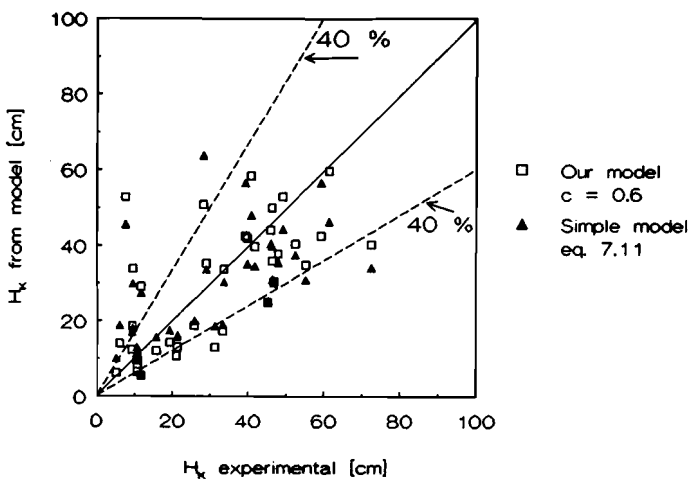


**Figure 7.3** *Model computations for the simple model and our model, based on our RTD experiments.*

The error ( $\sim 40\%$ ) appears to be quite large but it has to be considered that the experimental error in determining  $N_k$  was about  $20\%$  (as was mentioned in chapter 5). The bed height fluctuates during fluidization and therefore the error is enlarged when  $H_k$  is calculated, since  $H_k = H/N_k$ . Furthermore, in

computing  $H_k$  from the models certain process conditions have to be substituted in the equations, which also introduces certain errors.

Two points for the 106  $\mu\text{m}$  powder differed greatly. For these experiments the bed height was rather large ( $\sim 95$  cm), maybe introducing an extra error (as was mentioned in chapter 5), but there is no real explanation.

Summarizing our model gives:

$$H_k = \frac{U}{k_g \cdot a \cdot c \cdot E} \quad c \sim 0.6 \quad (7.15a)$$

$$a = \frac{6 \cdot \delta \cdot \psi}{d_b} \quad \begin{array}{ll} \psi \sim 1.67 & \text{for } d_p < \sim 200 \mu\text{m} \\ \psi \sim 1 & \text{for } d_p > \sim 200 \mu\text{m} \end{array}$$

$d_b$  from equation (7.2) ( $h^*$  from equation (6.27))

$\delta$  from equation (7.3)

$k_g$  from equation (7.5) (Sit and Grace, 1978)

$E$  from equation (7.13b)

The conversion  $X_a$  is computed from (see also chapter 3):

$$X_a = 1 - \exp \left[ - \frac{N_k \cdot N_r}{N_k + N_r} \right] \quad \begin{array}{l} N_k = H/H_k \\ N_r = \frac{k_d \cdot (1 - \delta) \cdot H}{U} \end{array} \quad (7.15b)$$

This means we have a model description with a simple theoretical and physical background, from which  $H_k$  and/or  $X_a$  can be calculated. If necessary  $c \cdot \psi$  can be used as the only fitting parameter, with a value of about 1.

The usefulness of our model was verified by comparing our model computations with RTD and chemical measurements reported in literature.

Figure 7.4. shows the results for the RTD experiments of de Groot (1968), van Swaaij and Zuiderweg (1972), Boonstra (1983) and Roes and Garnier (1984). From this figure it can be seen that our model also predicts  $H_k$  (within the expected accuracy) for other systems than those where a  $\text{CH}_4$  tracer was used and for much larger reactors than we used.

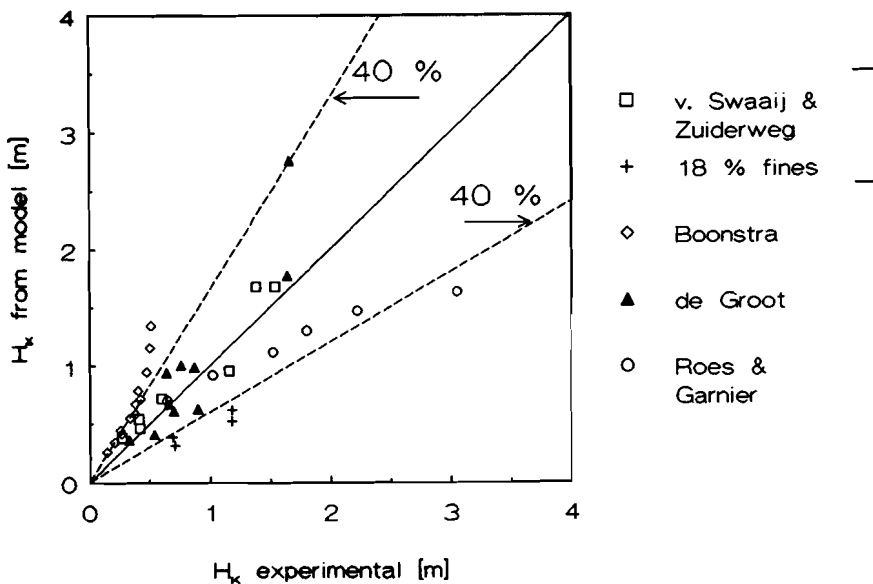


**Figure 7.4** Comparison of  $H_k$  values calculated from our model with  $H_k$  values actually measured from RTD experiments. From various authors. See also chapter 4.

It was found that the "simple model" predicted the conversion for the ozone decomposition reaction in a fluid bed with a porous plate well. However, calculations showed that the results of Fryer and Potter (1976) and Van Den Aarsen (1985) could not be fitted satisfactory.

Results of the computations with our model and the actually measured conversions for the ozone decomposition reaction are shown in fig. 7.5. Data from Orcutt et al. (1962) were left out. They used such a small catalyst that probably channeling occurred, which may have lowered the conversion.

From chapter 3 (Appendix 3.B) it can be seen that the error in measuring the ozone concentration is about 5 %. This means that the error in the conversion is about 10 %. If we appreciate the fact that an error in the model computations will be about 10 % (due to process parameter errors) an overall error of about 20 % can be expected. As can be seen from fig. 7.5 the model

prediction is quite satisfactory.

Figure 7.6 shows that also other reacting systems could be predicted well with our model. For the data of Massimilla and Johnstone (1961) the  $k_d$  value given by Werther and Hegner (1980) was used. However, as was mentioned in chapter 4 these data have to be considered with an appropriate reserve.

For all calculations  $\psi = 1.67$  was used, also for the larger particles (325  $\mu\text{m}$ ) used by Van Den Aarsen (1985), which shows that  $\psi$  may change with changing reactor conditions.

The results for the hydrogenation of ethylene from Lewis et al. (1959) can be explained from the fact that they used such a small reactor (diameter 5 cm) that slugging must have occurred (as was mentioned in chapter 4). This should lower the experimental conversion considerably, which is indeed found from fig. 7.6.

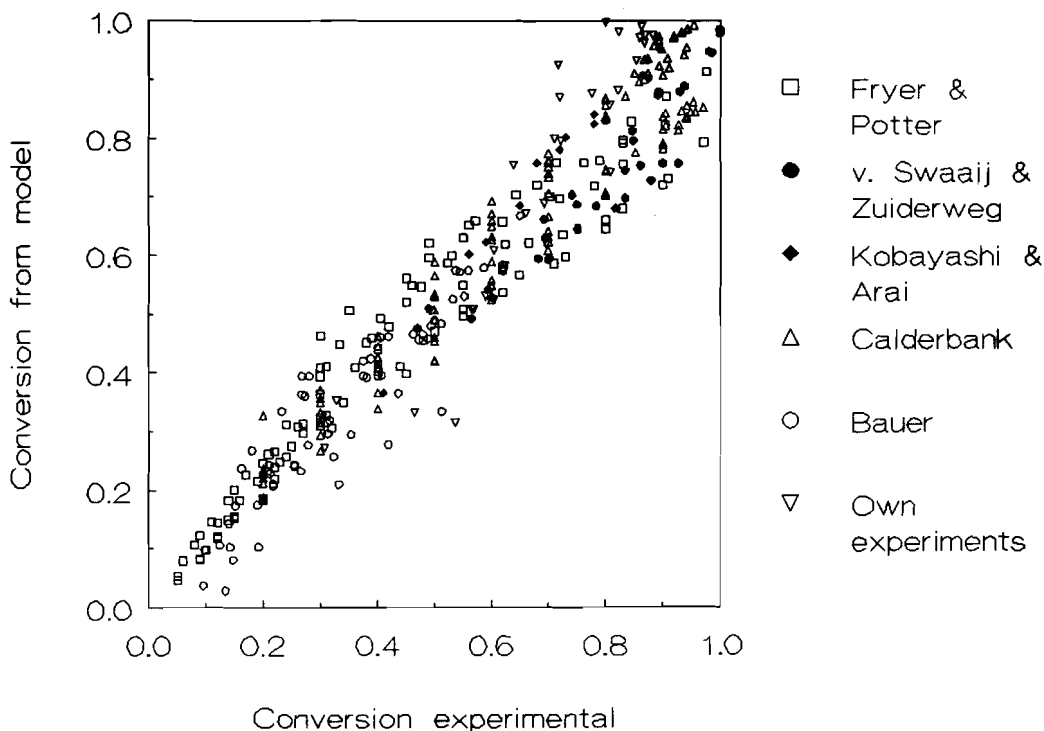


**Figure 7.5** Comparison of calculated and measured conversions for the ozone decomposition reaction. From various authors. See also table 4.2.

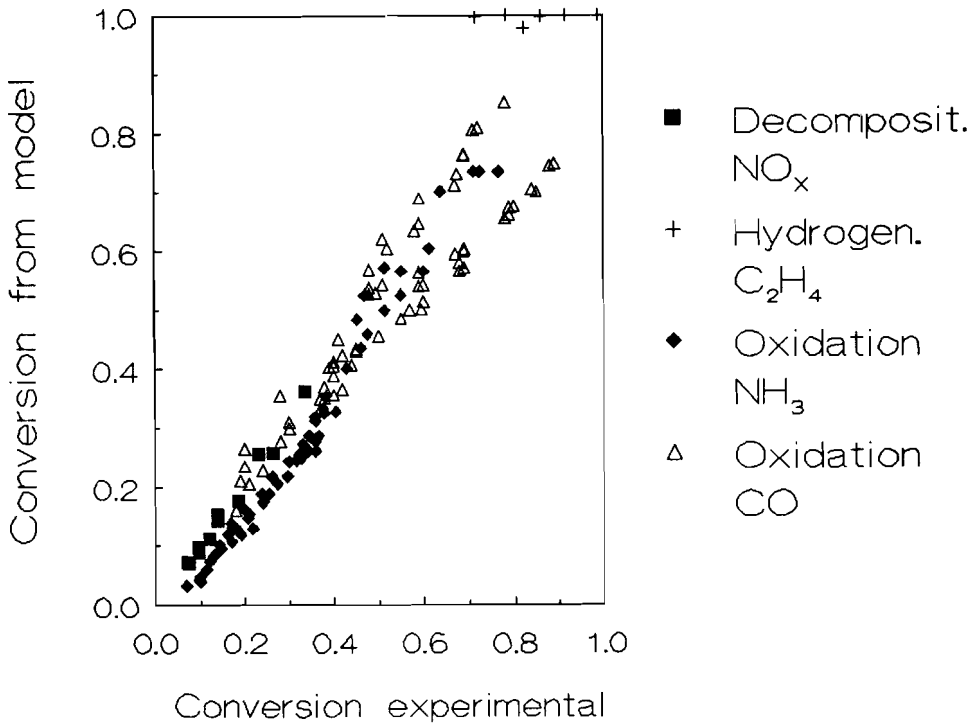


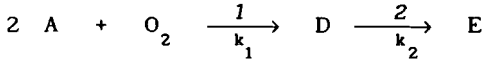
**Figure 7.6** Comparison of calculated and measured conversions, for various reactions. From various authors. See also Chapter 4.

- Decomposition of  $\text{NO}_x$  from Shen and Johnstone (1955).
- Hydrogenation of ethylene from Lewis et al. (1959).
- Oxidation of ammonia from Massimilla and Johnstone (1961).
- Oxidation of CO from Van Den Aarsen (1985).

**7.4. An example of a reactor design**

It was shown that our model was in agreement with the experimental data within the expected errors. Therefore this model was used to perform some simple design computations for a first order irreversible catalytic model reaction, to be carried out in a gas fluidized bed reactor.

Consider the exothermic oxidation of A (which may be a hydrocarbon):



where D is the desired product and  $k_1$  and  $k_2$  are reaction rate constants for the reactions 1 and 2 respectively. The reaction rate is defined by:

$$r_a = k \cdot p_a \quad (1^{st} \text{ order reaction in A}) \quad (7.16)$$

where  $p_a$  is the partial pressure in A.

The heat of reaction for the two reactions are respectively  $\Delta H_1$  [kJ/mol A] and  $\Delta H_2$  [kJ/mol D]. The conversion in A is  $X_a$ , the selectivity in D is  $S_D$  and the yield in D is  $Y_D$  ( $Y_D \equiv X_a \cdot S_D$ ).

Based on a mass balance for A, D, E and  $O_2$ , with dense phase and bubble phase in plug flow and assuming a  $k_1/k_2$ -ratio, a relation between the conversion  $X_a$  and selectivity  $S_D$  can be computed. Combined with process conditions this leads to an optimal combination of conversion and yield (fig 7.7).

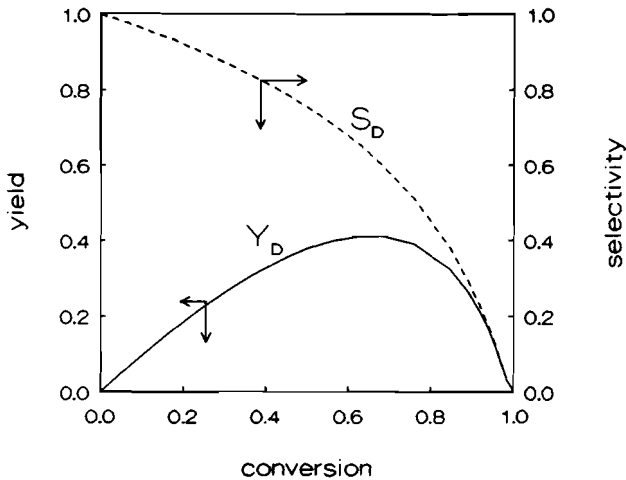


Figure 7.7 Hypothetical relation between selectivity, conversion and yield.

### Mass balance

If the production of D is  $P_D$  (mass per unit of time) then the molar flow rate of D,  $\phi_{\text{mol},D}$ , is given by:

$$\phi_{\text{mol},D} = \frac{P_D}{M_D} \quad (7.17)$$

where  $M_D$  is the molecular weight of D. The mass flow rate of A ( $\phi_{\text{m},A}$ ) necessary to obtain the desired production  $P_D$  is given by:

$$\phi_{\text{m},A} = \frac{2 \cdot M_A \cdot \phi_{\text{mol},D}}{X_a \cdot S_D} \quad (7.18)$$

Suppose that for the optimal selectivity a feed mole ratio of  $A/O_2 = 5$  is required and that the oxygen is fed to the reactor with air. Air contains about 20 % oxygen and therefore the following holds for the mass flow rate air  $\phi_{\text{m},\text{air}}$ :

$$\phi_{\text{m},\text{air}} = \frac{2 \cdot \phi_{\text{mol},D} \cdot M_{\text{air}}}{X_a \cdot S_D} \quad (7.19)$$

where  $M_{\text{air}}$  is the molecular weight of air. The total mass flow rate of the feed  $\phi_{\text{m},F}$  is given by:

$$\phi_{\text{m},F} = \phi_{\text{m},A} + \phi_{\text{m},\text{air}} \quad (7.20)$$

### Heat balance

The amount of heat released due to reaction  $Q_{\text{w},r}$  is:

$$Q_{\text{w},r} = X_a \cdot \phi_{\text{mol},A} \cdot (\Delta H_1 + \frac{1}{2} \cdot \Delta H_2 \cdot (1-S_D)) = X_a \cdot \phi_{\text{mol},A} \cdot \Delta H_{\text{TOT}} \quad (7.21)$$

where  $\Delta H_{\text{TOT}}$  is the total heat of reaction.

The amount of heat necessary to heat the feed gases is given by:



$$Q_{W,g} = (\phi_{m,air} \cdot c_{p,air} + \phi_{m,A} \cdot c_{p,A}) \cdot (T_{out} - T_{in}) \quad (7.22)$$

The produced heat  $Q_w$  ( $Q_w = Q_{w,r} - Q_{w,g}$ ) is removed by putting heat exchange pipes in the fluidized bed. The number of pipes is  $N_p$ , the diameter of the pipes is  $D_T$  and the length is equal to the bed height  $H$ . The overall heat transfer coefficient is  $h_w$  [ $W^2/(m^2 \cdot K)$ ] and is determined by the heat transfer between the fluid bed and the pipe surface. The following holds:

$$Q_w = h_w \cdot \pi \cdot D_T \cdot H \cdot N_p \cdot \Delta T \quad (7.23)$$

where  $\Delta T$  is the temperature difference between the fluid bed and the pipes. The reactor is assumed to be isothermal. This means that for a given production  $P_D$ , conversion, selectivity, reactor diameter,  $\Delta T$  and heat exchange pipe specifications, the bed height necessary to remove all heat can be calculated. From our mass transfer model discussed before, the height necessary to obtain a given conversion in  $A$  can be computed.

#### 7.4.1. Heat transfer

Many papers have dealt with the problem of heat transfer in gas fluidized beds. It would be out of the scope of this thesis to discuss all of these. Therefore a general description will be given and a model with which  $h_w$  can be computed.

The heat transfer coefficient  $h_w$  can be thought to consist of three additive components, namely:

- i)  $h_p$  : particle convection term (most important)
- ii)  $h_g$  : gas convection term (important with large  $U_{mf}$ )
- iii)  $h_r$  : radiative term (important at high temperatures, therefore often neglected).

The gas convection term  $h_g$  is calculated at two superficial velocity regimes:  $U_{mf} < U < U_{max}$  and  $U > U_{max}$  (Appendix 7.A). Here  $U_{max}$  is that velocity at

which a maximum in  $h_w$  is found. In general  $h_w$  is a function of  $U/U_{mf}$  as given in fig. 7.8.

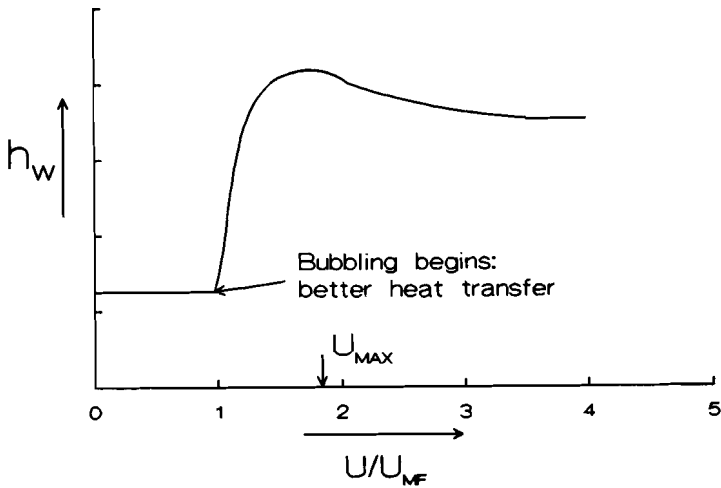


**Figure 7.8** General description of  $h_w$  [ $W/m^2 \cdot K$ ] as a function of  $U/U_{mf}$ .  
 $U = U_{max}$  at  $U/U_{mf} \sim 1.5 - 2$ .

The particle convection term  $h_p$  was computed with the model of Bock (1983) (see Appendix 7.A). With this model it is assumed that a small package of particles moves to the heat exchange pipes, exchanges heat and moves away. Heat transfer occurs according to the penetration theory.

**7.4.2. Design calculations.**

1) Reaction with  $k_2 \neq 0$ .

The input parameters given in table 7.1 were used in the design calculations. The reactor dimensions used are given in table 7.2. The particle size was taken to be variable. The process conditions were assumed to be such, that it was economically most favourable to use the conversion and selectivity given in table 7.1.

$X_a = 0.5$	$\Delta T = 300 \text{ }^\circ\text{C}$
$S_D = 0.4$	$T_{bed} = 500 \text{ }^\circ\text{C}$
$\Delta H_{TOT} = 300 \text{ kJ/mol}$	$(T_{out} - T_{in})_{gases} = 400 \text{ }^\circ\text{C}$
$M_{air} = 28.8 \text{ g/mol}$	$P = 1 \cdot 10^5 \text{ N/m}^2$
$M_A = 16 \text{ g/mol}$	$k_1 = 0.5 \text{ s}^{-1}$
$M_D = 28 \text{ g/mol}$	$D_g = 9.6 \cdot 10^{-5} \text{ m}^2/\text{s}$
$\rho_{g,A} = 0.25 \text{ kg/m}^3$	$\epsilon_d = 0.5$
$\rho_{g,air} = 0.46 \text{ kg/m}^3$	$f_{cat} \sim 0.95$
$\rho_p = 1500 \text{ kg/m}^3$	$c_{p,A} = 2200 \text{ J/(kg}\cdot\text{K)}$
$\mu_g = 3 \cdot 10^{-5} \text{ N}\cdot\text{s/m}^2$	$c_{p,air} = 1000 \text{ J/(kg}\cdot\text{K)}$
$\lambda_g = 0.055 \text{ W/(m}\cdot\text{K)}$	$c_{p,particles} = 700 \text{ J/(kg}\cdot\text{K)}$
$\lambda_e = 0.3 \text{ W/(m}\cdot\text{K)}$	

**Table 7.1** *Input values used for design example. All values are given at bed temperature.*

D [m]	6	8	10	12
$N_p$	150	260	500	700
$D_T$ [m]	0.10	0.10	0.10	0.10
pipe pitch [m]	0.40	0.40	0.40	0.40
$D_e$	5.87	7.84	9.75	11.70

**Table 7.2** *Reactor dimensions used in design example.*

The values for the input parameters were chosen based on values that are usually encountered in commercial units. To obtain comparable situations the value for the number of pipes was chosen in such a way that the fraction of catalyst in the reactor  $f_{cat}$  (given in eq. 7.24) was always about 0.95.

$$f_{cat} = \frac{\text{total bed volume} - \text{pipe volume}}{\text{total bed volume}} = 1 - \left( \frac{D_T}{D} \right)^2 \cdot N_p \quad (7.24)$$

Equations (A.7.1) to (A.7.8) were used to compute  $h_w$  at given conditions. The heat transfer coefficients  $h_w$  was found to change with  $d_p$  as shown in fig. 7.9. This trend and the same order of magnitude were also given by Botteril (1986).

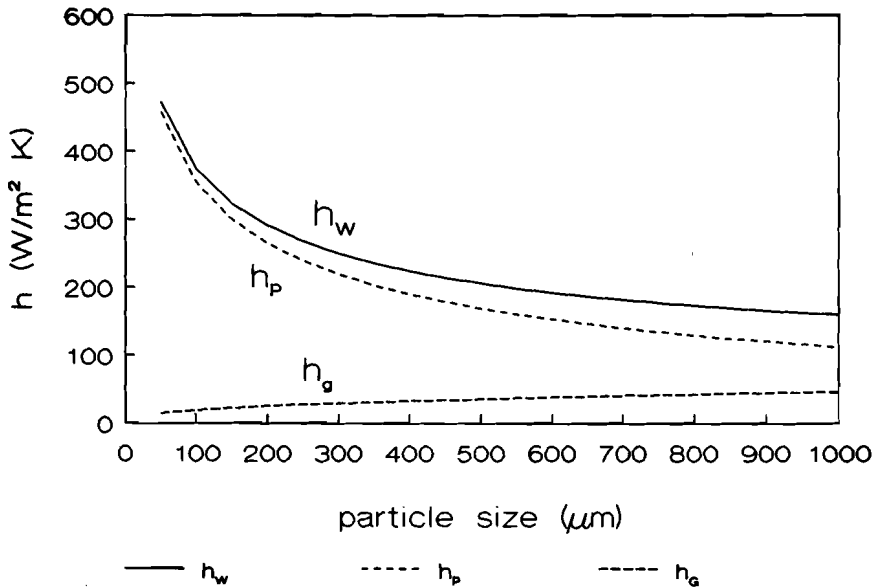


**Figure 7.9** Example of calculated heat transfer coefficients as a function of particle size. ( $P_D = 50,000$  ton/year,  $D = 10$  m, other parameters and values are given in table 7.1 and 7.2)

In computing the number of reaction units  $N_r$  a correction had to be made for the heat exchange pipes, because not the complete bed volume was occupied by

catalyst. Hence:

$$N_r = \frac{k_m \cdot M}{Q} = \frac{k_1 \cdot (1 - \delta) \cdot f_{cat} \cdot H}{U} \quad (7.25)$$

In the estimate of the bubble size the pipe arrangement had to be taken into account. Due to the heat exchange pipes it is very likely that bubble growth is disturbed and even limited (Botteril, 1986). According to Baeyens and Geldart (1980) pseudo slugging occurs between the tubes and they suggest therefore that an effective bubble diameter can be estimated from pipe diameter and pipe pitch. Based on a square array and a pipe pitch of 40 cm, an average bubble diameter  $d_b \sim 46$  cm was taken for all situations. The production  $P_D$  was varied, using reasonable values encountered in commercial units (30,000, 50,000, 70,000 or 100,000 (ton/year) per reactor). Also the bed diameter was varied in an attempt to estimate the most efficient reactor dimensions.

The height of a mass transfer unit  $H_k$  was calculated with our mass transfer model (eq. 7.15a). With the conversion given this means that the bed height is the only unknown variable in eq. 7.15b (with  $N_r$  given by eq. 7.25). This means that the bed height necessary to obtain the wanted conversion can be calculated with equations 7.15a, 7.15b and 7.25. With  $h_w$  calculated, the height necessary to remove all heat can be computed from eq. 7.19.

A general picture for the heights, necessary for heat transfer and conversion, as a function of particle size and at a fixed production  $P_D$  is given in fig. 7.10. With  $d_p < d_{p,opt}$  the system is mass transfer dominated. A bed height  $H_{X_a}$  is necessary to obtain the wanted conversion, meaning that the reactor has more than sufficient heat transfer area ( $H_{X_a}$  decreases with increasing  $d_p$ , because  $a$  is constant due to the constant average bubble size and at the same time  $k_g$  increases with increasing  $d_p$  due to the increasing  $U_{mf}$  (see eq. 7.6)). With  $d_p > d_{p,opt}$  a bed height of  $H_{h_w}$  is necessary to realize sufficient heat transfer (with increasing particle size, the heat transfer coefficient  $h_w$  decreases (fig. 7.9) and therefore  $H_{h_w}$  increases). However, this also implies an extra conversion (of  $X_{a,hw}$ ), leading to more heat production due to which  $H_{h_w}$  should increase, etc. This process goes on until the maximum obtainable conversion is reached. However, selectivity is much too low in this situation (see fig. 7.7). The  $H_{h_w}$  value can be lowered (from point P to Q) by increasing the number of pipes or temperature difference between

bed and pipes. This shows that for  $d_p < d_{p,opt}$  the reactor is too large and that for  $d_p > d_{p,opt}$  a new design is necessary. The most effective particle size is therefore  $d_{p,opt}$ : all heat can be removed and the wanted conversion combined with the desired selectivity are obtained.

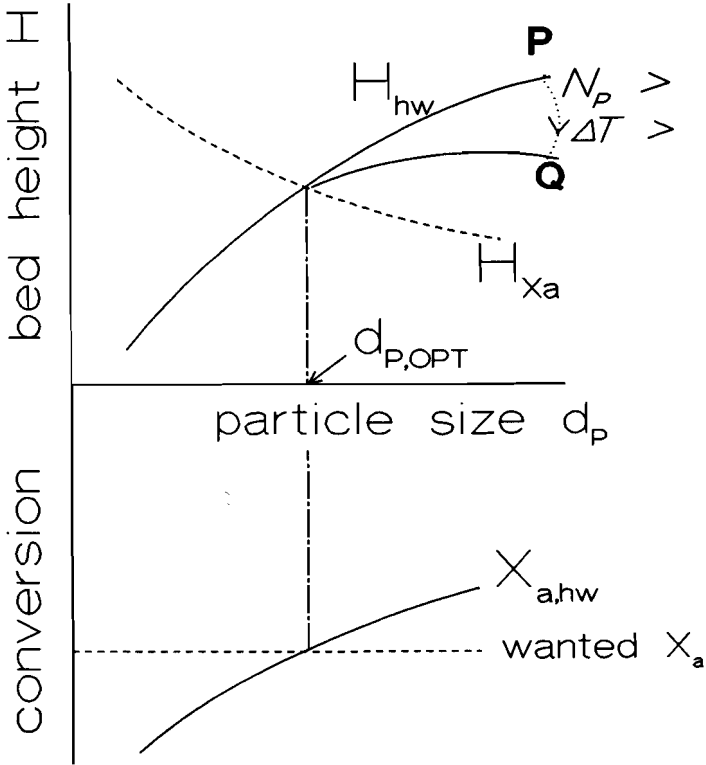


**Figure 7.10** Schematic drawing of bed heights necessary to obtain a certain conversion and heat transfer surface as a function of particle size. See text.

Results of the computations are shown in table 7.3. If the production  $P_D$  is to increase, a larger bed height is necessary at a given conversion. But also more heat has to be removed, which requires smaller particles. From this table it can be seen that the optimal particle size is always larger than  $\sim 400 \mu\text{m}$ , which is larger than the commonly encountered A powders. This shows that

particle size optimization is important in fluid bed reactor design and that there are situations where coarse particles are more favourable than fine particles.

D [m]	6			8		
	U [m/s]	$d_{p,opt}$ [ $\mu\text{m}$ ]	H [m]	U [m/s]	$d_{p,opt}$ [ $\mu\text{m}$ ]	H [m]
$P_D$ [ton/year]						
30,000	1.59	400	12.8	0.89	525	8.5
50,000	2.65	500	22.5	1.49	400	12.3
70,000	<i>non realistic bed heights</i>			2.09	375	16.4

D [m]	10			12		
	U [m/s]	$d_{p,opt}$ [ $\mu\text{m}$ ]	H [m]	U [m/s]	$d_{p,opt}$ [ $\mu\text{m}$ ]	H [m]
$P_D$ [ton/year]						
50,000	0.96	600	7.8	0.67	750	6.2
70,000	1.35	500	9.9	0.93	600	7.8
100,000	1.92	475	13.4	1.33	500	10.4

Table 7.3 Results from design calculations with  $k_2 \neq 0$ . See text.

2) Reaction with  $k_2 = 0$ .

In this situation the second reaction does not occur and therefore the selectivity is always equal to 1. The values for the input parameters were taken to be equal to those given in table 7.1. The conversion  $X_a$ , the reaction rate constant  $k_1$  and the particle size were taken to be variable. The reactor dimensions of the 8 m reactor were used and the desired production was 100,000 ton/year. The same considerations as mentioned for the case in which  $k_2 \neq 0$ , can now be used and the optimal particle size was determined in the same way. The results of the computations are shown in table 7.4 and fig. 7.11.

$k_1$ [s <sup>-1</sup> ]	$X_a$ [-]	U [m/s]	$d_{p,opt}$ [μm]	H [m]	$k_1$ [s <sup>-1</sup> ]	$X_a$ [-]	U [m/s]	$d_{p,opt}$ [μm]	H [m]
0.5	0.4	1.49	400	9.4	0.5	0.6	0.99	500	11.5
2.5			75	5.0	2.5			400	10.6
					5.0			300	10.1
$k_1$ [s <sup>-1</sup> ]	$X_a$ [-]	U [m/s]	$d_{p,opt}$ [μm]	H [m]	$k_1$ [s <sup>-1</sup> ]	$X_a$ [-]	U [m/s]	$d_{p,opt}$ [μm]	H [m]
0.5	0.8	0.74	800	14.7	2.5	0.9	0.66	950	16.0
2.5			625	13.4	5.0			850	15.4
5.0			600	13.2	10.0			800	15.1
10.0			500	11.4					

**Table 7.4** Results from design calculations with  $k_2 = 0$ ,  $D = 8$  m and  $P_D = 100,000$  ton/year.

Figure 7.11 shows the found optimal particle size as a function of reaction rate constant  $k_1$  and the conversion  $X_a$ .

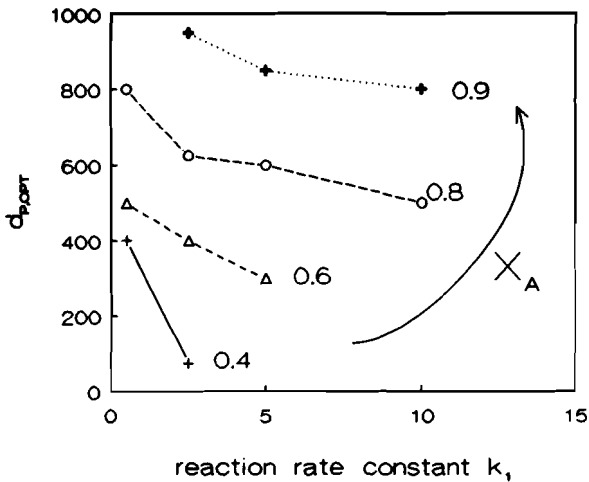


**Figure 7.11** Results from design calculations with  $k_2 = 0$ ,  $D = 8$  m and  $P_D = 100,000$  ton/year. See table 7.4 and text.



Table 7.4 shows that the optimal particle size is mostly larger than the size of the commonly encountered A powders. The results shown in fig. 7.11 can be explained from fig. 7.10. If  $k_1$  increases with the conversion fixed, the bed height necessary to obtain this conversion decreases, because then the number of reaction units  $N_r$  has the same value. The height necessary to remove all heat remains the same and therefore a smaller  $d_{p,opt}$  is found (fig. 7.10). If the conversion increases with  $k_1$  fixed, the bed height necessary to obtain the wanted conversion increases, because now more reaction units are needed. The bed height necessary to remove all heat also increases, but not as much as the bed height necessary to obtain the wanted conversion and therefore  $d_{p,opt}$  increases (fig. 7.10).

### 7.5. Concluding remarks.

A simple and physical model was defined, based on theories known from literature. The constant  $c$  was determined from our RTD experiments and it was shown that with our model it was possible to explain RTD and conversion data for various reactors and reactor dimensions.

Based on our model, design and experiments can be planned more efficiently. Then results from these experiments can be scaled up by the scaling parameter, making design more simple and reliable.

A simple design example showed that there are cases that it is indeed more efficient to use coarser particles than usually encountered in gas fluidized beds. This could be concluded for reactions with and without secondary reactions.

## Appendix 7.A

### Computation of heat transfer coefficients $h_g$ and $h_p$ .

The gas convection term  $h_g$  is calculated at two superficial velocity regimes:  $U_{mf} < U < U_{max}$  and  $U > U_{max}$ . Here  $U_{max}$  is that velocity at which a maximum in  $h_w$  is found. In general  $h_w$  is a function of  $U/U_{mf}$  as given in fig. 7.8. In our case only those situations were regarded in which  $U > U_{max}$  (because  $U/U_{mf} > 2$ ). Then the following equation describes the heat transfer coefficient  $h_g$  (Botteril, 1986):

$$Nu = \frac{h_g \cdot d_p}{\lambda} = 0.175 \cdot Ar^{0.46} \cdot Pr^{0.33} \quad (A.7.1)$$

Here  $d_p$  is the particle size in [m] and  $\lambda$  the thermal conductivity of the gas in [W/(m·K)]. For air at 300 °K,  $\lambda = 26 \cdot 10^{-3}$  W/(m·K) and  $\lambda = 55 \cdot 10^{-3}$  at 800 °K (Perry and Chilton (1972)). The influence of pressure on  $\lambda$  is negligible. Ar (Archimedes number) has the same definition as given in equation (1.1) and Pr is the Prandtl number:

$$Ar = \frac{\rho_f \cdot d_p^3 \cdot (\rho_p - \rho_f) \cdot g}{\mu^2} \quad \text{and} \quad Pr = \frac{\mu \cdot c_p}{\lambda} \quad (A.7.2)$$

If necessary the relation given by Bock (1983) can be used for  $U_{mf} < U < U_{max}$ .

The particle convection term  $h_p$  was computed with the model of Bock (1983). With this model it is assumed that a small package of particles moves to the heat exchange pipes, exchanges heat and moves away. Heat transfer is assumed to follow the penetration theory.

Bock (1983) gave the following equations:

(A.7.3)

$$\frac{1}{h_p} = \frac{1}{(1 - \epsilon_b)} \cdot \left[ \frac{3}{h_{max} (1 - \epsilon_{mf})} + \frac{\pi^{1/2}}{2} \cdot \sqrt{\frac{t_c}{(\lambda_e \cdot \rho \cdot c_p)_E}} \right]$$

with:

$$h_{max} = \frac{4 \cdot \lambda}{d_p} \cdot \left[ \left( 1 + \frac{2B}{d_p} \right) \cdot \ln \left( 1 + \frac{d_p}{2B} \right) - 1 \right]$$

and

$$2B = 4 \cdot \lambda_m \cdot \left( \frac{2}{\gamma} - 1 \right) \quad \lambda_m = \frac{16}{5} \cdot \sqrt{\frac{R \cdot T}{2 \cdot \pi \cdot M}} \cdot \frac{\mu}{P}$$

$$\log\left(\frac{1}{\gamma} - 1\right) = 0.6 - \left(\frac{1000 [^{\circ}\text{K}]}{T} + 1\right) \cdot \frac{1}{C}$$

The factor  $\gamma$  is the accommodation coefficient, accounting for the incomplete energy transfer during a molecule-wall collision. In  $(\lambda \cdot \rho \cdot c)_E$  the subscript E means "effective". The effective  $\rho \cdot c_p$  is additive:

$$(\rho \cdot c_p)_E \sim (\rho \cdot c_p)_{\text{gas}} + (\rho \cdot c_p)_{\text{particles}} = \varepsilon_d \cdot (\rho \cdot c_p)_{\text{gas}} + (1 - \varepsilon_d) \cdot (\rho \cdot c_p)_{\text{part}} \quad (\text{A.7.4})$$

The effective heat conductivity coefficient  $\lambda_e$  was calculated from Botteril (1986). The factor  $\lambda_m$  is the mean free path length of the gas molecules and is taken from the gas theory. Here is M the molecular weight of the gas and P the absolute pressure [N/m<sup>2</sup>]. For most gases considered, Bock (1983) found a value of about 3 for the empirical constant C.

The contact time t is calculated from from:

$$t_c = 2.5 \cdot \left(\frac{d_p}{U - U_{mf}}\right)^{0.5} \cdot z^{0.8} \cdot \left(\frac{(\rho_p - \rho_f) \cdot (1 - \varepsilon_{mf})}{\rho_f}\right)^{0.4} \quad (\text{A.7.5})$$

where z is the height above the distributor plate. The bubble hold up  $\varepsilon_b$  was defined by:

$$\varepsilon_b = 0.15 \cdot \left(\frac{U - U_{mf}}{(g \cdot D_e)^{0.5}}\right)^{0.5} \cdot z^{-0.65} \quad (\text{A.7.6})$$

where  $D_e$  is the effective bed diameter:

$$D_e = \sqrt{D^2 - N_p \cdot D_T^2} \quad (\text{A.7.7})$$

For a height  $z \geq z'$  the fluid dynamics were defined to be independent of height z:

$$\begin{aligned} z' &= 3 \cdot D_e && \text{for one pipe} \\ z' &= 3 \cdot \text{pipe pitch} && \text{for a bundle of pipes} \end{aligned} \tag{A.7.8}$$

A pipe pitch of 40 cm was used, hence  $z' = 120$  cm. This was neglected compared to expected bed heights of several meters. Therefore  $t$  and  $\varepsilon_b$  were computed with  $z = 1.2$  m.

## REFERENCES

- Argyriou D.T., List H.L. and Shinnar R. (1971), Bubble growth by coalescence in gas fluidized beds, *A. I. Ch. E. J.*, 17 (1), 122.
- Bauer W. (1980), Einfluss der Gasverteilerkonstruktion auf Stoffaustausch- und Reaktionsverhalten flacher Wirbelschichten., Ph. D. Thesis, Universität Erlangen.
- Baeyens J. and Geldart D. (1980), Modelling approach to the effect of equipment scale on fluidized bed heat transfer data, *J. Powder & Bulk Solids Technology*, 4 (4), 1-9.
- Bock H.J. (1983), Heat transfer in fluidized beds, in *Fluidization*. Edited by Kunii D. and Toei R., p. 323, Engineering Foundation, New York.
- Bohle W. and Van Swaaij W.P.M. (1978), In "*Fluidization*" (edited by J.F. Davidson and D.L. Keairns), pp 167 - 172. Cambridge University Press, London and New York
- Boonstra J. (1983), Interim report, University of Technology Eindhoven, Laboratory of Chemical Process Technology, June.
- Borodulya V.A., Buevich Yu. A. and Dikalenka V.I. (1981), Motion and mass transfer of bubbles in fluidized beds, *J. Eng. Phys*, 41, 1123.  
Translated from: *Inzh.- Fiz. Zh.* 41, 678 (1981).
- Botteril J.S.M. (1986), Fluid Bed Heat Transfer, in *Gas Fluidization Technology*. Edited by D. Geldart, p.219, John Wiley and Sons, Ltd.
- Calderbank P.H., Toor F.D. and Lancaster F.H. (1967), Reaction kinetics in gas fluidized catalyst bed (experimental), *Proc. Int. Symp. Fluidization*, p. 652, Netherlands Univ. Press, Amsterdam.
- Chiba T. and Kobayashi H. (1970), Gas exchange between the bubble and emulsion phases in gas-solid fluidized beds, *Chem. Eng. Sci.*, 25, 1375 - 1385.
- Clift R. and Grace J.R. (1985), Continuous Bubbling and Slugging, in *Fluidization*, 2<sup>nd</sup> edition, Academic Press. Edited by Davidson J.F., Clift R. and Harrison D., p. 73.
- Clift R., Grace J.R. and Weber M.E. (1974), Stability of bubbles in fluidized beds, *Ind. Eng. Chem. Fundam.*, 13 (1), 45.
- Cottaar E.J.E. (1985), The influence of interstitial gas on powder handling, Ph.D. Thesis, University of Technology Eindhoven.
- Darton R.C., LaNeuze R.D., Davidson J.F. and Harrison D. (1977), Bubble growth due to coalescence in fluidised beds, *Trans. I. Chem. E.*, 55, 274.
- Davidson J.F. and Harrison D. (1963), *Fluidised Particles*, Cambridge University Press.
- Davidson J.F., Harrison D., Darton R.C. and LaNueze R.D. (1977), The two phase theory of fluidization and its application to chemical reactors, In "Chemical Reactor Theory: A Review", edited by Lapidus L. and Amundsen N.R., p. 583, Prentice-Hall Englewood, New Jersey.

- De Groot J.H. (1967), Scaling up of gas fluidized bed reactors, *Proc. Int. Symp. Fluidization*, p. 348, edited by A.A.H. Drinkenburg, Netherlands Univ. Press, Amsterdam.
- Drinkenburg A.A.H. (1970), Gas transfer in a fluidized bed, Ph.D. Thesis, University of Technology Eindhoven.
- Dry R.J. and Judd M.R. (1985), Fluidized beds of fine, dense powders. Scale-up and reactor modeling, *Powder Technology*, **43**, 41-53.
- Edelman A. (1967), Design and operation of an ozonator, Ph. D. Thesis, University of Delft.
- Eigenberger G. and Butt J.B. (1976), A modified Crank-Nicholson technique with equidistant space steps, *Chem. Eng. Sci.*, **3**, 681 - 691.
- Ergun S. (1952), Fluid flow through packed columns, *Chem. Engng. Prog.*, **48**, 89
- Fan L.T., Tho-Ching Ho, Yutani N. and Walawender W.P. (1983), Statistical study of the frequency of free bubbling in a shallow fluidized bed. In *Fluidization*. Edited by Kunii D. and Toei R., p. 15 - 24. Engineering Foundation, New York.
- Fan L.T. and Fan Liang-Shin (1979), Simulation of catalytic fluidized bed reactors by a transient axial dispersion model with invariant physical properties and nonlinear chemical reactions, *Chem. Eng. Sci.*, **34**, 171-179.
- Fan Liang-Shin and Fan L.T. (1980), Transient and steady state characteristics of a gaseous reactant in catalytic fluidized bed reactors, *A.I.Ch.E. Journal*, **26** (1), 139.
- Frye C.G. Lake W.C. and Eckstrom H.C. (1958), Gas-solid contacting with ozone decomposition reaction, *A.I.Ch.E. Journal*, **4** (4), 403.
- Fryer C. and Potter O.E. (1976), Experimental investigation of model for fluidized bed catalytic reactors, *A.I.Ch.E. Journal*, **22** (1), 39.
- Geldart D. (1967), The expansion of bubbling fluidised beds, *Powder Techn.*, **1**, 335.
- Geldart D. (1973), Types of fluidization, *Powder Techn.*, **7**, 285.
- Geldart D. and Cranfield R.R. (1972), The gas fluidisation of large particles, *Chem. Eng. Journ.*, **3**, 211.
- Glicksman L.R. and McAndrews G. (1985), The effect of bed width on the hydrodynamics of large particle fluidised beds, *Powder Techn.*, **42**, 159.
- Grace J.R. and Harrison D. (1969), On the two phase theory of fluidization, *Chem. Eng. Sci.*, **29**, 327.
- Grace J.R. and Clift R. (1974), On the two-phase theory of fluidization, *Chem. Eng. Sci.*, **29**, 327 - 334.
- Hayes J.G. (1974), Numerical methods for curve and surface fitting, *Bull. Inst. Math. Applics.*, **10**, 144.
- Hlavacek V. and Van Rompay P. (1981), Current problems of multiplicity, stability and sensitivity of states in chemically reacting systems, *Chem. Eng. Sci.*, **36** (10), 1587 - 1597.

- Kato K. and Wen C.Y. (1969), Bubble assemblage model for fluidized bed catalytic reactors, *Chem. Eng. Sci.*, **24**, 1351.
- Krishna R. (1981), *Nato Adv. Study Inst. Ser., Ser. E52*.
- Kunii D. and Levenspiel O. (1968), Bubbling bed model, *Ind. Eng. Chem. Fund.*, **7**, 446.
- Kunii D. and Levenspiel O. (1969), *Fluidization Engineering*, John Wiley and Sons Inc., New York.
- Kunii D. and Levenspiel O. (1990), Fluidized Reactor models. 1) For the bubbling beds of fine, intermediate and large particles. 2) For the lean phase: freeboard and fast fluidization, *Ind. Eng. Chem. Res.*, **29**, 1226 - 1234.
- Kobayashi H. and Arai F. (1965), *Kagaku Kogaku (Chem. Eng. Japan)* **29**, 885
- Lewis W.K., Gilliland E.R. and Glass W. (1959), Solid catalyzed reaction in a fluidized bed, *A.I.Ch.E. Journal*, **5** (4), 419.
- Massimilla L. and Johnstone H.F. (1961), Reaction kinetics in fluidized beds, *Chem. Eng. Sci.*, **16**, 105 - 112.
- Matsen J.M. (1973), Evidence of maximum stable bubble size in a fluidized bed, *A. I. Ch. E. Symp. Series*, **69** (128), 30.
- Mori S. and Wen C.Y. (1975), Estimation of bubble diameter in gaseous fluidized beds, *A. I. Ch. E. Journal*, **21**, 109.
- NAG-library (1980), Mark 8, Numerical Algorithm Group Limited, 1980 - 1989, NAG FORTRAN Library, Oxford.
- Orcutt J.C. Davidson J.F. and Pigford R.L. (1976), Reaction time distribution in fluidized catalytic reactors, *Chem. Eng., Prog. Symp. Series*, **58** (38), 1.
- Palm W.J. (1983), Advanced matrix methods for dynamic system analysis. Chapter 9 from "*Modeling analysis and control of dynamic systems*", p.583, John Wiley and Sons, Inc.
- Perry R.H. and Chilton C.H. (1973), *Chemical Engineers' Handbook* 5<sup>th</sup> ed., Mc. Graw-Hill Book Company.
- Pollard J.H. (1977), Numerical and statistical techniques, Cambridge University Press.
- Pyle D.L. and Harrison D. (1967), An experimental investigation on the two phase theory of fluidization, *Chem. Eng. Sci.*, **22**, 1199.
- Rietema K. (1967), Application of mechanical stress theory to fluidization. In *Proc. Int. Symp on Fluidization*, edited by A.A.H. Drinkenburg, p.154, Neth. Univ. Press.
- Roes A.W.M. en Garnier C.N. (1986), Investigation into the bubble to dense phase mass transfer rate in a gas-solid fluidized bed with cohesive powders, In *Heat and Mass transfer in fixed and fluidized bed*, ed. by W.P.M. van Swaaij and Naim H. Afgan, Berlin Springer.
- Rowe P.N. (1962), The effect of bubbles on gas-solids contacting in fluidized beds, *Chem. Eng. Prog. Symp Series*, **58** (38), 42.

- Rowe P.N. (1976), Prediction of bubble size in a gas fluidized bed, *Chem. Eng. Sci.*, **31**, 285-288.
- Rowe P.N., Macgillivray H.J. and Cheesman D.J. (1979), Gas discharge from an orifice into a gas fluidized bed, *Trans. I. Chem. E.*, **57**, 194.
- Rowe P.N. and Masson H. (1981), Interaction of bubbles with probes in gas fluidised beds. *Trans. I. Chem. E.*, **59**, 177.
- Shah B.H., Ramkrishna D. and Borwanker J.D. (1977a), Simulation of bubble populations in a gas fluidized bed, *Chem. Eng. Sci.*, **32**, 1419.
- Shah B.H., Ramkrishna D. and Borwanker J.D. (1977b), Simulation of particulate systems using the concept of the interval of quiescence, *A. I. Ch. E. Journal*, **23** (6), 897.
- Shen C.Y. and Johnstone H.F. (1955), Gas solid contact in fluidized beds, *A.I.Ch.E. Journal*, **1** (3), 349.
- Sit S.P. and Grace J.R. (1978), Interphase mass transfer in aggregative fluidized beds, *Chem. Eng. Sci.*, **33**, 1115 - 1122.
- Sit S.P. and Grace J.R. (1981), Effect of bubble interaction on interphase mass transfer in gas fluidized beds, *Chem. Eng. Sci.*, **36**, 327 - 335.
- Skoog D.A. and West D.M. (1982), *Fundamentals of Analytical Chemistry*, 4<sup>th</sup> edition, CBS College Publishing, pp 539 - 545.
- Sun G. and Grace J.R. (1990), The effect of particle size distribution on the performance of a catalytic fluidized bed reactor, *Chem. Eng. Sci.*, **45** (8), 2187.
- Sweet I.R., Gustafson S.S. and Ramkrishna D. (1987), Population balance modeling of bubbling fluidized bed reactors - I. Well stirred dense phase, *Chem. Eng. Sci.*, **42** (2), 341- 351.
- Thoenes D. (1972), Grundlagen der chemischen Reaktionskinetik, in *Ullmans Encyklopadie der Technischen Chemie*, Band 1, p. 216, Verlag GmbH, Weinheim.
- Tuin B.J.W. (1989), Extraction of heavy metals from contaminated clay soils, p.166, Ph. D. Thesis, Univ. of Techn. Eindhoven.
- Toomey R.D. and Johnstone H.F. (1952), Gaseous fluidization of solid particles, *Chem. Eng. Prog.* **48**, 220.
- Van Den Aarsen F.G. (1985), Fluidised bed wood gasifier performance and modeling, PhD. Thesis, Univ. of Techn. Twente.
- Van Deemter J.J. (1961), Mixing and contacting in gas-solid fluidized beds, *Chem. Eng. Sci.*, **13**, 143-154.
- Van Lare C.E.J., Piepers H.W. and Thoenes D., (1990), Scaling and particle size optimization of mass transfer in gas fluidized beds, *Chem. Eng. Sci.*, **45** (8), 2211 - 2217.
- Van Loon P. (1987), Continuous decoupling transformations for linear boundary value problems, Ph. D. Thesis, Techn. Univ. Eindhoven.
- Van Swaaij W.P.M. (1985), Chemical Reactors, in *Fluidization*, 2<sup>nd</sup> edition, Academic Press. Edited by Davidson J.F., Clift R. and Harrison D., p. 595



- Van Swaaij W.P.M. and Zuiderweg F.J. (1972), Investigation of ozone decomposition in fluidized beds on the basis of a two-phase model, *Chem. React. Eng., Proc. Eur. Symp.* 5<sup>th</sup>, B9-25.
- Villadsen J.V. and Stewart W.E. (1967), Solution of boundary-value problems by orthogonal collocation, *Chem. Eng. Sci.*, 22, 1483-1501.
- Wen C.Y. and Yu Y.H. (1966), Mechanics of Fluidization, *Chem. Eng. Prog. Symp. Series*, 62, 100.
- Werther J. (1972), Experimentelle Untersuchungen zur Hydrodynamik von Gas/Feststoff Wirbelschichten, Ph. D. Thesis, Univ. of Erlangen.
- Werther J. (1976), Bubble growth in large diameter fluidized beds, in *Fluidization Technology*, Vol I, p. 215. Edited by D.L. Keairns, Hemisphere Publishing Corp. in association with Mc Graw Hill, Washington.
- Werther J. (1978), Mathematische modellierung von Wirbelschichtreaktoren, *Chem. Ing. Techn.*, 50, 850.
- Werther J. (1983), Hydrodynamics and mass transfer between the bubble and emulsion phases in fluidised beds of sand and cracking catalyst, In *Fluidization*. Edited by Kunii D. and Toei R., p.93, Engineering Foundation, New York.
- Werther J. and Hegner B. (1980), Ermittlung optimaler Betriebseinstellungen für technische Wirbelschichtreaktoren, *Chem. Ing. Techn.*, 2, 106-113.
- Westerterp K.R., Van Swaaij W.P.M. and Beenackers A.A.C.M. (1984), *Chemical Reactor Design and Operation*, John Wiley and Sons Ltd.
- Whitehead A.B. and Young A.D. (1967), In *Proceedings of the international symposium on fluidization*, p. 294. Edited by Drinkenburg A.A.H., Neth. Univ. Press, Amsterdam.
- Yates J.G. (1983), Fundamentals of Fluidized-bed chemical processes, Butterworths.

## CURRICULUM VITAE

Coert van Lare werd geboren op 20 augustus 1964 te Horn. In 1982 behaalde hij het VWO diploma aan het Boschvelcollege te Venray en begon hij met de studie Scheikundige Technologie aan de Technische Hogeschool Eindhoven (nu Technische Universiteit Eindhoven). Hij studeerde in 1986 af bij de vakgroep Organische Chemie op een onderzoek naar DNA stukturen. Hierna begon hij in hetzelfde jaar met het promotieonderzoek (AIO-4) bij de vakgroep Fysische Technologie (nu Chemische Proceskunde). Per 1 januari 1991 is hij werkzaam bij het Unilever Research Laboratorium te Vlaardingen.

## NAWOORD

Bij deze wil ik iedereen bedanken die mij al die tijd moreel en/of vakmatig heeft ondersteund. Prof. Thoenes wil ik bedanken voor alle hulp en het feit dat hij mij de mogelijkheid heeft gegeven het promotieonderzoek op een zelfstandige wijze uit te voeren. Prof. Marin wil ik bedanken voor de nuttige discussies tijdens het schrijven van het artikel over de decoupling methode en voor het kritisch doorlezen van het manuscript. Mijn dank gaat ook uit naar dr. Paul van Loon voor alle hulp en uitleg betreffende die decoupling methode. Prof. van Swaaij en Prof. Kerkhof wil ik danken voor het kritisch doornemen van het manuscript.

De samenwerking binnen de groep Fluidizatie heb ik als zeer waardevol ervaren. Mijn oprechte dank gaat dan ook uit naar ir. Huub Piepers voor alle geduld en ondersteuning en naar Joop Boonstra voor de technische adviezen, die weer vakkundig werden uitgevoerd door de technische staf. De afstudeerders ir. Martien Rutten en ir. Jeroen Schoonderbeek hebben, samen met Bart van Beers, veel bijgedragen aan het uiteindelijke resultaat. Verder wil ik de hele vakgroep Chemische Proceskunde danken voor de fijne en ontspannen sfeer waarin ik al die tijd gewerkt heb en voor alle interesse en steun.

## Stellingen behorende bij het proefschrift van C.E.J. van Lare

1. De in de literatuur vermelde afwijkingen van de twee-fasen theorie van Toomey en Johnstone (1952) zijn in feite minder groot dan vaak gesuggereerd wordt, omdat deze "afwijkingen" veelal geconcludeerd worden uit resultaten van experimentele technieken waarmee het niet mogelijk is de volledige bellengasstroom te bepalen.

Dit proefschrift, hoofdstuk 5 en 6.

Toomey R.D. en Johnstone H.F., *Chem. Eng. Prog.*, **48**, 220 (1952).

2. De hoogte waarop een stabiele belgrootte wordt bereikt is voornamelijk afhankelijk van de deeltjesgrootte van het gefluïdiseerde poeder.

Dit proefschrift, hoofdstuk 6.

3. Gezien de overeenkomsten in hydrodynamica en stofoverdracht tussen gas/vast- en gas/vloeistof-gefluïdiseerde bedden, kunnen inzichten uit de gas/vloeistof-combinatie gebruikt worden voor deelbeschrijvingen van een gas/vast-fluïdbed.

Dit proefschrift, hoofdstuk 7.

4. Het gebruik van B/D poeders (volgens de classificatie van Geldart (1973)) kan, ondanks de zogenaamde slechte fluïdisatie-eigenschappen, duidelijke voordelen hebben bij de toepassing in fluïdbed-reactoren.

Dit proefschrift, hoofdstuk 7.

Geldart D., *Powder Techn.*, **7**, 285 (1973).

5. Een fundamentele discussie over de werkelijke bellengasstroom in een gefluïdiseerd bed is alleen zinnig indien er een (arbitraire) definitie bestaat over een minimale belgrootte.

Grace J.R. en Clift R., *Chem. Eng. Sci.*, **29**, 327 (1974).

6. Bij het vergelijken van correlaties voor het berekenen van warmteoverdrachtscoëfficiënten in geschraapte warmtewisselaars, dient de schraperbladgeomtrie als parameter meegenomen te worden.

Maingonnat J.F. en Corrieu G., *Entropie* N° 111, p. 29 - 36 (1983).

Lazer I. en Reher E., *Wissen. Zeitschr.*, **15** (4), 356 (1973).

7. Bij de oplossing van de diffusievergelijking in droogprocessen met behulp van kortsluitmethoden, kan tegenwoordig nog nauwelijks gesproken worden van een vereenvoudiging ten opzichte van de numerieke oplossing.

Coumans W.J., Proefschrift, Techn. Univ. Eindhoven, 1987.

8. Het deeltjesaantal als functie van de conversie bij de emulsie-polymerisatie van vinyl acetaat, zoals gegeven door Zollars (1981), is onjuist.

Zollars R.L., In *Emulsion Polymerisation of Vinyl Acetate*. Editors: M.S. El-Aaser en J.W. VanderHoff, Applied Science Publishers Ltd., 1981.

9. De complexiteit van modellen moet in verhouding staan tot de nauwkeurigheid en het bereik van experimenten en rekenmethoden.

10. In verband met de verkeersveiligheid moet het altijd voeren van minstens dimlichten, voor al het gemotoriseerde verkeer, verplicht gesteld worden.

11. Het is onvermijdelijk dat een aantal boerenbedrijven moet sluiten. Er is immers geen enkele andere bedrijfstak die de overschotten produceert, het milieu belast en nog zoveel subsidie ontvangt als zij doet.